Control of Redox Behaviors of Heteroaromatic Coenzymes with Coordination to Transition-Metal Complexes

著者	見留 広海
内容記述	この博士論文は全文公表に適さないやむを得ない事由があり要約のみを公表していましたが、解消したため、2017年10月2日に全文を公表しました。
year	2016
その他のタイトル	遷移金属錯体を用いた複素環補酵素の酸化還元挙動の制御
学位授与大学	筑波大学 (University of Tsukuba)
学位授与年度	2015
報告番号	12102甲第7650号
URL	http://hdl.handle.net/2241/00144168

Control of Redox Behaviors of Heteroaromatic Coenzymes with Coordination to Transition-Metal Complexes

Hiroumi Mitome

February 2016

Control of Redox Behaviors of Heteroaromatic Coenzymes with Coordination to Transition-Metal Complexes

Hiroumi Mitome
Doctoral Program in Chemistry

Submitted to the Graduate School of
Pure and Applied Sciences
in Partial Fulfillment of the Requirements
for the Degree of Doctor of Philosophy in
Science

at the
University of Tsukuba

Contents

Chapter 1 General Introduction

1–1. Substrate Oxidation by Natural Enzymes

In biological systems, enzymes perform various reactions to keep the lives. Among the reactions, oxidations are especially important, as observed in metabolism, photosynthesis, and so on. In the oxidation processes, transition-metal elements such as iron and copper, which are coordinated by amino-acid residues, porphyrin, or heteroaromatic enzymes as ligands, play principal roles.[1-3] Oxidation enzymes including cytochrome P450, flavin-containing monooxygenases and pterin-dependent enzymes form active species to oxidize substrates with use of one dioxygen molecule as a sacrificial oxidant.[1a] As described below, dioxygen activation in the oxidation enzymes is well sophisticated to let the active center of the enzymes efficiently react with a dioxygen molecule, which is known to be inert due to its triplet ground state.[4] In nature, both of the dioxygen activation and substrate oxidation with the active species in the oxidation enzymes utilize "Proton-Coupled Electron Transfer (PCET)" to lower the energy barrier of the reactions (See Chapter 1-4).

Cytochrome P450s are one of representative examples of oxidation enzymes conducting dioxygen activation to obtain the active species, and they contain an iron(III)-porphyrin complex at their active center. In the dioxygen activation process, the iron(III)-porphyrin accepts one electron and the reduced porphyrin

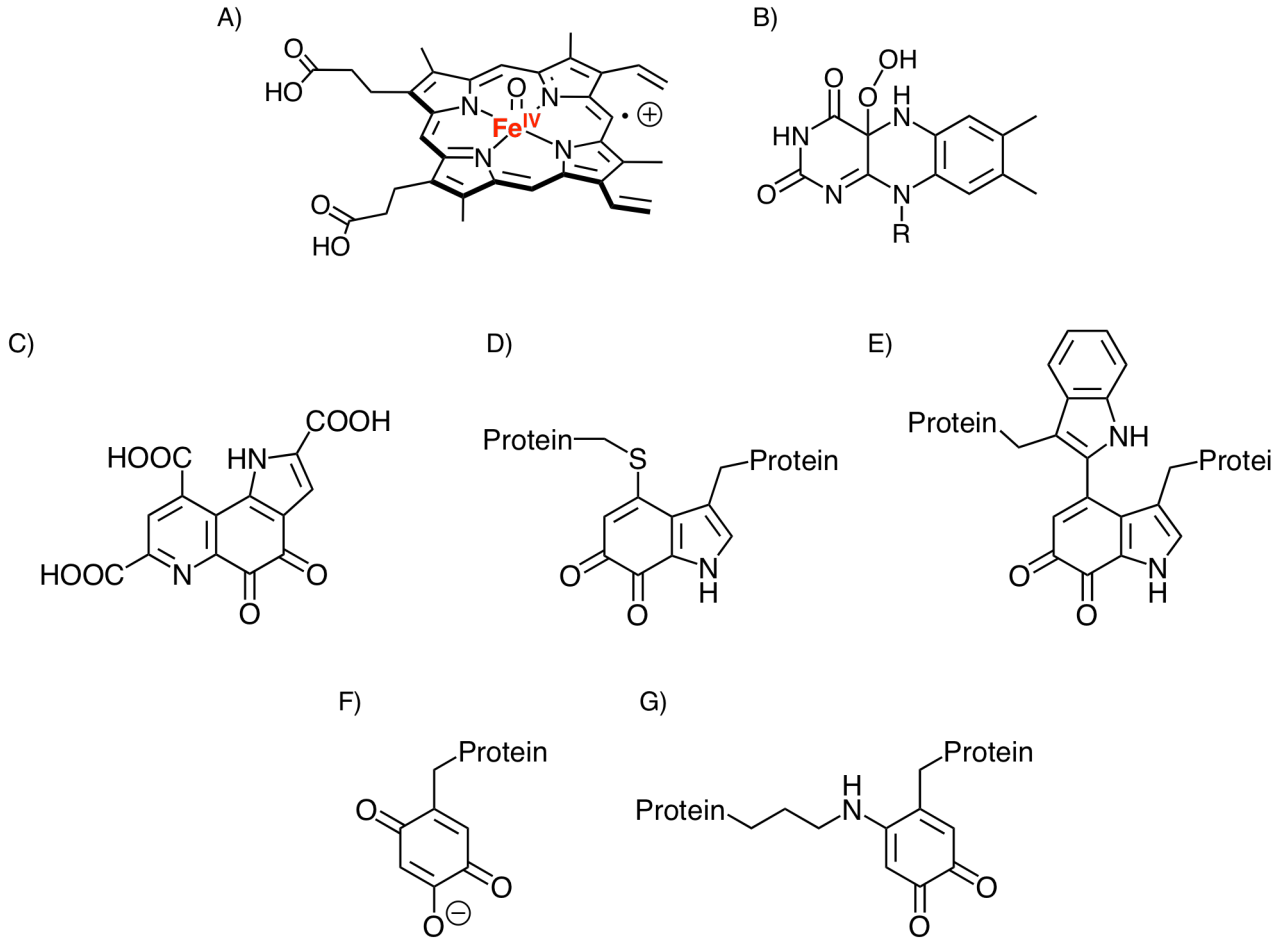

Figure 1. Coenzymes of oxidation enzymes in their active forms. (A) Compound I, (B) flavin-hydroperoxide, (C) PQQ, (D) CTQ, (E) TTQ, (F) TPQ, (G) LTO.

reacts with a dioxygen molecule to generate the active species, so-called "Compound I" (Figure 1-1), which is an iron(IV)-oxo-(porphyrin-π-radical-cation) species.[1] Compound I shows high electron-acceptability with use of the high-valent metal center and also exhibits high proton-acceptability with use of the –2-charged oxo ligand, and the acceptabilities bring the high oxidation power to compound I to oxidize even C-H bonds.

Flavins are heteroaromatic coenzymes to perform various redox reactions that are important in metabolism.[3a] In flavin-dependent enzymes, $2e^-$-reduced flavin reacts with dioxygen to form flavin C4a-hydroperoxide species as the active species to oxidize organic substrates (Figure 1-1).[3b] The formation of flavin C4a-hydroperoxide was supported with experiments performed by Anderson, in which Anderson formed flavin C4a-hydroperoxide by pulse radiolysis to an aerated solutions of riboflavin.[5] Flavin-dependent monooxygenases catalyze various oxidation reactions of substrates such as hydroxylation, Baeyer-Villiger-type oxidation, sulfoxidation, epoxidation, and halogenation.[3a] Inspired by the high reactivity, flavins have been utilized to develop catalytic systems, which performed oxidation reactions of organic molecules with dioxygen or hydrogen peroxide as the sacrificial oxidant.[6-11]

On the other hand, quinoproteins have been known to perform substrate oxidation reactions without activating dioxygen. Quinoproteins have quinone molecules such as pyrroloquinolinequinone (4,5-dihydro-4,5-dioxo-1*H*-pyrrolo-[2,3-*f*]quinoline-2,7,9-tricarboxylic acid, PQQ), cysteine tryptophylquinone (CTQ), tryptophan tryptophylquinone (TTQ), topaquinone (TPQ), and lysine tyrosylquinone (LTQ), which behave as cofactors or a part of the protein chain (Figure 1-1).[12] Organic substrates oxidized by quinoproteins in biological systems include alcohols, amines, and sugars; however, apart from PQQ-dependent enzymes, most of all quinoproteins oxidize primary amines as the main substrates to obtain corresponding aldehydes in biological systems.[12a] The reaction mechanism of the substrate oxidation with quinoproteins is direct oxidation with the quinone molecule.[12] The reduced quinones derived from the substrate oxidation are reoxidized by a heme cofactor in the quinoprotein, by a heme-iron enzyme, or by a copper enzyme, and thus, a dioxygen molecule is not required for substrate oxidation reactions by quinoproteins.[12]

1–2. PQQ, a Heteroaromatic Coenzyme

In contrast to other quinone cofactors, PQQ is known for its high reactivity to oxidize alcohols and sugars.[12a] PQQ was found by Hauge in 1964 from soluble PQQ-glucose dehydrogenase as the first quinoprotein cofactor.[13] The discovery of PQQ was not only the start of quinoprotein chemistry but also the third report of redox-active coenzymes following nicotinamide and flavin.[14] As another example of enzymes containing PQQ, methanol dehydrogenase in methylotrophs has been reported,[15,16] which can oxidize methanol to formaldehyde.[12i] To utilize the high reactivity of PQQ-dependent enzymes, various investigations aiming for its practical applications have been performed, such as sensors of glucose, which detected electronic currents generated by oxidation of glucose with PQQ-dependent quinoproteins.[17] On the basis of crystal structures, quinoproteins containing PQQ was revealed to form a PQQ-calcium ion complex at the active center and use the PQQ-calcium ion complex to oxidize substrates.[12a]

Salisbury and co-workers succeeded in explicit determination of the X-ray single-crystal structure of an acetone-adduct of PQQ, which was extracted from *Pseudomonas* TP1, in 1979.[18] From the structural analysis

and spectroscopic findings reported by Duine and co-workers,[19] the structure of PQQ was determined as a quinoline-quinone derivative having a fused pyrrole ring at the C-C bond between C5 and C6 of the quinoline ring, and three carboxyl groups are substituted at the 2, 7 and 9 positions of the pyrrolo-quinoline-quinone structure.

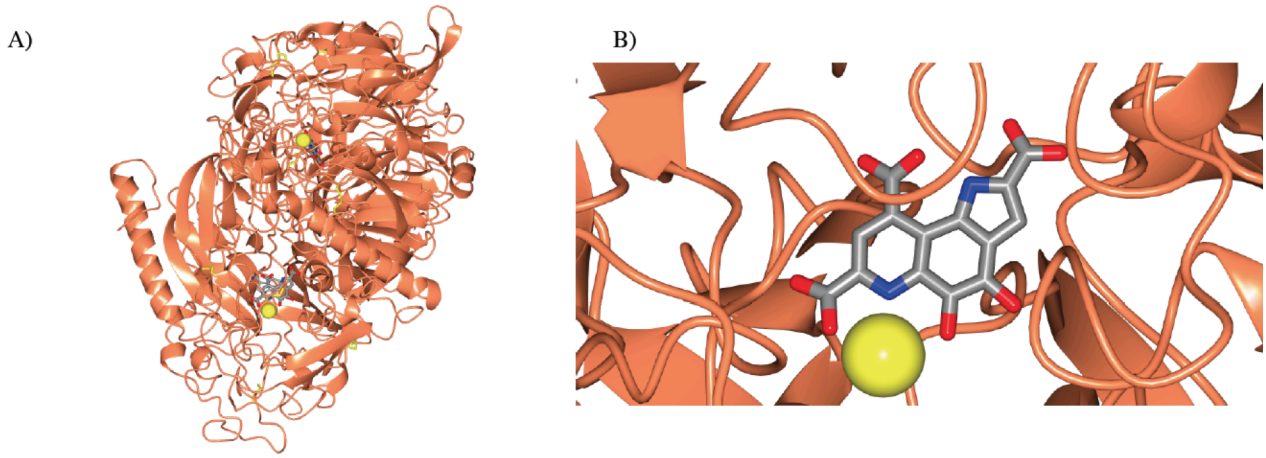

Figure 1-2. (A) Crystal Structure of methanol dehydrogenase, and (B) a magnified figure around the active center.[15c]

In 1981, Corey and co-workers reported a total synthesis of PQQ and its methyl ester (PQQTME).[20] Since then, investigation of PQQ molecules outside of enzymes became possible,[21] which had been unavailable because of difficulty in extraction of PQQ itself from living animals or plants due to its high reactivity. However, PQQ itself is a weak oxidant with the first reduction potential at –0.53 V vs SCE (for PQQTME in MeCN) in the absence of the Ca^{2+} ion.[21j] Besides, methanol dehydrogenase catalytically oxidizes methanol, which cannot be oxidized even by DDQ with higher electron-acceptability (+0.51 V vs SCE),[22] by virtue of

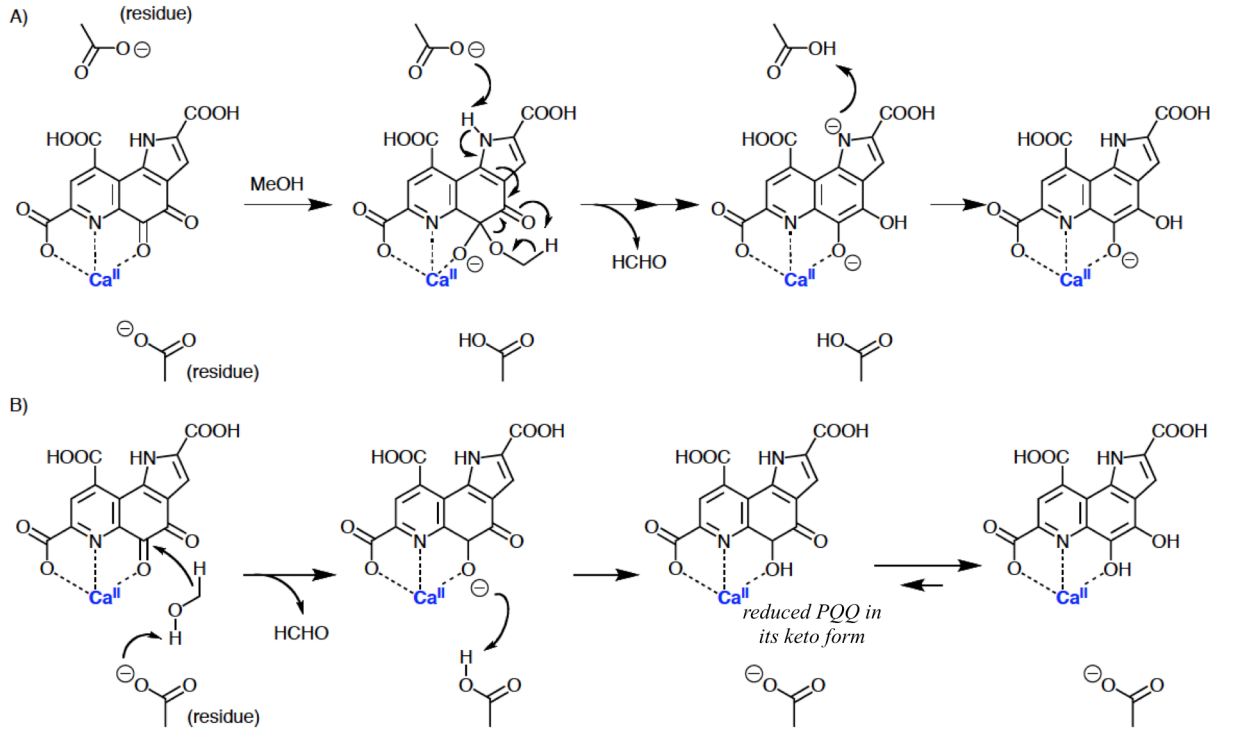

Figure 1-3. Proposed mechanisms for the oxidation reaction by methanol dehydrogenase; (A) "addition-elimination mechanism" and (B) hydride-transfer mechanism (extracted from Ref. 12a).

the activation of the cofactor through Ca^{2+} binding and proton uptake by an aspartate residue of the protein framework.[15a,15c,23]

For the oxidation reactions with PQQ, "addition-elimination mechanism" has been proposed on the basis of kinetic analyses of the substrate oxidation (Figure 1-3).[16a] In the addition-elimination mechanism, a substrate attacks a carbonyl carbon of PQQ, which is activated by a Lewis acid such as a calcium ion and also by strong electronegativity of the nitrogen atom in the pyridine ring of PQQ, and resultantly the substrate and PQQ form an intermediate. Theoretical calculations by Toscano's group also support the addition-elimination mechanism.[24] On the other hand, hydride-transfer mechanism also has been proposed on the basis of a crystallographic high-resolution structure of methanol dehydrogenase from *Methylophilus methylotrophus* and theoretical investigations into the structure of the reduced PQQ, which was suggested to be included in the enzyme used for the X-ray analysis (Figure 1-3).[12f, 25, 26] Bruice *et al.* reported that methanol dehydrogenase contained a reduced PQQ derivative in the keto form on the basis of the high-resolution structure (Figure 1-3B), and also proposed that the reduced PQQ in the keto form could be generated only in the hydride-transfer mechanism.[25] As described above, the reaction mechanism of substrate oxidation with PQQ still remains controversial.

Oxidation reactions of biologically important molecules, such as thiols, amines, amino acids, and aldoses, with use of PQQ outside of enzymatic environments, have been reported since 1984;[21a-f] however, oxidation of alcohols with PQQ was hard to be achieved. Catalytic methanol oxidation using a synthetic PQQ derivative was first achieved by Itoh and co-workers in 1997.[21g-i] Addition of a calcium ion and DBU (= 1,8-diazabicyclo[5.4.0]undec-7-ene) as a strong base into a PQQTME solution in methanol, ethanol, 1-propanol, or 2-propanol induced oxidation reactions of the solvent molecules to give corresponding aldehydes or ketone.[21h] In this reaction, dioxygen was used as a sacrificial oxidant. As one of the reasons why PQQTME could oxidize methanol, effects of calcium ion was proposed as mentioned above; *i.e.*, the PQQTME-Ca^{2+} complex shows much higher reduction potential at 0.0 V vs SCE in MeCN than that of free

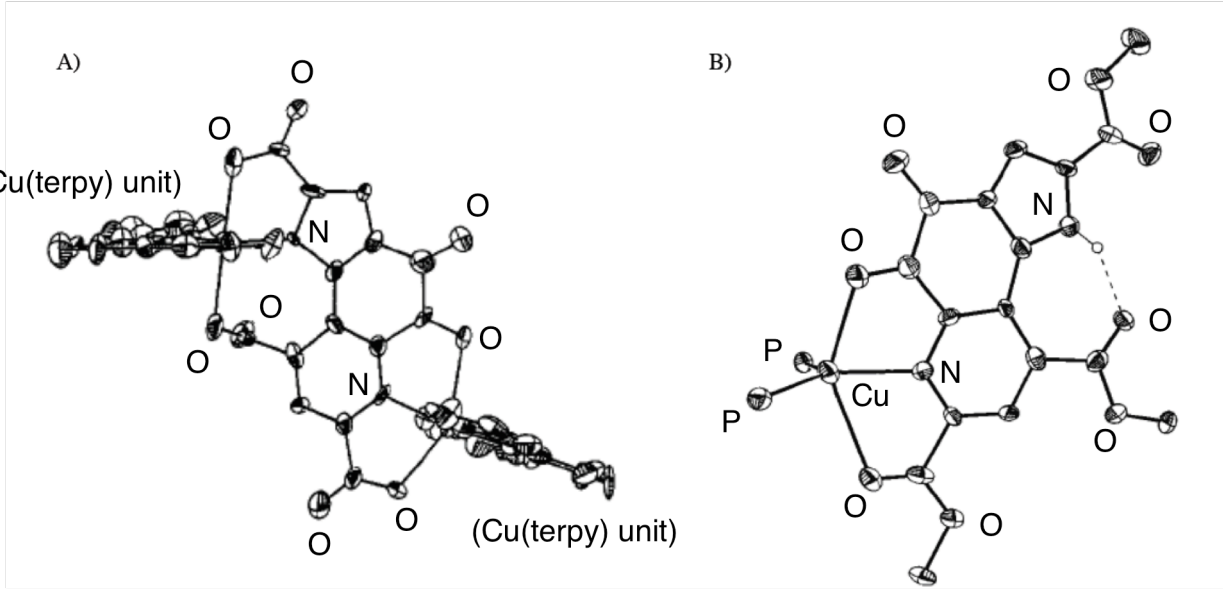

Figure 1-4. Crystal structures of PQQTME metal-complexes: (A) $[Cu^{II}(PQQ^{4-})(terpy)_2]$[27c] and (B) $[Cu^{I}(PQQTME)(PPh_3)_2]^+$.[28] Phenyl rings of the PPh_3 ligands are omitted for clarity in (B).

PQQTME (–0.53 V vs SCE in MeCN).[21j] However, the complexation constant between PQQTME and a calcium ion is not so large (K = 1900 M^{-1}) and the acid-base equilibrium between DBU and PQQTME interrupts the aiming oxidation reaction, and thus, the observed reaction rate was much small. In fact, under Itoh's conditions, PQQTME spent 65 h to oxidize 14.5 equiv ethanol even in the ethanol solution.[21h]

As mentioned above, interaction of PQQ with metal ions can dramatically enhance the reactivity of PQQ, in relation to the association of the calcium ion as demonstrated in the substrate oxidation; however, only a few researches on PQQ-transition-metal complexes have been reported so far, and the reported researches focused on the X-ray single crystal analyses of the complexes and no attention has been paid to the impact of coordination of PQQ derivatives to transition-metal ions on their redox properties and electronic structures (Figure 1-4).[27, 28]

1–3 Pterin: A Dioxygen Activator in Nature

Pterins are also heteroaromatic coenzymes and known to activate a dioxygen molecule at the active sites in metalloenzymes (Figure 1-5). Through the dioxygen activation, organic substrates such as aromatic molecules and phenol derivatives are oxidized by, for example, tryptophan hydroxylase,[29] phenylalanine hydroxylase,[30] and tyrosine hydroxylase,[31] which involve tetrahydropterin as the cofactor. Tetrahydropterins in the tetrahydropterin-dependent hydroxylases exist in the vicinity of an iron center, and the reaction of dioxygen with tetrahydrobiopterin has been proposed to produce a metal-peroxo species, a 4a-pterin-OO-iron complex, as precursors of active species (Figure 1-5).[32]

Mimicking the oxidation reactions performed by tetrahydropterin-dependent hydroxylases should be a powerful strategy for development of artificial oxidation systems for organic compounds, because of its high

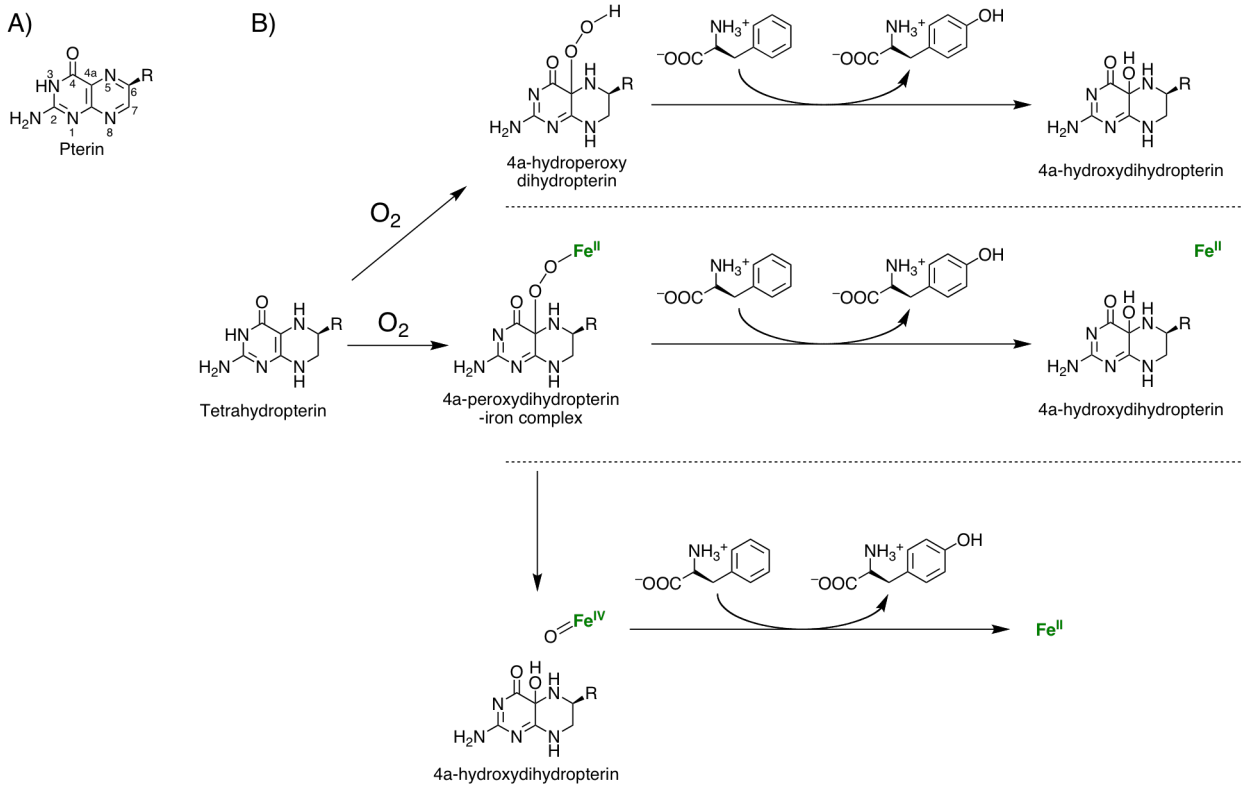

Figure 1-5. (A) Structure of pterins, and (B) a proposed reaction mechanism in the substrate oxidation at the active center of phenylalanine hydroxylase.[32-35]

oxidation power to oxidize aromatic C-H bonds and high selectivity without oxidizing functional groups of substrates, which are more prone to oxidation reactions, such as amino groups.[32] However, the active species of the oxidation reactions have never been detected nor isolated yet due to its instability, and the artificial models also have never been reported. Due to the lack of information on the structure of the active species, the mechanism of the oxidation reactions by tetrahydrobiopterin-dependent hydroxylases has not been well elucidated in spite of intensive efforts,[33] and applications of pterins to oxidation reactions have yet to be achieved.

Based on efforts to shed light on the mechanism of substrate oxidation performed by tetrahydropterin-dependent hydroxylases in nature, it is revealed that the tetrahydropterin at the vicinity of an iron center directly reacts with a dioxygen molecule at the 4a-position to form 4a-hydroperoxy-dihydropterin (Figure 1-5).[33] However, the subsequent reaction of the obtained 4a-hydroperoxydihydropterin remains controversial, and there are three hypotheses (Figure 1-5): (1) 4a-hydroperoxy-dihydropterin directly reacts with an organic substrate to give an alcohol as the product and 4a-hydroxydihydropterin,[34] (2) 4a-hydroperoxy-dihydropterin reacts with the iron center to form the pterin-OO-iron complex, and then, the iron-peroxo species oxidizes substrates,[32] and (3) the iron-peroxo species are converted to iron(IV)-oxo species as active species,[35] which are regarded as important oxidants in biological systems as mentioned in the next section of this thesis.

1–4 Proton-Coupled Electron Transfer (PCET)

As mentioned above, various oxidation enzymes oxidize organic substrates in biological systems; *i.e.* the enzymes can perform the oxidation reactions at a body temperature under mild conditions in spite of low reactivity of the C–H bonds in organic substrates. In fact, oxidation of C–H bonds of organic compounds is very difficult to be achieved in artificial systems due to their high oxidation potentials (> 2 V vs SCE)[36] and large bond-dissociation energies (BDE). To oxidize organic substrates sufficiently under mild conditions, the oxidation enzymes in biological systems adopt PCET as an energetically feasible pathway.[37] In PCET reactions, the oxidants obtain not only electron(s) but also proton(s) from substrates to give a neutral radical product. The thermal stabilities of the products give positive driving forces in the oxidation reactions to make it possible to promote the reactions in spite of the high oxidation potentials and large BDEs of organic substrates. To learn oxidation of organic substrates from biological systems, PCET reactions have been intensively investigated.[38-51]

In both natural and artificial systems, high-valent metal-oxo species such as compound I in cytochrome P450s are regarded as one of the most powerful oxidants, which oxidize C-H bonds of aliphatic substrates through a PCET mechanism. In the formation process of compound I, the iron(II)-porphyrin react with O_2 to form iron(III)-porphyrin-$O_2^{\bullet-}$ species, and then, the iron(III)-porphyrin-$O_2^{\bullet-}$ receives one electron and one proton to give an iron(III)-porphyrin-OOH^- species through a PCET mechanism. The iron(III)-porphyrin-OOH^- species subsequently accepts one proton and releases a water molecule and the metal center formally loses two electrons to give compound I (Figure 1-6). Compound I in the catalytic cycle of cytochrome P450s mainly oxidizes C-H bonds of organic substrates to give alcohols, and also oxidizes C=C bonds including that of benzene to give epoxide species (Figure 1-6).[1] Due to its splendid oxidation reactivity to oxidize even benzene, compound I has attracted considerable attention, and the mechanistic insights into the PCET

oxidation of C-H bonds have been intensively investigated with use of high-valent metal-oxo complexes.[43-51] In PCET oxidation reactions, both of basicity and electron-acceptability of oxidants are important; because PCET oxidants receive not only electron(s) but also proton(s) from substrates. However, determination of basicity and electron-acceptability of high-valent metal-oxo species are generally difficult. The lack of knowledge on such characteristics of oxidants interrupts entire understanding of PCET chemistry in C-H oxidation reactions, especially in correlation among electron- and proton-acceptability and reactivity of oxidants.

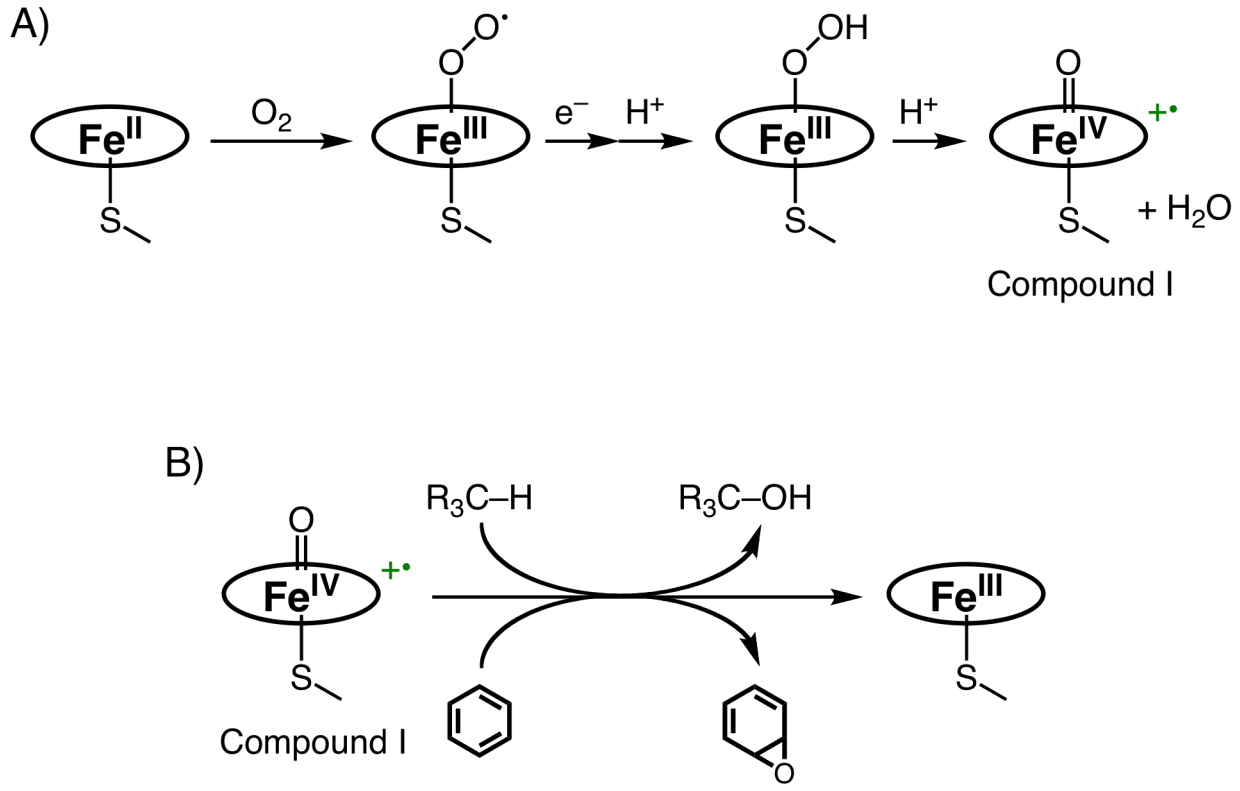

Figure 1-6. Formation process of compound I (A) and substrate oxidation with the compound I in nature (B).[1]

1–5 Ruthenium(II)-Polypyridyl Units as Platforms of Heteroaromatic Coenzymes

As mentioned above, to explore the reactivity of heteroaromatic coenzymes, achievement of reversible redox behaviors outside of enzymatic environments are very important. However, the heteroaromatic coenzymes generally form unstable species upon the redox processes *in vitro*, as expected for organic molecules. However, the problems on the reduction of stable fully-oxidized forms of heteroaromatic coenzymes to afford unstable species can be solved by coordination of the coenzymes to transition-metal ions. In transition-metal-coenzyme complexes, the positive charge of the coordinated metal center can exert higher electron-acceptability on the coordinating coenzyme, and resultantly suppress decomposition of the unstable reduced coenzymes. The coordination to a transition-metal center also can afford new functions to coenzymes, such as photochromic behaviors[52] and oxidation abilities of organic substrates through a PCET mechanism.[53] Along this line, many transition-metal complexes of flavin,[54, 55] alloxazine,[56] and pterin[57] have been synthesized and redox behaviors of the complexes have been well investigated.

Kojima and coworkers also have reported the redox behaviors of ruthenium(II)-TPA-heteroaromatic

coenzyme complexes; for example, a ruthenium-TPA complex having deprotonated *N*,*N*-dimethyl-6,7-dimethylpterin (dmdmp) as a ligand showed a reversible reduction behavior of the pterin ligand, which allowed detailed characterization of $1e^-$-reduced pterin species.[58] Such a $1e^-$-reduced species is hard to be obtained and handled with use of free pterin molecules, since the free pterin molecules exhibit irreversible redox behavior.[58] In addition, the ruthenium(III)-TPA-pterin complex, formed with oxidation of the corresponding ruthenium(II) complex by an Fe^{III} complex as an oxidant, showed substrate oxidation reactivity through a PCET mechanism.[53] For example, the ruthenium(III)-pterin complex caught phenols at the amino group of the deprotonated 6,7-dimethylpterin (dmp) ligand through hydrogen bonding, and then, one electron and one proton were transferred from the phenol molecule to the pterin ligand and ruthenium center, respectively, to afford the corresponding phenoxyl radical (Figure 1-7A).[53]

A ruthenium(II)-TPA-complex of alloxazine, a derivative of flavin, has been also reported, in which the ruthenium(II) center is bound to the two nitrogen atoms of the alloxazine ligand.[59] The 1,10-coordination in the alloxazine complex allows the alloxazine ligand to behave as a hydrogen-bonding acceptor at the 2-O, 3-NH, and 4-O sites (Figure 7B). Upon addition of 2,6-bis(acetamido)pyridine into a solution of the ruthenium-TPA-alloxazine complex, a 1:1 adduct was formed as confirmed by spectroscopic observations and X-ray crystallographic analysis.[59] The adduct formation caused a positive shift of the redox potentials of the alloxazine ligand and also induced changes in the electronic structure of the $1e^-$-reduced species.[59] The ruthenium(II)-TPA-pterin complex also forms a 1:1 adduct with guanine and thymine through hydrogen bonding. In the case of guanine, the ruthenium(II)-bound $dmdmp^-$ ligand forms three-point complementary hydrogen-bonding adduct to exert a positive shift of the reduction potential of the pterin ligand by 300 mV.[60]

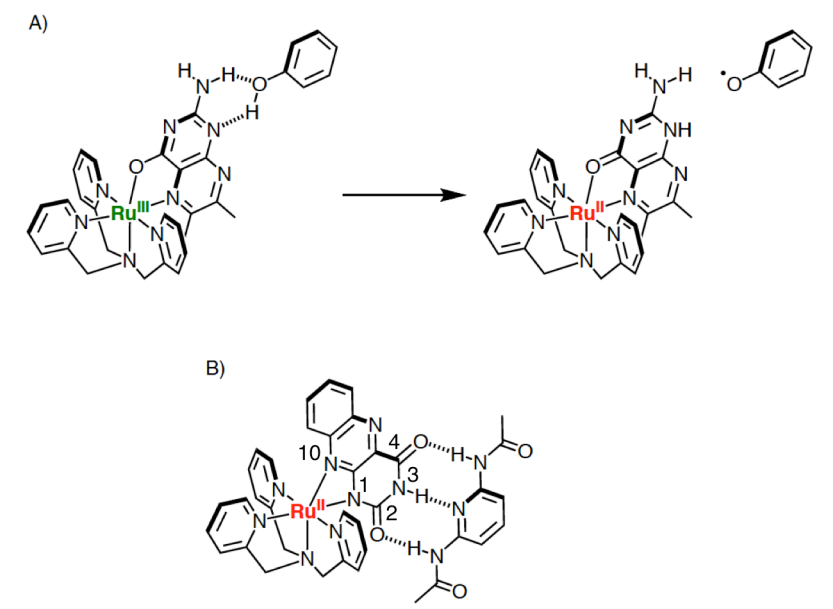

Figure 1-7. Functions of coenzymes derived from coordination to a ruthenium-TPA unit: (A) PCET oxidation of phenol,[53] (B) hydorogen bonding of a ruthenium-TPA-alloxazine complex with 2,6-bis(acetamido)pyridine.[59]

1–6 Purpose of This Research

As mentioned above, developments of novel functions with ruthenium-heteroatomatic coenzyme

complexes such as substrate oxidation have been successful so far,[46a,59,60] and thus, the author expected that the ruthenium-polypyridyl unit was a useful platform also for researches on PQQ. Additionally, the formation and detection of pterin-OO-metal species, which is a plausible candidate for the active species in pterin-dependent hydroxylases, has yet to be achieved in spite of its importance for gaining mechanistic insights into substrate oxidation reactions performed by pterin-dependent oxidation enzymes in nature. Therefore, the author has synthesized PQQ- and pterin-complexes, coordinating to ruthenium- or rhodium-polypyridyl units, and investigated their redox properties for development of their novel functions on the basis of detailed characterization of those complexes using spectroscopic, electrochemical, and crystallographic methods.

In Chapter 2, the author describes synthesis and characterization of two ruthenium-silver-terpy-PQQ complexes; their properties have been investigated in detail to clarify the electronic effect of coordination of PQQ to transition-metal ions.

In Chapter 3, synthesis and characterization of ruthenium(II)- and rhodium(III)-pterin complexes toward the formation of a pterin-OO-metal species as the final goal. MeBPA (= *N*-methyl-*N*,*N*-bis(pyridylmethyl)amine) and TPMOM (= tris(2-pyridyl)-methoxy-methane) were employed herein as tridentate ligands to provide a vacant coordination site at the metal centers for coordination of the terminal oxygen of a pterin-OO^- ligand. Since ruthenium(II) and rhodium(III) ions have similar electronic structures of d^6-low spin state, and thus, formation of stable complexes with pterin can be expected.

In Chapter 4, the author describes detailed mechanistic insights into C-H oxidation of organic substrates by two ruthenium(III)-pterin complexes on the basis of kinetic analysis. The author focuses on the impact of the electron-acceptability of the ruthenium center and the proton-acceptability of the pterin ligand on the PCET oxidation of C-H bonds. Herein, the author has clarified that the electron- and proton-acceptability of the ruthenium(III)-pterin complexes control the arrangements of the oxidants and the substrates in the transition states of the oxidation reactions.

Reference and Notes

(1) (a) Denisov, I. G.; Makris, T. M.; Sligar, S. G.; Schlichting, I. *Chem*. *Rev*. **2005**, *105*, 2253. (b) Bernauer, U.; Vieth, B.; Ellrich, R.; Heinrich-Hirsch, B.; Jänig, G.-R.; Gundert-Remy, U. *Arch*. *Toxicol*. **1999**, *73*, 189.

(2) (a) Dix, T. A.; Bollag, G. E.; Domanico, P. L.; Benkovic, S. J. *Biochemistry* **1985**, *24*, 2955. (b) Erlandsen, H.; Bjørgo, E.; Flatmark, T.; Stevens, R. C. *Biochemistry* **2000**, *39*, 2208. (c) Solomon, E. I.; Brunold, T. C.; Davis, M. I.; Kemsley, J. N.; Lee, S.-K.; Lehnert, N.; Neese, F.; Skulan, A. J.; Yang, Y.-S.; Zhou, J. *Chem*. *Rev*. **2000**, *100*, 235.

(3) (a) Huijbers, M. M. E.; Montersino, S.; Westphal, A. H.; Tischler, D.; van Berkel, W. J. H. *Arch*. *Bio*. *Biophys*. **2014**, *544*, 2. (b) Massey, V. *J*. *Biol*. *Chem*. **1994**, *269*, 22459. (c) Branchaund, B. P.; Walsh, C. T. *J*. *Am*. *Chem*. *Soc*. **1985**, *107*, 2153. (d) Yachnin, B. J.; Sprules, T.; McEvoy, M. B.; Lau, P. C. K.; Berghuis, A. M. *J*. *Am*. *Chem*. *Soc*. **2012**, *134*, 7788.

(4) Frimer, A. A. *The Chemistry of Functional Group, Peroxides*; Patai, S., Eds.; John Wiley & Sons: New York, 1983; Chapter 7.

(5) Anderson, R. F. in "Flavins and Flavoproteins"; Massey, V.; Williams, C. H., Jr. Eds; Elsevier/North-Holland: New York, 1982; pp. 287-283.

(6) Iida, H.; Imada, Y.; Murahashi, S.-I. *Org*. *Biomol*. *Chem*. **2015**, *13*, 7599.

(7) (a) Murahashi, S.-I.; Oda, T.; Masui, Y. *J*. *Am*. *Chem*. *Soc*. **1989**, *111*, 5002. (b) Bergstad, K.; Bäckvall, J.-E. *J*. *Org*. *Chem*. **1998**, *63*, 6650. (c) Lindén, A. A.; Krüger, L.; Bäckvall, J.-E. *J*. *Org*. *Chem*. **2003**, *68*, 5890. (d) Bergstad, K.; Jonsson, S. Y.; Bäckvall, J.-E. *J*. *Am*. *Chem*. *Soc*. **1999**, *121*, 10424. (e) Jonsson, S. Y.; Färnegårdh, K.; Bäckvall, J.-E. *J*. *Am*. *Chem*. *Soc*. **2001**, *123*, 1365. (f) Jonsson, S. Y.; Adolfsson, H.; Bäckvall, J.-E. *Org*. *Lett*. **2001**, *3*, 3463. (g) Piera, J.; Bäckvall, J.-E. *Angew*. *Chem*., *Int*. *Ed*. **2008**, *47*, 3506. (h) Li, W.-S.; Zhang N.; Sayre, L. M.; *Tetrahedron* **2001**, *57*, 4507. (i) Marsh, B. J.; Carbery, D. R. *Tetrahedron Lett*. **2010**, *51*, 2362. (j) Minidis, A. B. E.; Bäckvall, J.-E. *Chem*.*–Eur*. *J*. **2001**, *7*, 297. (k) Lindén, A. A.; Hermanns, N.; Ott, S.; Krüger, L.; Bäckvall, J.-E. *Chem*.*–Eur*. *J*. **2005**, *11*, 112. (l) Ménová, P.; Cibulka, R. *J*. *Mol*. *Catal*. *A: Chem*. **2012**, *363-364*, 362. (m) Ménová, P.; Dvořáková, H.; Eigner, V.; Ludvík, J.; Cibulka, R. *Adv*. *Synth*. *Catal*. **2013**, *355*, 3451. (n) Lindén, A. A.; Johansson, M.; Hermanns, A. A.; Bäckvall, J.-E. *J*. *Org*. *Chem*. **2006**, *71*, 3849. (o) Baxová, L.; Cibulka, R.; Hampl, F. *J*. *Mol*. *Catal*. *A: Chem*. **2007**, *277*, 53. (p) Zelenka, J.; Hartman, T.; Klímová, K.; Hampl, F.; Cibulka, R. *ChemCatChem*, **2014**, *6*, 2843.

(8) (a) Polyak, I.; Reetz, M. T.; Thiel, W. *J*. *Am*. *Chem*. *Soc*. **2012**, *134*, 2732. (b) Reetz, M. T.; Wu, S. *J*. *Am*. *Chem*. *Soc*. **2009**, *131*, 15424. (c) ten Brink, G. J.; Arends I. W. C. E.; Sheldon, R. A. *Chem*. *Rev*. **2004**, *104*, 4105. (d) Mazzini, C.; Lebreton, J.; Furstoss, R. *J*. *Org*. *Chem*. **1996**, *61*, 8. (e) Chen, S.; Hossain, M. S.; Foss, F. W., Jr. *Org*. *Lett*. **2012**, *14*, 2806. (f) Murray, A. T.; Matton, P.; Fairhurst, N. W. G.; John, M. P.; Carbery, D. R. *Org*. *Lett*. **2012**, *14*, 3656. (g) Shinkai, S.; Yamaguchi, T.; Manabe, O.; Toda, F. *J*. *Chem*. *Soc*., *Chem*. *Commun*. **1988**, 1399. (h) Žurek, J.; Cibulka, R.; Dvořáková, H.; Svoboda, J. *Tetrahedron Lett*. **2010**, *51*, 1083. (i) Jurok, R.; Cibulka, R.; Dvořáková, H.; Hampl, F.; Hodačová, J. *Eur*. *J*. *Org*. *Chem*. **2010**, 5217. (j) Jurok, R.; Hodačová, J.; Eigner, V.; Dvořáková, H.; Setnička V.; Cibulka, R. *Eur*. *J*. *Org*. *Chem*. **2013**, 7724. (k) Mojr, V.; Herzig, V.; Buděšínský, M.; Cibulka, R.; Kraus, T. *Chem*. *Commun*. **2010**, *46*, 7599. (l) Mojr, V.; Buděšínský, M.; Cibulka, R.; Kraus, T. *Org*. *Biomol*. *Chem*. **2011**, *9*, 7318. (m) Hartman,

T.; Herzig, V.; Buděšínský, M.; Jindřich, J.; Cibulka, R.; Kraus, T. *Tetrahedron Asymm.* **2012**, *23*, 1571. (n) Iida, H.; Iwahana, S.; Mizoguchi, T.; Yashima, E. *J. Am. Chem. Soc.* **2012**, *134*, 15103. (o) Murahashi, S.-I.; Ono, S.; Imada, Y. *Angew. Chem., Int. Ed.* **2002**, *41*, 2366.

(9) (a) Imada, Y.; Iida, H.; Murahashi, S.-I.; Naota, T. *Angew. Chem., Int. Ed.*, **2005**, *44*, 1704. (b) Murahashi, S.-I.; Oda, Y.; Naota, T. *Tetrahedron Lett.* **1992**, *33*, 7557. (c) Chen, S.; Foss, F. W., Jr. *Org. Lett.* **2012**, *14*, 5150. (d) Imada, Y.; Iida, H.; Ono, S.; Murahashi, S.-I. *J. Am. Chem. Soc.* **2003**, *125*, 2868. (e) Imada, Y.; Iida, H.; Ono, S.; Masui, Y.; Murahashi, S.-I. *Chem.–Asian J.* **2006**, *1*, 136. (f) Imada, Y.; Kitagawa, T.; Wang, H.-K.; Komiya, N.; Naota, T. *Tetrahedron Lett*, **2013**, *54*, 621. (g) Murahashi, S.-I.; Zhang, D.; Iida, H.; Miyawaki, T.; Uenaka, M.; Murano, K.; Meguro, K. *Chem. Commun.* **2014**, *50*, 10295. (h) Yano, Y.; Nakazato, M.; Ohya, E. *J. Chem. Soc., Perkin Trans. 2* **1985**, 77. (i) Kotoučová, H.; Strnadová, I.; Kovandová, M.; Chudoba, J.; Dvořáková, H.; Cibulka, R. *Org. Biomol. Chem.* **2014**, *12*, 2137. (j) Imada, Y.; Iida, H.; Naota, T. *J. Am. Chem. Soc.* **2005**, *127*, 14544. (k) Imada, Y.; Kitagawa, T.; Ohno, T.; Iida, H.; Naota, T. *Org. Lett.* **2010**, *12*, 32. (l) Imada, Y.; Iida, H.; Kitagawa, T.; Naota, T. *Chem.–Eur. J.* **2011**, *17*, 5908. (m) Smit, C.; Fraaije, M. W.; Minnaard, A. J. *J. Org. Chem.* **2008**, *73*, 9482. (n) Teichert, J. F.; den Hartog, T.; Hanstein, M.; Smit, C.; ter Horst, B.; Hernandez-Olmos, V.; Feringa, B. L.; Minnaard, A. J. *ACS Catal.* **2011**, *1*, 309. (o) Marsh, B. J.; Heath, E. L.; Carbery, D. R. *Chem. Commun.* **2011**, *47*, 280. (p) Imada, Y.; Osaki, M.; Noguchi, M.; Maeda, T.; Fujiki, M.; Kawamorita, S.; Komiya, N.; Naota, T. *ChemCatChem* **2015**, *7*, 99.

(10) (a) Chen, S.; Hossain, M. S.; Foss, F. W., Jr. *ACS Sustainable. Chem. Eng.* **2013**, *1*, 1045. (b) Shinkai, S.; Yamashita, T.; Kusano, Y.; Manabe, O. *J. Org. Chem.* **1980**, *45*, 4947. (c) Yano, Y.; Hoshino, Y.; Tagaki, W. *Chem. Lett.* **1980**, *9*, 749. (d) Iwahana, S.; Iida, H.; Yashima, E. *Chem.–Eur. J.* **2011**, *17*, 8009. (e) Fukuzumi, S.; Kuroda, S.; Tanaka, T. *J. Am. Chem. Soc.* **1985**, *107*, 3020. (f) Fukuzumi, S.; Tanii, K.; Tanaka, T. *J. Chem. Soc., Chem. Commun.* **1989**, 816. (g) Fukuzumi, S.; Yasui, K.; Suenobu, T.; Ohkubo, K.; Fujitsuka, O.; Ito, O. *J. Phys. Chem. A* **2001**, *105*, 10501. (h) Yasuda, M.; Nakai, T.; Kawahito, Y.; Shiragami, T. *Bull. Chem. Soc. Jpn.* **2003**, *76*, 601. (i) Svoboda, J.; Schmaderer, H.; König, B. *Chem.–Eur. J.* **2008**, *14*, 1854. (j) Schmaderer, H.; Hilgers, P.; Lechner, A.; König, B. *Adv. Synth. Catal.* **2009**, *351*, 163. (k) Daďová, J.; Kümmel, S.; Feldmeier, C.; Cibulková, J.; Pažout, R.; Maixner, J.; Gschwind, R. M.; König, B.; Cibulka, R. *Chem.–Eur. J.* **2013**, *19*, 1066. (l) Megerle, U.; Wenninger, M.; Kutta, R.-J.; Lechner, R.-J.; König, B.; Dick, B.; Riedle, E. *Phys. Chem. Chem. Phys.* **2011**, *13*, 8869. (m) Celdmeier, C.; Bartling, H.; Margerl, K.; Gschwind, R. M. *Angew. Chem., Int. Ed.* **2015**, *54*, 1347. (o) Lechner, R.; König, B. *Synthesis* **2010**, 1712.

(11) (a) Mirzakulova, E.; Khatmullin, R.; Walpita, J.; Corrigan, T.; Vargas-Barbosa, N. M.; Vyas, S.; Oottikkal, S.; Manzer, S. F.; Hadad, C. M.; Glusac, K. D. *Nat. Chem.* **2012**, *4*, 794. (b) Pouy, M. J.; Milczek, E. M.; Figg, T. M.; Otten, B. M.; Prince, B. M.; Gunnoe, T. B.; Cundari, T. R.; Groves, J. T. *J. Am. Chem. Soc.* **2012**, *134*, 12920. (c) Šturala, J.; Boháčová, S.; Chudoba, J.; Metelková, R.; Cibulka, R. *J. Org. Chem.* **2015**, *80*, 2676.

(12) (a) Anthony, C. *Biochem. J.* **1996**, *320*, 697. (b) Davidson, V. L. *Arch. Biochem. Biophys.* **2004**, *428*, 32. (c) Oubrie, A.; Rozeboom, H. J.; Kalk, K. H.; Olsthoorn, A. J. J.; Duine, J. A.; Dijkstra, B. W. *EMBO J.* **1999**, *18*, 5187. (d) Govindaraj, S.; Einstein, E.; Jones, L. H.; Sanders-Loehr, J.; Chistoserdov, A. Y.;

Davidson, V. L.; Edwards, S. L. *J. Bacteriol*. **1994**, *176,* 2922. (e) Takagi, K.; Torimura, M.; Kawaguchi, K.; Kano, K.; Ikeda, T. *Biochemistry* **1999**, *38*, 6935. (f) Satoh, A.; Kim, J.-K.; Miyahara, I.; Devreese, B.; Vandenberghe, I.; Hacisalihoglu, A.; Okajima, T.; Kuroda, S.; Adachi, O.; Duine, J. A.; Beeumen, J. V.; Tanizawa, K.; Hirotsu, K. *J. Biol. Chem*. **2002**, *277*, 2830. (g) Chang, C. M.; Klema, V. J.; Johnson, B. J.; Mure, M.; Klinman, J. P.; Wilmot, C. M. *Biochemistry* **2010**, *49*, 2540. (h) Rucker, R. B.; Kosonen, T.; Clegg, M. S.; Mitchel, A. E.; Rucker, B. R.; Uriu-Hare, J. Y.; Keen, C. L. *Am. J. Clin. Nutr*. **1998**, *67*, 996S. (i) Oubrie, A.; Dijkstra, B. W. *Protein Science* **2000**, *9*, 1265.

(13) Hauge, J. G. *J. Biol. Chem*. **1964**, *239*, 3630.

(14) (a) Matsushita, K.; Toyama, H.; Yamada, M.; Adachi, O. *Appl. Microbiol. Biotechnol*. **2002**, *58*, 13. (b) Ge, X.; Wang, W.; Du, B.; Wang, J.; Xiong, X.; Zhang, W. *J. Basic Microbilo*. **2015**, *312*, 323.

(15) (a) Xia, Z.-X.; Dai, W.-W.; Xiong, J.-P.; Hao, Z.-P. *J. Biol. Chem*. **1992**, *267*, 22289. (b) White, S.; Boyd, G.; Mathews, F. C.; Xia, Z.-X.; Dai, Z.-Z.; Zhang. Y.-F.; Davidson, V. L. *Biochemistry* **1993**, *32*, 12955. (c) Xia, Z.-X.; Dai, W.-W.; Zhang, Y.-F.; White, S. A.; Boyd, G. D.; Mathews, F. S. *J. Mol. Biol*. **1996**, *259*, 480.

(16) (a) Anthony, C.; Ghosh, M.; Blake, C. C. F. *Biochem. J*. **1994**, *304*, 665. (b) Anthony, C.; Williams, P. *Biochim. Biophys. Acta* **2003**, *1647*, 18.

(17) (a) Ikeda, T.; Kobayashi, D.; Matsushita, F. *J. Electroanal. Chem*. **1993**, *361*, 221. (b) D'Costa, E. J.; Higgins, I. J.; Turner, A. P. F. *Biosensor* **1986**, *2*, 71. (c) Ikebukuro, K.; Saito, Y.; Igarashi, S.; Sode, K. *Electrochemisry* **2003**, *71*, 490. (d) Ikeda, T.; Kano, K. *Biochim. Biophys. Acta* **2003**, *1647*, 121. (e) Tkac, J.; Svitel, J.; Vostiar, I.; Navratil, M.; Gemeiner, P. *Bioelectrochemistry* **2009**, *76*, 53. (f) Niculescu, M.; Erichsen, T.; Sukharev, V.; Kerenyi, Z.; Csöregi, E.; Schuhmann, W. *Anal. Chim. Acta* **2002**, *463*, 39. (g) Kamitaka, Y.; Tsujimura, S.; Setoyama, N.; Kajino, T.; Kano, K. *Phys. Chem. Chem. Phys.* **2007**, *9*, 1793. (h) Yakushi, T.; Matsushita, K. *Appl. Microbiol. Biotechnol.* **2010**, *86*, 1257.

(18) Salisbury, S. A.; Forrest, H. S.; Cruse, W. B. T.; Kennard, O. *Nature* **1979**, *280*, 843.

(19) (a) de Beer, R.; van Ormondt, D.; van Ast, M. A.; Banen, R.; Duine, J. A.; Frank, J. *J. Chem. Phys*. **1979**, *70*, 4491. (b) Duine, J. A.; Frank, J. *Biochem. J*. **1980**, *187*, 221.

(20) Corey, E. J.; Tramontano, A. *J. Am. Chem. Soc*. **1981**, *103*, 5599.

(21) (a) Ohshiro, Y.; Itoh, S.; Kurokawa, K.; Kato, J.; Hirano, T.; Agawa, T. *Tetrahedron Lett*. **1983**, *24*, 3465. (b) Itoh, S.; Kato, N.; Ohshiro, Y.; Agawa, T. *Tetrahedron Lett*. **1984**, *25*, 4753. (c) Itoh, S.; Kato, N.; Mure, M.; Ohshiro, Y. *Bull. Chem. Soc. Jpn*. **1987**, *60*, 420. (d) Itoh, S.; Mure, M.; Ohshiro, Y. *J. Chem. Soc., Chem. Commun*. **1987**, 1580. (e) Rodriguez, E. J.; Bruice, T. C. *J. Am. Chem. Soc*. **1989**, *111*, 7947. (f) Itoh, S.; Mure, M.; Ogino, M.; Ohshiro, Y. *J. Org. Chem*. **1991**, *56*, 6857. (g) Itoh, S.; Kawakami, H.; Fukuzumi, S. *J. Am. Chem. Soc*. **1997**, *119*, 439. (h) Itoh, S.; Kawakami, H.; Fukuzumi, S. *Biochemistry* **1998**, *37*, 6562. (i) Itoh, S.; Kawakami, H.; Fukuzumi, S. *J. Mol. Catal. B: Enzymatic* **2000**, *8*, 85. (j) Itoh, S.; Kawakami, H.; Fukuzumi, S. *J. Am. Chem. Soc*. **1998**, *120*, 7271. (k) Fukuzumi, S.; Itoh, S.; Komori, T.; Suenobu, T.; Ishida, A.; Fujitsuka, M.; Ito, O. *J. Am. Chem. Soc*. **2000**, *122*, 8435.

(22) Evans, D. H. *Encyclopedia of Electrochemistry of the Elements, Organic Selection*; Bard, A. J.; Lund, H., Eds.; Marcel Dekker: New York, 1987; Chapter XII–1 and references cited therein.

(23) (a) Blake, C. C. F.; Ghosh, M.; Harlos, K.; Avezoux, A.; Anthony, C. *Nat. Struct. Biol.* **1994**, *1*, 102. (b)

Cozier, G. E.; Giles, I. G.; Anthony, C. *Biochem. J.* **1995**, *308*, 375. (c) Ghosh, M.; Anthony, C.; Harlos, K.; Goodwin, M. G.; Blake, C. *Structure* **1995**, *3*, 177.

(24) Leopoldini, M.; Ruso, N.; Toscano, M. *Chem.–Eur. J.* **2007**, *13*, 2109.

(25) Zing, Y.-J.; Xia, Z.-X.; Chen, Z.-W.; Mathews, F. S.; Bruice, T. C. *Proc. Natl. Acad. Sci. USA* **2001**, *98*, 432.

(26) Reddy, Y. S.; Bruice, T. C. *J. Am. Chem. Soc.* **2003**, *125*, 8141.

(27) (a) Suzuki, S.; Sakurai, T.; Itoh, S.; Ohshiro, Y. *Chem. Lett.* **1988**, 777. (b) Suzuki, S.; Sakurai, T.; Itoh, S.; Ohshiro, T. *Inorg. Chem.* **1988**, *27*, 591. (c) Nakamura, N.; Kohzuma, T.; Kuma, H.; Suzuki, S. *Inorg. Chem.* **1994**, *33*, 1594.

(28) Wanner, M.; Sixt, T. Klinkhammer, K.-W.; Kaim, W. *Inorg. Chem.* **1999**, *38*, 2753.

(29) McKinney, J.; Teigen, K.; Frøystein, N. Å.; Salaün, C.; Knappskog, P. M.; Haavik, J.; Martínez, A. *Biochemistry* **2001**, *40*, 15591.

(30) Andersen, O. A.; Flatmark, T.; Hough, E. *J. Mol. Biol.* **2001**, *314*, 279.

(31) Haavik, J.; Toska, K. *Mol. Neurobiol.* **1998**, *16*, 285.

(32) (a) Dix, T. A.; Bollag, G. E.; Domanico, P. L.; Benkovic, S. J. *Biochemistry* **1985**, *24*, 2955. (b) Benkovic, S.; Wallick, D.; Bloom, L.; Gaffney, B. J.; Domanico, P.; Dix, T.; Pember, S. *Biochem. Soc. Trans.* **1985**, *13*, 436. (c) Lazarus, R. A.; Wallick, D. E.; Dietrich, R. F.; Gottschall, D. W.; Benkovic, S. J.; Gaffney, B. J.; Shiman, R. *Fed. Proc., Fed. Am. Soc. Exp. Biol.* **1982**, 41, 2605.

(33) Kappock T. J.; Caradonna, J. P. *Chem. Rev.* **1996**, *96*, 2659.

(34) Such a coenzyme-OOH species is also proposed as the active species of oxidation reactions performed by flavoproteins. See ref. 31 and Entsch, B.; Ballou, D. P.; Massey, V. *J. Biol. Chem.* **1976**, *251*, 2550.

(35) Dix, T. A.; Benkovic, S. J. *Acc. Chem. Res.* **1981**, *21*, 101.

(36) Warren, J. J.; Tronic, T. A.; Mayer, J. M. *Chem. Rev.* **2010**, *110*, 6961.

(37) Huynh, M. H. V.; Meyer, T. J. *Chem. Rev.* **2007**, *107*, 5004.

(38) (a) Reece, S. Y.; Nocera, D. G. *Annu. Rev. Biochem.* **2009**, *78*, 673. (b) Jackson, J. A.; Mussell, R. D.; Nocera, D. G.; *Inorg. Chem.* **1993**, *32*, 4643. (c) Rosenthal, J.; Luckett, T. D.; Hodgkiss, J. M.; Nocera, D. G. *J. Am. Chem. Soc.* **2006**, *128*, 6546. (d) Irebo, T.; Reece, S. Y.; Sjödin, M.; Nocera, D. G.; Hammarström, L. *J. Am. Chem. Soc.* **2007**, *129*, 15462.

(39) (a) Du Bois, J.; Mizoguchi, T. J.; Lippard, S. J. *Coord. Chem. Rev.* **2000**, *200-202*, 443. (b) Choi, S.-Y.; Eaton, P. E.; Hollenberg, P. F.; Liu, K. E.; Lippard, S. J.; Newcomb, M.; Putt, D. A.; Upadhyaya, S. P.; Xiong, Y. *J. Am. Chem. Soc.* **1996**, *118*, 6547. (c) LeCloux, D. D.; Barrios, A. M.; Lippard, S. J. *Bioorg. Med. Chem.* **1999**, *7*, 763. (d) Brandstetter, H.; Whittington, D. A.; Lippard, S. J.; Frederick, C. A. *Chem. Biol.* **1999**, *6*, 441. (e) Yoon, S.; Lippard, S. J. *Inorg. Chem.* **2003**, *42*, 8606. (f) Kuzelka, J.; Mukhopadhyay, S.; Spingler, B.; Lippard, S. J. *Inorg. Chem.* **2003**, *42*, 6447. (g) Moreira, R. F.; Tshuva, E. Y.; Lippard, S. J. *Inorg. Chem.* **2004**, *43*, 4427. (h) Beauvais, L. G.; Lippard S. J. *J. Am. Chem. Soc.* **2005**, *127*, 7370. (i) Yoon, S.; Lippard, S. J. *Inorg. Chem.* **2006**, *45*, 5438. (j) Kim, Y.; Feng, X.; Lippard, S. J. *Inorg. Chem.* **2007**, *46*, 6099. (k) Newcomb, M.; Chandrasena, R. E. P.; Lansakara-P., D. S. P.; Kim, H.-Y.; Lippard, S. J.; Beauvais, L. G.; Murray, L. J.; Izzo, V.; Hollenberg, P. F.; Coon, M. J. *J. Org. Chem.* **2007**, *72*, 1121. (l) Zhao, M.; Helms, B.; Slonkina, E.; Friedle, S.; Lee, D.; DuBois, J.; Hedman, B.; Hodgson, K. O.; Fréchet, J. M. J.;

Lippard, S. J. *J. Am. Chem. Soc.* **2008**, *130*, 4352. (m) Behan, R. K.; Lippard, S. J. *Biochemistry* **2010**, *49*, 9679. (n) Tinberg, C. E.; Lippard, S. J. *Biochemistry* **2010**, *49*, 7902. (o) Majumdar, A.; Apfel, U.-P.; Jiang, Y.; Moënne-Loccoz, P.; Lippard, S. J. *Inorg. Chem.* **2014**, *53*, 167.

(40) (a) Que, L., Jr. *Acc. Chem. Res.* **2007**, *40*, 493. (b) Oloo, W. N.; Que, L., Jr. *Acc. Chem. Res.* **2015**, *48*, 2612. (c) Leising, R. A.; Brennan, B. A.; Que, L., Jr.; Fox, B. G.; Munck, E. *J. Am. Chem. Soc.* **1991**, *113*, 3988. (d) Leising, R. A.; Norman, R. E.; Que, L., Jr. *Inorg. Chem.* **1990**, *29*, 2553. (e) Leising, R. A.; Zang, Y.; Que, L., Jr. *J. Am. Chem. Soc.* **1991**, *113*, 8555. (f) Leising, R. A.; Kim, J.; Perez, M. A.; Que, L., Jr. *J. Am. Chem. Soc.* **1993**, *115*, 9524. (g) Chiou, Y.-M. *J. Am. Chem. Soc.* **1995**, *117*, 3999. (h) Kim, J.; Kim, C.; Harrison, R. G.; Wilkinson, E. C.; Que, L., Jr. *J. Mol. Catal. A: Chem.* **1997**, *117*, 83. (i) Roelfes, G.; Lubben, M.; Hage, R.; Que, L., Jr.; Feringa, B. L. *Chem.–Eur. J.* **2000**, *6*, 2152. (j) Chen, K.; Costas, M.; Kim, J.; Tipton, A. K.; Que, L., Jr. *J. Am. Chem. Soc.* **2002**, *124*, 3026. (k) Kaizer, J.; Klinker, E. J.; Oh, N. Y.; Rohde, J.-U.; Song, W. J.; Stubna, A.; Kim, J.; Münck, E.; Nam, W.; Que, L., Jr. *J. Am. Chem. Soc.* **2004**, *126*, 472. (l) Bassan, A.; Blomberg, M. R. A.; Siegbahn, P. E. M.; Que, L., Jr. *Chem.–Eur. J.* **2005**, *11*, 692. (m) Shan, X.; Que, L., Jr. *J. Inorg. Biochem.* **2006**, *100*, 421. (n) Mas-Ballesté, R.; Fujita, M.; Hemmila, C.; Que, L., Jr. *J. Mol. Catal. A: Chem.* **2006**, *251*, 49. (p) Mukherjee, A.; Martinho, M.; Bominaar, E. L.; Münck, E.; Que, L., Jr. *Angew. Chem., Int. Ed.* **2009**, *48*, 1780. (o) Makhlynets, O. V.; Das, P.; Taktak, S.; Flook, M.; Mas-Ballesté, R.; Rybak-Akimova, E. V.; Que, L., Jr. *Chem.–Eur. J.* **2009**, *15*, 13171. (p) England, J.; Martinho, M.; Farquhar, E. R.; Frisch, J. R.; Bominaar, E. L.; Münck, E.; Que, L., Jr. *Angew. Chem., Int. Ed.* **2009**, *48*, 3622. (q) Wang, D.; Farquhar, E. R.; Stubna, A.; Münck, E.; Que, L., Jr. *Nat. Chem.* **2009**, *1*, 145. (t) Wang, D.; Zhang, M.; Bühlmann, P.; Que, L., Jr. *J. Am. Chem. Soc.* **2010**, *132*, 7638. (r) Paria, S.; Que, L., Jr.; Paine, T. K. *Angew. Chem., Int. Ed.* **2011**, *50*, 11129. (s) Company, A.; Prat, I.; Frisch, J. R.; Mas-Ballestè, D. R.; Güell, M.; Juhàsz, G.; Ribas, X.; Münck, D. E.; Luis, J. M.; Que, L., Jr.; Costas, M. *Chem.–Eur. J.* **2011**, *17*, 1622. (t) McDonald, A. R.; Que, L., Jr. *Nat. Chem.* **2011**, *3*, 761. (u) Farquhar, E. R.; Emerson, J. P.; Koehntop, K. D.; Reynolds, M. F.; Trmčć M.; Que, L., Jr. *J. Biol. Inorg. Chem.* **2011**, *16*, 589. (v) Prat, I.; Company, A.; Postils, V.; Ribas, X.; Que, L., Jr.; Luis, J. M.; Costas M. *Chem.–Eur. J.* **2013**, *19*, 6724. (w) Xue, X.; Geng, C.; Ye, S.; Fiedler, A. T.; Neese, F.; Que, L., Jr. *Inorg. Chem.* **2013**, *52*, 3976. (x) Oloo, W. N.; Feng, Y.; Iyer, S.; Parmelee, S.; Xuea, G.; Que, L., Jr. *New J. Chem.* **2013**, *37*, 3411. (y) Iyer, S. R.; Javadi, M. M.; Feng, Y.; Hyun, M. Y.; Oloo, W. N.; Kimb, C.; Que, L., Jr. *Chem. Commun.* **2014**, *50*, 13777. (z) Kleespies, S. T.; Oloo, W. N.; Mukherjee, A.; Que, L., Jr. *Inorg. Chem.* **2015**, *54*, 5053.

(41) (a) Cox, D. D.; Que, L., Jr. *J. Am. Chem. Soc.* **1988**, *110*, 8085. (b) White, L. S.; Que, L., Jr. *J. Mol. Cat.* **1985**, *33*, 139. (c) White, L. S.; Hellman, E. J.; Que, L., Jr. *J. Org. Chem.* **1982**, *47*, 3766. (d) Lauffer, R. B.; Heistand II, R. H.; Que, L., Jr. *J. Am. Chem. Soc.* **1981**, *103*, 3947. (e) Paine, T. K.; Pariaa, S.; Que, L., Jr. *Chem. Commun.* **2010**, *46*, 1830. (f) Garcia-Bosch, I.; Company, A.; Frisch, J. R.; Torrent-Sucarrat, M.; Cardellach, M.; Gamba, I.; Güell, M.; Casella, L.; Que, L., Jr.; Ribas, X.; Luis, J. M.; Costas, M. *Angew. Chem., Int. Ed.* **2010**, *49*, 2406. (g) Pap, J. S.; Cranswick, M. A.; Balogh-Hergovich, É.; Baráth, G.; Giorgi, M.; Rohde, G. T.; Kaizer, J.; Speier, G.; Que, L., Jr. *Eur. J. Inorg. Chem.* **2013**, 3858.

(42) (a) Que, L., Jr.; Dong, Y. *Acc. Chem. Res.* **1996**, *29*, 190. (b) Kim, J.; Harrison, R. G.; Kim, C.; Que, L., Jr. *J. Am. Chem. Soc.* **1996**, *118*, 4373. (c) Oldenburg, P. D.; Feng, Y.; Pryjomska-Ray, I.; Ness, D.; Que, L.,

Jr. *J. Am. Chem. Soc.* **2010**, *132*, 17713. (d) Biswas, A. N.; Puri, M.; Meier, K. K.; Oloo, W. N.; Rohde, G. T.; Bominaar, E. L.; Münck, E.; Que, L., Jr. *J. Am. Chem. Soc.* **2015**, *137*, 2428.
(43) (a) Groves, J. T.; Nemo, T. E.; Myers, R. S. *J. Am. Chem. Soc.* **1979**, *101*, 1032. (b) Groves, J. T.; Haushalter, R. C.; Nakamura, M.; Nemo, T. E.; Evans, B. J. *J. Am. Chem. Soc.* **1981**, *103*, 2884. (c) Liu, W.; Groves, J. T. *Acc. Chem. Res.* **2015**, *48*, 1727. (d) Breslow, R.; Groves, J. T.; Olin, S. S. *Tetrahedron Lett.* **1966**, *7*, 4717. (e) Groves, J. T. *Tetrahedron Lett.* **1975**, *16*, 3113. (f) Groves, J. T.; der Puy, M. V. *J. Am. Chem. Soc.* **1975**, *97*, 7118. (g) Groves, J. T.; der Puy, M. V. *J. Am. Chem. Soc.* **1976**, *98*, 5290. (h) Groves, J. T; Kruper, W. J., Jr. *J. Am. Chem. Soc.* **1979**, *101*, 7613. (i) Groves, J. T.; Kruper, W. J., Jr.; Nemo, T. E.; Myers, R. S. *J. Mol. Cat.* **1980**, *7*, 169. (j) Groves, J. T.; Kruper, W. J., Jr.; Haushalter, R. C. *J. Am. Chem. Soc.* **1980**, *102*, 6375. (k) Groves, J. T.; Neumann, R. *J. Am. Chem. Soc.* **1989**, *111*, 2900. (l) Groves, J. T.; Gross, Z.; Stern, M. K. *Inorg. Chem.* **1994**, *33*, 5065. (m) Groves, J. T.; Bonchio, M.; Carofiglio, T.; Shalyaev, K. *J. Am. Chem. Soc.* **1996**, *118*, 8961. (n) Groves, J. T. *J. Porphyrins Phthalocyanines* **2000**, *4*, 350. (o) Brazeau, B. J.; Austin, R. N.; Tarr, C.; Groves, J. T.; Lipscomb, J. D. *J. Am. Chem. Soc.* **2001**, *123*, 11831. (p) Moe, L. A.; Hu, Z.; Deng, D.; Austin, R. N.; Groves, J. T.; Fox, B. G. *Biochemistry* **2004**, *43*, 15688. (q) Austin, R. N.; Deng, D.; Jiang, Y.; Luddy, K.; van Beilen, J. B.; de Montellano, P. R. O.; Groves, J. T. *Angew. Chem., Int. Ed.* **2006**, *45*, 8192. (r) Wang, C.; Shalyaev, K. V.; Bonchio, M.; Carofiglio, T.; Groves, J. T. *Inorg. Chem.* **2006**, *45*, 4769. (s) Chakrabarty, S.; Austin, R. N.; Deng, D.; Groves, J. T.; Lipscomb, J. D. *J. Am. Chem. Soc.* **2007**, *129*, 3514. (t) Bell, S. R.; Groves, J. T. *J. Am. Chem. Soc.* **2009**, *131*, 9640. (u) Liu, W.; Groves, J. T. *Angew. Chem., Int. Ed.* **2013**, *52,* 6024. (v) Konnick, M. M.; Hashiguchi, B. G.; Devarajan, D.; Boaz, N. C.; Gunnoe, T. B.; Groves, J. T.; Gunsalus, N.; Ess, D. F.; Periana, R. A. *Angew. Chem., Int. Ed.* **2014**, *53*, 10490. (w) Boaz, N. C.; Bell, S. R.; Groves, J. T. *J. Am. Chem. Soc.* **2015**, *137*, 2875.
(44) (a) Mayer, J. M. *Acc. Chem. Res.* **2011**, *44*, 36. (b) DuMez, D. D.; Mayer, J. M. *Inorg. Chem.* **1995**, *34*, 6396. (c) DuMez, D. D.; Mayer, J. M. *J. Am. Chem. Soc.* **1996**, *118*, 12416. (d) Brown, S. N.; Mayer, J. M. *J. Am. Chem. Soc.* **1996**, *118*, 12119. (e) Lockwood, M. A.; Blubaugh, T. J.; Collier, A. M.; Lovell, S.; Mayer, J. M. *Angew. Chem., Int. Ed.* **1999**, *38*, 226. (f) Lockwood, M. A.; Wang, K.; Mayer, J. M. *J. Am. Chem. Soc.* **1999**, *121*, 11894. (g) Roth, J. P.; Mayer, J. M. *Inorg. Chem.* **1999**, *38*, 2760. (h) Bennett, B. K.; Crevier, T. J.; DuMez, D.; Matano, Y.; McNeil, W. S.; Mayer, J. M. *J. Organomet. Chem.* **1999**, *591* 96. (i) Matano, Y.; Northcutt, T. O.; Brugman, J.; Bennett, B. K.; Lovell, S.; Mayer, J. M. *Organometallics* **2000**, *19*, 2781. (j) Bryant, J. R.; Taves, J. E.; Mayer, J. M. *Inorg. Chem.* **2002**, *41*, 2769. (k) Larsen, A. S.; Wang, K.; Lockwood, M. A.; Rice, G. L.; Won, T.-J.; Lovell, S.; Sadílek, M.; Tureček, F.; Mayer, J. M. *J. Am. Chem. Soc.* **2002**, *124,* 10112. (l) Bryant, J. R.; Mayer, J. M. *J. Am. Chem. Soc.* **2003**, *125*, 10351. (m) Matsuo, T.; Mayer, J. M. *Inorg. Chem.* **2005**, *44*, 2150. (n) Osako, T.; Watson, E. J.; Dehestani, A.; Bales, B. C.; Mayer, J. M. *Angew. Chem., Int. Ed.* **2006**, *45*, 7433. (o) Wu, A.; Masland, J.; Swartz, R. D.; Kaminsky, W.; Mayer, J. M. *Inorg. Chem.* **2007**, *46*, 11190. (p) Mader, E. A.; Davidson, E. R.; Mayer, J. M. *J. Am. Chem. Soc.* **2007**, *129*, 5153. (q) Mader, E. A.; Manner, V. W.; Markle, T. F.; Adam, W.; Franz, J. A.; Mayer, J. M. *J. Am. Chem. Soc.* **2009**, *131*, 4335. (r) Waidmann, C. R.; Zhou, X.; Tsai, E. A.; Kaminsky, W.; Hrovat, D. A.; Borden, W. T.; Mayer, J. M. *J. Am. Chem. Soc.* **2009**, *131*, 4729. (s) Dehestani, A.; Wu, A.; Hayoun, R.; Kaminsky, W.; Mayer, J. M. *Inorg. Chim. Acta* **2009**, *362*, 4534. (t) Waidmann, C. R.; DiPasquale, A. G.;

Mayer, J. M. *Inorg. Chem.* **2010**, *49*, 2383. (u) Schrauben, J. N.; Cattaneo, M.; Day, T. C.; Tenderholt, A. L.; Mayer, J. M. *J. Am. Chem. Soc.* **2012**, *134*, 16635.
(45) (a) Cook, G. K.; Mayer, J. M. *J. Am. Chem. Soc.* **1994**, *116*, 1855. (b) Cook, G. K.; Mayer, J. M. *J. Am. Chem. Soc.* **1995**, *117*, 7139. (c) Wang, K.; Mayer, J. M. *J. Org. Chem.* **1997**, *62*, 4248. (d) Wang, K.; Mayer, J. M. *J. Am. Chem. Soc.* **1997**, *119*, 1470. (e) Gardner, K. A.; Kuehnert, L. L.; Mayer, J. M. *Inorg. Chem.* **1997**, *36*, 2069. (f) Bales, B. C.; Brown, P.; Dehestani, A.; Mayer, J. M. *J. Am. Chem. Soc.* **2005**, *127*, 2832. (g) Mayer, J. M.; Mader, E. A.; Roth, J. P.; Bryant, J. R.; Matsuo, T.; Dehestania, A.; Bales, B. C.; Watson, E. J.; Osako, T.; Valliant-Saunders, K.; Lam, W. H.; Hrovat, D. A.; Bordena, W. T.; Davidsona, E. R. *J. Mol. Catal. A: Chem.* **2006**, *251*, 24. (h) Valliant-Saunders, K.; Gunn, E.; Shelton, G. R.; Hrovat, D. A.; Borden, W. T.; Mayer, J. M. *Inorg. Chem.* **2007**, *46*, 5212.
(46) (a) Rhile, I. J.; Mayer, J. M. *J. Am. Chem. Soc.* **2004**, *126*, 12718. (b) Bryant, J. R.; Matsuo, T.; Mayer, J. M. *Inorg. Chem.* **2004**, *43*, 1587. (c) Rhile, I. J.; Markle, T. F.; Nagao, H.; DiPasquale, A. G.; Lam, O. P.; Lockwood, M. A.; Rotter, K.; Mayer, J. M. *J. Am. Chem. Soc.* **2006**, *128*, 6075. (d) Markle, T. H.; Mayer, J. M. *Angew. Chem., Int. Ed.* **2008**, *47*, 738. (e) Markle, T. F.; Rhile, I. J.; Mayer, J. M. *J. Am. Chem. Soc.* **2011**, *133*, 17341. (f) Markle, T. F.; Tenderholt, A. L.; Mayer, J. M. *J. Phys. Chem. B* **2012**, *116*, 571.
(47) (a) Nam, W. *Acc. Chem. Res.* **2007**, *40*, 522. (b) Nam, W. *Acc. Chem. Res.* **2015**, *48*, 2415. (c) Nam, W.; Goh, Y. M.; Lee, Y. J.; Lim, M. H.; Kim, C. *Inorg. Chem.* **1999**, *38*, 3238. (d) Nam, W.; Kim, H. J.; Kim, S. H.; Ho, R. Y. N.; Valentine, J. S. *Inorg. Chem.* **1996**, *35*, 1045. (e) In, J.-H.; Park, S.-E.; Song, R.; Nam. W. *Inorg. Chim. Acta* **2003**, *343*, 373. (f) Oh, N. Y.; Suh, Y.; Park, M. J.; Seo, M. S.; Kim, J.; Nam, W. *Angew. Chem., Int. Ed.* **2005**, *44*, 4235. (g) Nehru, K.; Seo, M. S.; Kim, J.; Nam, W. *Inorg. Chem.* **2007**, *46*, 293. (h) de Visser, S. P.; Oh, K.; Han, A.-R.; Nam, W. *Inorg. Chem.* **2007**, *46*, 4632. (i) de Visser, S. P.; Nam, W. *J. Phys. Chem. A* **2008**, *112*, 12887. (j) Nehru, K.; Jang, Y.; Oh, S.; Dallemer, F.; Nam, W.; Kim, J. *Inorg. Chim. Acta* **2008**, *361*, 2557. (k) Yoon, J.; Wilson, S. A.; Jang, Y. K.; Seo, M. S.; Nehru, K.; Hedman, B.; Hodgson, K. O.; Bill, E.; Solomon, E. I.; Nam, W. *Angew. Chem., Int. Ed.* **2009**, *48*, 1257. (l) Arunkumar, C.; Lee, Y.-M.; Lee, J. Y.; Fukuzumi, S.; Nam, W. *Chem.–Eur. J.* **2009**, *15*, 11482. (m) Cho, J.; Sarangi, R.; Annaraj, J.; Kim, S. Y.; Kubo, M.; Ogura, T.; Solomon, E. I.; Nam, W. *Nat. Chem.* **2009**, *1*, 568. (n) Tahsini, L.; Bagherzadeh, M.; Nam, W.; de Visser, S. P. *Inorg. Chem.* **2009**, *48*, 6661. (o) Fukuzumi, S.; Kishi, T.; Kotani, K.; Lee, Y.-M.; Nam, W. *Nat. Chem.* **2011**, *3*, 38. (p) Fukuzumi, S.; Kotani, H.; Suenobu, T.; Hong, S.; Lee, Y.-M.; Nam, W. *Chem.–Eur. J.* **2010**, *16*, 354. (q) Cho, J.; Jeon, S.; Wilson, S. A.; Liu, L. V.; Kang, E. A.; Braymer, J. J.; Lim, M. H.; Hedman, B.; Hodgson, K. O.; Valentine, J. S.; Solomon, E. I.; Nam, W. *Nature* **2011**, *478*, 502. (r) Park, J.; Morimoto, Y.; Lee, Y.-M.; You, Y.; Nam, Y.; Fukuzumi, S. *Inorg. Chem.* **2011**, *50*, 11612. (s) Hong, S.; Lee, Y.-M.; Cho, K.-B.; Sundaravel, S.; Cho, J.; Kim, M. J.; Shin, W.; Nam, W. *J. Am. Chem. Soc.* **2011**, *133*, 11876. (t) Hong, S.; Lee, Y.-M.; Cho, K.-B.; Sundaravel, K.; Cho, J.; Kim, M. J.; Shin, W.; Nam, W. *J. Am. Chem. Soc.* **2011**, *133*, 11876. (u) Latifi, R.; Valentine, J. S.; Nam, W.; de Visser, S. P. *Chem. Commun.* **2012**, *48*, 3491. (v) Morimoto, Y.; Park, J.; Suenobu, T.; Lee, Y.-M.; Nam, W.; Fukuzumi, S. *Inorg. Chem.* **2012**, *51*, 10025. (w) Park, J.; Lee, Y.-M.; Nam, W.; Fukuzumi, S. *J. Am. Chem. Soc.* **2013**, *135*, 5052. (y) Morimoto, Y.; Lee, Y.-M.; Nam, W.; Fukuzumi, S. *Chem. Commun.*, **2013**, *49*, 2500. (x) Chen, J.; Lee, Y.-M.; Davis, K. M.; Wu, X.; Seo, M. S.; Cho, K.-B.; Yoon, H.; Park, Y. J.; Fukuzumi, S.; Pushkar, Y. N.; Nam, W. *J. Am. Chem. Soc.* **2013**, *135*, 6388. (z) Park, J.; Morimoto, Y.; Lee,

Y-M.; Nam, W.; Fukuzumi. S. *Inorg. Chem.* **2014**, *53*, 3618.
(48) (a) Kim, S. J.; Latifi, R.; Kang, H. Y.; Nam, W.; de Visser, S. P. *Chem. Commun.* **2009**, 1562. (b) Cho, J.; Sarangi, R.; Kang, H. Y.; Lee, J. Y.; Kubo, M.; Ogura, T.; Solomon, E. I.; Nam, W. *J. Am. Chem. Soc.* **2010**, *132*, 16977. (c) Wu, X.; Seo, M. S.; Davis, K. M.; Lee, Y.-M.; Chen, J.; Cho, K.-B.; Pushkar, Y. N.; Nam, W. *J. Am. Chem. Soc.* **2011**, *133*, 20088. (d) Cho, K.-B.; Kang, H.; Woo, J.; Park, Y. J.; Seo, M. S.; Cho, J.; Nam, W. *Inorg. Chem.* **2014**, *53*, 645. (e) Goo, Y. R.; Maity, A. C.; Cho, K.-B.; Lee, Y.-M.; Seo, M. S.; Park, Y, J.; Cho, J.; Nam, W. *Inorg. Chem.* **2015**, *54*, 10513. (f) Dhuri, S. N.; Lee, Y.-M.; Seo, M. S.; Cho, J.; Narulkar, D. D.; Fukuzumi, S.; Nam, W. *Dalton Trans.* **2015**, *44*, 7634. (g) Dhuri, S. N.; Cho, K.-B.; Lee, Y.-M.; Shin, S. Y.; Kim, J. H.; Mandal, D.; Shaik, S.; Nam, W. *J. Am. Chem. Soc.* **2015**, *137*, 8623. (h) Wu, X.; Yang, X.; Lee, Y.-M.; Nam, W.; Sun, L. *Chem. Commun.* **2015**, *51*, 4013. (i) Ray, K.; Pfaff, F. F.; Wang, B.; Nam, W. *J. Am. Chem. Soc.* **2014**, *136*, 13942.
(49) (a) Nam, W.; Lee, Y.-M.; Fukuzumi, S. *Acc. Chem. Res.* **2014**, *47*, 1146. (b) Fukuzumi, S. *Dalton Trans.* **2015**, *44*, 6696. (c) Fukuzumi, S.; Mochizuki, S.; Tanaka, T. *Inorg. Chem.* **1989**, *28*, 2459. (d) Ishikawa, M.; Matsuda, Y.; Yamamoto, K.; Fukuzumi, S. *Chem. Lett.* **1992**, *21*, 2269. (e) Fukuzumi, S.; Yorisue, T. *Bull. Chem. Soc. Jpn* **1992**, *65*, 715. (f) Fukuzumi, S.; Fujita, M.; Otera, J.; Fujita, Y. *J. Am. Chem. Soc.* **1992**, *114*, 10271. (g) Fukuzumi, S.; Fujita, M. *J. Mol. Cat.* **1994**, *90*, L225. (h) Fukuzumi, S.; Nakanishi, I.; Maruta, J.; Yorisue, T.; Suenobu, T.; Itoh, S.; Arakawa, R.: Kadish, K. M. *J. Am. Chem. Soc.* **1998**, *120*, 6673. (i) Itoh, S.; Bandoh, H.; Nagatomo, S.; Kitagawa, T.; Fukuzumi, S. *J. Am. Chem. Soc.* **1999**, *121*, 8945. (j) Taki, M.; Kumei, H.; Itoh, S.; Fukuzumi, S. *J. Inorg. Biochem.* **2000**, *78*, 1. (k) Fukuzumi, S.; Yasui, K.; Suenobu, T.; Ohkubo, K.; Fujitsuka, M.; Ito, O. *J. Phys. Chem. A* **2001**, *105*, 10501. (l) Osako, T.; Ohkubo, K.; Taki, M.; Tachi, M.; Fukuzumi, S.; Itoh, S. *J. Am. Chem. Soc.* **2003**, *125*, 11027. (m) Ohkubo, K.; Suga, K.; Fukuzumi, S. *Chem. Commun.* **2006**, 2018. (n) Fukuzumi, S. *Helv. Chim. Acta* **2006**, 89, 2425. (o) Zhang, M.; E, W.; Ohkubo, K.; Sanchez-Garcia, D.; Yoon, D.-Y.; Sessler, J.-L.; Fukuzumi, S.; Kadish, K. M. *J. Phys. Chem. A* **2008**, *112*, 1633. (p) Matsumoto, T.; Ohkubo, K.; Honda, K.; Yazawa, A.; Furutachi, H.; Fujinami, S.; Fukuzumi, S.; Suzuki, M. *J. Am. Chem. Soc.* **2009**, *131*, 9258. (q) Fukuzumi, S.; Kotani, H.; Prokop, K. A.; Goldberg, D. P. *J. Am. Chem. Soc.* **2011**, *133*, 1859. (r) Maenaka, Y.; Suenobu, T.; Fukuzumi, S. *J. Am. Chem. Soc.* **2012**, 134, 9417. (s) Takaichi, J.; Ohkubo, K.; Sugimoto, K.; Nakano, M.; Usa, D.; Maekawa, H.; Fujieda, N.; Nishiwaki, N.; Seki, S.; Fukuzumi, S.; Itoh, S. *Dalton Trans.* **2013**, *42*, 2438. (t) Jung, J.; Ohkubo, K.; Goldberg, D. P.; Fukuzumi, S. *J. Phys. Chem. A* **2014**, *118*, 6223. (u) Lee, J. Y.; Peterson, R. L.; Ohkubo, K.; Garcia-Bosch, I.; Himes, R. A.; Woertink, J.; Moore, C. D.; Solomon, E. I.; Fukuzumi, S.; Karlin, K. D. *J. Am. Chem. Soc.* **2014**, *136*, 9925. (v) Ohkubo, K.; Hirose, K.; Fukuzumi, S. *Chem.–Eur. J.* **2015**, *21*, 2855. (w) Aratani, Y.; Yamada, Y.; Fukuzumi, S. *Chem. Commun.* **2015**, *51*, 4662. (x) Isaka, Y.; Kato, S.; Hong, D.; Suenobu, T.; Yamada, Y.; Fukuzumi, S. *J. Mater. Chem. A* **2015**, *3*, 12404.
(50) (a) Sastri, C. V.; Lee, J.; Oh, K.; Lee, Y. J.: Lee, J.; Jackson, T. A.; Ray, K.; Hirao, H.; Shin, W.; Halfen, J. A.; Kim, J.; Que, L., Jr.; Shaik, S.; Nam, W. *Proc. Natl. Acad. Sci. USA* **2007**, *104*, 19181. (b) Hirao, H.; Que, L., Jr.; Nam, W.; Shaik, S. *Chem.–Eur. J.* **2008**, *14*, 1740. (c) Kumar, D.; Hirao, H.; Que, L., Jr.; Shaik, S. *J. Am. Chem. Soc.* **2005**, *127*, 8026. (d) Mas-Ballesté, R.; McDonald, A. R.; Reed, D.; Usharani, D.; Schyman P.; Milko, P.; Shaik, S.; Que, L., Jr. *Chem.–Eur. J.* **2012**, *18*, 11747. (e) Oloo, W. N.; Meier, K. K.; Wang, Y.; Shaik, S.; Münck, E.; Que, L., Jr. *Nat. Commun.* **2013**, *5*, 3046. (f) Dhuri, S. N.; Seo, M. S.; Lee,

Y.-M.; Hirao, H.; Wang, Y.; Nam, W.; Shaik, S. *Angew*. *Chem*., *Int*. *Ed*. **2008**, *47*, 3356. (g) Kang, Y.; Chen, H.; Jeong, Y. J.; Lai, W.; Bae, E. H.; Shaik, S.; Nam, W. *Chem.–Eur*. *J*. **2009**, *15*, 10039. (h) Cho, K.-B.; Shaik, S.; Nam, W. *J*. *Phys*. *Chem*. *Lett*. **2012**, *3*, 2851.

(51) (a) Kojima, T.; Leising, R. A.; Yan, S.; Que, L., Jr. *J*. *Am*. *Chem*. *Soc*. **1993**, *115*, 11328. (b) Ishizuka, T.; Ohzu, S.; Kojima, T. *Synlett* **2014**, *25*, 1667. (c) Kojima, T. *Chem. Lett*. **1996**, *25*, 121. (d) Kojima, T.; Matsuo, H.; Matsuda, Y. *Chem. Lett*. **1998**, *27*, 1085. (e) Kojima, T.; Ishioka, Y.; Matsuda, Y. *Chem*. *Commun*. **2004**, 366. (f) Shiota, Y.; Herrera, J. M.; Juhász, G.; Abe, T.; Ohzu, S.; Ishizuka, T.; Kojima, T.; Yoshizawa, K. *Inorg*. *Chem*. **2011**, *50*, 6200. (g) Ohzu, S.; Ishizuka, T.; Kotani, H.; Kojima, T. *Chem. Commun.* **2014**, *50*, 15018. (h) Kojima, T.; Hayashi, K.-I.; Iizuka, S.; Tani, F.; Naruta, Y.; Kawano, M.; Ohashi, Y.; Hirai, Y.; Ohkubo, K.; Matsuda, Y. Fukuzumi, S. *Chem.–Eur. J.* **2007**, *13*, 8212. (i) Hirai, Y.; Kojima, T.; Mizutani, Y.; Shiota, Y.; Yoshizawa, K.; Fukuzumi, S. *Angew*. *Chem*., *Int*. *Ed*. **2008**, *47*, 5772. (j) Kojima, T.; Hirai, Y.; Ishizuka, T.; Shiota, Y.; Yoshizawa, Y.; Ikemura, K.; Ogura, T.; Fukuzumi, S. *Angew*. *Chem*., *Int*. *Ed*. **2010**, *49*, 8449. (k) Kojima, T.; Nakayama, K.; Ikemura, K.; Ogura, T.; Fukuzumi, S. *J*. *Am*. *Chem*. *Soc*. **2011**, *133*, 11692. (l) Ohzu, S.; Ishizuka, T.; Hirai, Y.; Fukuzumi, S.; Kojima, T. *Chem.–Eur. J.* **2013**, *19*, 1563.

(52) (a) Miyazaki, S.; Kojima, T.; Fukuzumi, S. *J. Am. Chem. Soc.* **2008**, 130, 1556. (b) Ishizuka, T.; Sawaki, T.; Miyazaki, S.; Kawano, M.; Shiota, Y.; Yoshizawa, K.; Fukuzumi, S.; Kojima, T. *Chem.–Eur. J.* **2011**, *17*, 6652.

(53) Miyazaki, S.; Kojima, T.; Mayer, J. M.; Fukuzumi, S. *J*. *Am*. *Chem*. *Soc*. **2009**, *131*, 11615.

(54) (a) Clarke, M. J.; Dowling, M. G.; Garafalo, A. R.; Brennan, T. F. *J*. *Am*. *Chem*. *Soc*. **1979**, *101*, 223. (b) Clarke, M. J.; Dowling, M. G.; Garafalo, A. R.; Brennan, T. F. *J*. *Biol*. *Chem*. **1980**, *255*, 3472. (c) Clarke, M. J.; Dowling, M. G. *Inorg*. *Chem*. **1981**, *20*, 3506. (d) Dowling, M. G.; Clarke, M. J. *Inorg*. *Chim*. *Acta* **1983**, *78*, 153. (e) Shinkai, S.; Nakao, H.; Honda, N.; Manabe, O.; Mueller, F. *J. Chem. Soc.*, *Perkin Trans. 1* **1986**, 1825. (f) Shinkai, S.; Ishikawa, Y.; Manabe, O. *Bull. Chem. Soc. Jpn.* **1983**, *56*, 1694. (g) Shinkai, S.; Nakano, H.; Ueda, K.; Manabe, O. *Tetrahedron Lett.* **1984**, *25*, 5295. (h) Fukuzumi, S.; Kuroda, S.; Tanaka, T. *J. Am. Chem. Soc.* **1985**, *107*, 3020.

(55) (a) Schwederski, B.; Kaim, W. *Inorg. Chim. Acta* **1992**, *195*, 123. (b) Bessenbacher, C.; Kaim, W. *Anorg. Z. Allg. Chem.* **1989**, *577*, 39. (c) Kunkely, H.; Vogler, A. *Z. Naturforsch.* **1998**, *536*, 423.

(56) Selbin, J.; Sherrill, J.; Bigger, C. H. *Inorg. Chem.* **1974**, *13*, 2544.

(57) (a) Kohzuma, T.; Masuda, H.; Yamauchi, O. *J*. *Am*. *Chem*. *Soc*. **1989**, *111*, 3431. (b) Fischer, B.; Strähle, J.; Viscontini, M. *Helv*. *Chim*. *Acta* **1991**, *74*, 1544. (c) Fischer, B.; Schmalle, H. W.; Dubler, E.; Schäfer, A.; Viscontini, M *Inorg. Chem*. **1995**, *34*, 5726. (d) Fischer, B.; Schmalle, H. W.; Baumgartner, M. R.; Viscontini, M. *Helv. Chim. Acta* **1997**, *80*, 103. (e) Burgmayer, S. J. N.: Arkin, M. R.; Bostick, L.; Dempster, S.; Everett, K. M.; Layton, H. L.; Paul, K. E.; Rogge, C.; Rheingold, A. L. *J*. *Am*. *Chem*. *Soc*. **1995**, *117*, 5812. (f) Lee, D. H.; Murthy, N. N.; Lin, Y.; Nasir, N. S.; Karlin, K. D. *Inorg. Chem.* **1997**, *36*, 6328. (g) Hille, R. *Chem. Rev.* **1996**, *96*, 2757. (h) Collison, R.; Garner, C. D.; Joule, J. A. *Chem. Soc. Rev.* **1996**, *25*, 25. (i) Rees, D. C.; Hju, Y.; Kisker, C.; Schindelin, H. *J. Chem. Soc.*, *Dalton Trans.* **1997**, 3909. (j) Etiefel, E. I. *J. Chem. Soc.*, *Dalton Trans.* **1997**, 3915. (k) Davies, E. S.; Beddoes, R. L.; Collison, D.; Dinsmore, A.; Docrat, A.; Joule, J. A.; Wilson, C. R.; Garner, C. D. *J. Chem. Soc.*, *Dalton Trans.* **1997**, 3985. (l) Garton, S.

D.; Hilton, J.; Oku, H.; Crouse, B. R.; Rajagopalan, K. V.; Johnson, M. K. *J. Am. Chem. Soc.* **1997**, *119*, 12906. (m) Westcott, B. L.; Gruhn, N. E.; Enemark, J. H. *J. Am. Chem. Soc.* **1998**, *120*, 3382. (n) Greulich, S.; Kaim, W.; Stange, A.; Stoll, H.; Fiedler, J.; Zalis, S. *Inorg. Chem.* **1996**, *35*, 3998. (o) Heilmann, O.; Hornung, F. M.; Kaim, W.; Fiedler, J. *J. Chem. Soc.*, *Faraday Trans.* **1996**, *92*, 4233. (p) Kaim, W.; Reinhardt, R.; Fiedler, J. *Angew. Chem.*, *Int. Ed. Engl.* **1997**, *36*, 2493. (q) Kaim, W.; Reinhardt, R.; Waldhör, E.; Fiedler, J. *J. Organomet. Chem.* **1996**, *524*, 195. (r) Abelleira, A.; Galang, R. D.; Clarke, M. J. *Inorg. Chem.* **1990**, *29*, 633. (s) Nasir, M. S.; Karlin, K. D.; Chen, Q.; Zubieta, J. *J. Am. Chem. Soc*. **1992**, *114*, 2264. (t) Fischer, B.; Enemark, J. H.; Basu, P. *J. Inorg. Biochem.* **1998**, *72*, 13.

(58) (a) Kojima, T.; Sakamoto, T.; Matsuda, Y.; Ohkubo, K.; Fukuzumi, S. *Angew*. *Chem*., *Int*. *Ed*. **2003**, *42*, 4951. (b) Miyazaki, S.; Ohkubo, K.; Kojima, T.; Fukuzumi, S. *Angew*. *Chem*., *Int*. *Ed*. **2008**, *47*, 9669.

(59) Miyazaki, S.; Ohkubo, K.; Kojima, T.; Fukuzumi, S. *Angew*. *Chem*., *Int*. *Ed*. **2007**, *46*, 905.

(60) Inui, Y.; Miyazaki, S.; Ohkubo, K.; Fukuzumi, S.; Kojima, T. *Angew. Chem.*, *Int. Ed.* **2012**, *51*, 4623.

Chapter 2 Syntheses and Characterizations of Ruthenium(II)-PQQTME-terpy Complexes

2–1 Introduction

As described in Section 1-2 in Chapter 1, PQQ is a redox-active heteroaromatic coenzyme, which has been first found by Hauge in a glucose dehydrogenase of *bacterium anitratum*[1] as the third redox-active coenzyme, after the discovery of nicotinamide and flavins. The biosynthesis of PQQ is achieved using a peptide precursor containing glutamic acid and tyrosine residues.[2] PQQ catalytically oxidizes glucose and alcohols at the active sites of quinoproteins as key steps of biological metabolic reactions, and the resultant reduced form of PQQ is reoxidized by cytochrome *c* or azurin through electron transfer.[3-5] Because of the facts that the catalytic efficiency of PQQ in its substrate oxidation is quite high and PQQ can utilize molecular oxygen as a sacrificial oxidant, exploration of the reaction mechanism for the substrate oxidation

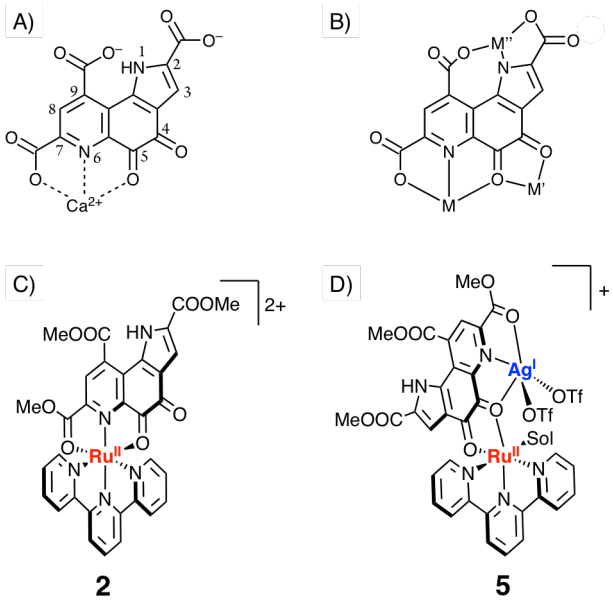

Figure 2-1. (A) Structure of a Ca^{2+}-bound PQQ. (B) Three potential metal-coordination sites (M, M', and M") of PQQ. (C) Structure of $[Ru^{II}(\eta^3\text{-PQQTME})(terpy)]^{2+}$ (**2**). (D) Structure of $[\{Ru^{II}(terpy)(sol)\}(\mu\text{-PQQTME})\{Ag^{I}(OTf)_2\}]^{+}$ (**5**, sol = a coordinating solvent).

by PQQ has attracted considerable attention.[6-9] An X-ray crystallographic analysis of quinoproteins having PQQ as a cofactor shows that the PQQ cofactor is strongly bound to a calcium ion in a tridentate fashion through 5-oxo-O, 6-pyidine-N, and 7-carboxylate-O atoms of PQQ (Figure 2-1A).[10-12]

Anthony and Richardson have demonstrated that the Ca^{2+} ion is essential for oxidation of the substrates, on the basis of the experiments with use of a mutated methanol dehydrogenase lacking the Ca^{2+} ion.[13] In addition, Itoh and co-workers have performed the kinetic analyses on oxidation reactions catalyzed by PQQ derivatives to reveal the roles of the Ca^{2+} ion.[6f-h] In consequence, the rate constant of the methanol addition at the carbonyl carbon of a trimethyl ester derivative of PQQ (PQQTME) is accelerated by 3300 times in the presence of Ca^{2+} ions relative to that in the absence of Ca^{2+} ions.[6f-h] Additionally, oxidation of methanol is achieved with addition of a strong base into the methanol solution of PQQTME and Ca^{2+}, despite the fact that metal-free PQQ is known to be unable to oxidize methanol in non-enzymatic environments.[6f-h] As

another effect of Ca^{2+} ion, the reduction potential of PQQTME is also positively shifted by *ca.* 0.57 V in the presence of Ca^{2+} ions.[14]

Since PQQ has several potential sites for metal coordination in the structure (Figure 2-1B), PQQ can act as a ligand in transition-metal complexes. To elucidate the reactivity of PQQ for substrate oxidation and to clarify roles of the coordinated Ca^{2+} ion in the biological activity of PQQ, several metal complexes of PQQ and the derivatives have been synthesized and the redox properties of metal-bound PQQ have been investigated.[15-18] For instance, a Cu^{I}-PQQTME complex exhibited the reduction potential of the PQQ moiety at –0.02 V vs SCE in CH_2Cl_2, which was positively shifted by 0.42 V in comparison with that of free PQQTME.[17] The properties of metal-PQQ complexes, however, have yet to be well explored, and heteronuclear transition-metal complexes of PQQ derivatives had never been reported. Due to the shortage of examples in transition-metal complexes of PQQ, it has not been well explored yet how the difference in

Scheme 2-1. Syntheses of Ru^{II}-Ag^{I}-PQQTME and Ru^{II}-PQQTME complexes

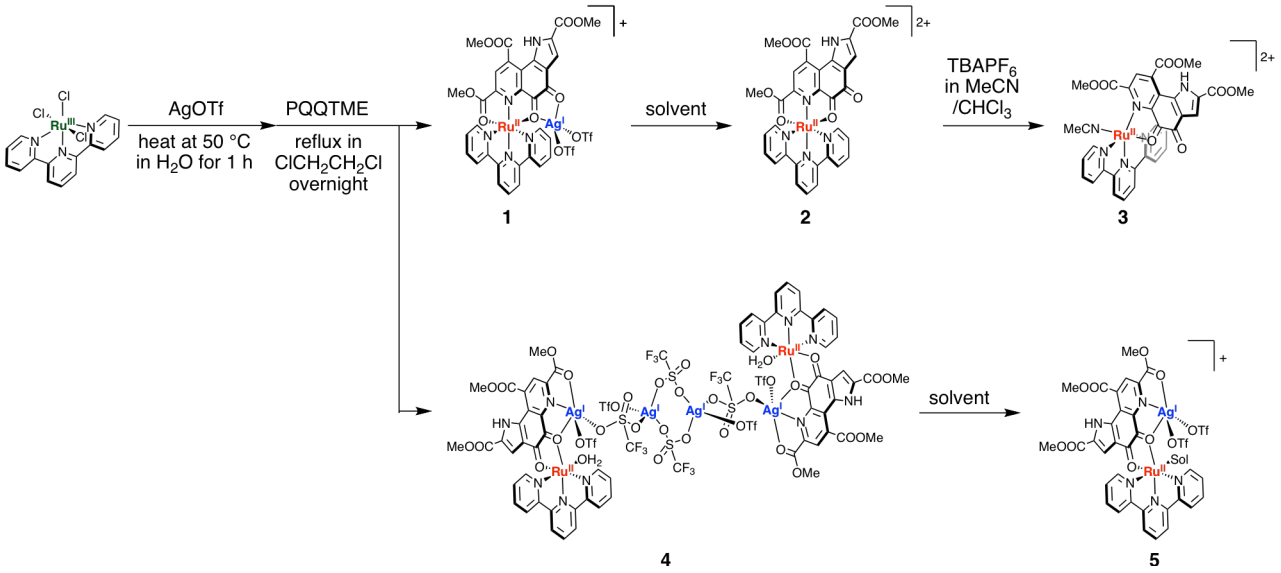

the coordination sites of PQQ in the transition-metal complexes influences the electrochemical properties of the PQQ ligand and the reactivity in oxidation reactions. To shed light on the point, the author newly synthesized Ru^{II} complexes of PQQTME, **2** and **5,** and compared their properties. Complex **2** has the ONO coordination mode for the Ru^{II} coordination, whereas compound **5** coordinates to the Ru^{II} center through the OO coordination mode at the *o*-quinone moiety and has an additional Ag^{I} ion at the ONO coordination site (Figure 2-1C and 2-1D). The author also measured the reduction potentials and compared the electronic structures of the PQQTME moieties for **2** and **5**.

2–2 Syntheses of Two Ruthenium(II)-Silver(I)-PQQTME-terpy Complexes

In this work, 2,2':6',2''-terpyridine (terpy) was employed as an auxiliary ligand of a Ru^{II} ion, since terpy is a strongly π-accepting ligand and thus $d\pi$ electrons of the Ru^{II} center are donated to the terpy ligand by π-back bonding.[19] Therefore, the back donation of the $d\pi$ electrons of the Ru^{II} center to the PQQ ligand should be reduced and thus the electron density of the PQQ moiety is expected to be lowered and more electron-deficient. PQQTME was synthesized with 4-amino-2-hydroxybenzoic acid as a starting material by

the reported procedure.[20-23] Ru^{II}-PQQTME complexes used in this study were prepared in good yields from PQQTME and $[Ru^{II}(terpy)(OH_2)_3](OTf)_2$, which was prepared by treatment of $[Ru^{III}Cl_3(terpy)]$ with excess amount of $Ag^{I}(OTf)$ in H_2O (Scheme 2-1).[24] The resulting aqueous solution of $[Ru^{II}(terpy)(OH_2)_3](OTf)_2$ was filtered, and dried up under vacuum to obtain a mixture of $[Ru^{II}(terpy)(OH_2)_3](OTf)_2$ and excess silver salts. The mixture was heated overnight at reflux together with PQQTME in 1,2-dichloroethane, and then, the resulting suspension was filtered. The filtrate was slowly concentrated to afford crystals of a Ru^{II}-Ag^{I}-PQQTME hetero-multinuclear complex. Interestingly, the amount of $Ag^{I}(OTf)$ used for the preparation of $[Ru^{II}(terpy)(OH_2)_3](OTf)_2$ controlled the products of the reaction of PQQTME with $[Ru^{II}(terpy)(OH_2)_3](OTf)_2$. Using 4 equiv of $Ag^{I}(OTf)$ per ruthenium, a dinuclear complex, $[(terpy)Ru^{II}(\mu\text{-PQQTME})Ag^{I}(OTf_2)](OTf)_2$ (**1**), was obtained, whereas usage of 7 equiv of $Ag^{I}(OTf)$ per ruthenium gave a hexanuclear complex, $[\{(terpy)(OH_2)Ru^{II}(\mu\text{-PQQTME})\text{-}Ag^{I}(OTf)(\mu\text{-OTf})\}_2\{(OTf)Ag^{I}(\mu\text{-OTf})_2Ag^{I}(OTf)\}]$ (**4**).

The structure of **1** was deduced from the results of the elemental analysis for the solid sample of **1**·(OTf), the spectroscopic data of **2**, and the crystal structure of **3**·$(PF_6)_2$ (See below). The result of the elemental analysis indicates that the solid of **1**·(OTf) contains an $Ag(OTf)_3$ unit per a Ru^{II}(PQQTME)(terpy) unit. In addition, relevance to the crystal structure of **3**·$(PF_6)_2$, the Ru^{II}(terpy) unit of **1** is considered to be coordinated to the ONO coordination site of the PQQTME ligand. The solid of **1**·(OTf) was dissolved in a coordinating solvent such as MeCN to give the mononuclear Ru^{II} complex, **2**. The purity of **4** was confirmed by elemental analysis and the explicit structural determination of **4** was done by X-ray crystallography on a single crystal (See below).

2–3 Characterizations of Ruthenium(II)-PQQTME-terpy Complexes

2–3–1 ^{1}H NMR Spectrum of 2

Since complexes **4** and **5** do not have enough solubility in deuterated solvents usually used for ^{1}H NMR measurements, or exhibit decomposion after dissolving the complexes, only the ^{1}H NMR spectrum of **2** could be measured. In the ^{1}H NMR spectrum of **2** in CD_3CN (Figure 2-2), the ^{1}H NMR signal of the methoxycarbonyl group at the 7'-position of the PQQTME ligand appeared at δ 4.22 ppm (red diamond in

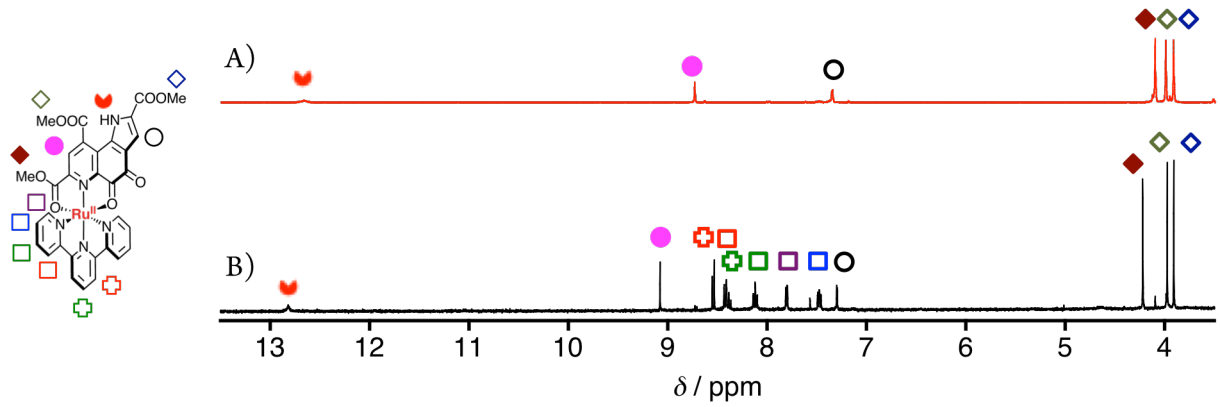

Figure 2-2. ^{1}H NMR spectra of PQQTME (A) and **2** (B) in CD_3CN at room temperature.

Figure 2-2B), which was downfield-shifted in comparison with that of free PQQTME (δ 4.00 ppm) due to

the coordination to the Ru^{II} ion. A similar downfield shift was also observed for the PQQTME-Ca^{2+} complex, which has a Ca^{2+} ion at the ONO coordination site of PQQTME,[6f] and thus, complex **2** probably also has the ONO-coordination mode (Figure 2-1C).

2–3–2 ESI-TOF-MS Spectra of the PQQ Complexes

The ESI-TOF-MS spectrum of **2** in acetonitrile (MeCN) showed peak clusters at *m/z* = 337.6, 353.6, 358.1, 707.2 and 738.1. All of those clusters exhibited distribution patterns corresponding to species having one ruthenium and no sliver atom (Figure 2-3). The former three peak clusters showed peak separations of 0.5, whereas those of the latter two of them were 1.0. Hence, complex **1** is assumed to lose the Ag^{I} ion to give the mononuclear complex **2** upon being dissolved in a coordinating solvent such as MeCN, as shown in Scheme 2-1. The peak clusters at *m/z* = 353.6 and 707.2 were assigned to **2** (calcd. for $[Ru^{II}(\eta^3\text{-PQQTME})(terpy)]^{2+}$: *m/z* = 353.5) and $1e^{-}$-reduced species of **2** (calcd. for $[Ru^{II}(\eta^3\text{-PQQTME}^{\bullet-})(terpy)]^{+}$: *m/z* = 707.1), respectively. Thus, complex **2** derived from **1** in MeCN should be $[Ru(terpy)(PQQTME)]^{2+}$, in which both terpy and PQQTME bind to the Ru^{II} center as tridentate ligands in the meridional geometry as shown in Scheme 2-1. The peak clusters at *m/z* = 337.6 and 358.1 can be ascribed to fragment signals of **2**; the former should be derived from the fragment species that complex **2** loses a methoxy group and one proton from the PQQTME moiety (calcd. for $[Ru^{II}(PQQTME - H - OMe)(terpy)]^{2+}$: *m/z* = 337.5), and the latter can be assigned to the species that **2** loses a methoxy group and one proton from the PQQTME moiety and then induces additional coordination of an acetonitrile molecule (calcd. for $[Ru^{II}(PQQTME - H - OMe)(terpy)(MeCN)]^{2+}$: *m/z* = 358.0). The methoxycarbonyl group at the 7'-position of the PQQTME moiety in **2** is possibly activated by coordination to the Ru^{II} center and is apt to be cleaved between the oxygen atom of the methoxy group and the carbon atom of the carbonyl group at 7'-position of the PQQTME moiety during ionization processes for ESI-TOF-MS measurements (Figure. 2-4). The cleavage gave the fragment showing a signal at *m/z* = 337.6. In addition, the complex losing the methoxy group can be attacked by an acetonitrile molecule from the solvent at the Ru^{II} center, to give the peak cluster at *m/z* = 358.0, which has been mentioned above. The mass signal derived from acetonitrile-coordinating species was not observed without the loss of the methoxy group of PQQTME in the ESI-TOF-MS measurements, suggesting that acetonitrile molecules cannot coordinate to the Ru^{II} center of **2** under mild conditions, even in the acetonitrile solution. The peak cluster at 738.1 was assigned to $[\mathbf{2} + OMe]^{+}$ ion (calcd. for $\{[Ru^{II}(PQQTME\text{- }OMe)(terpy)]\}^{+}$: *m/z* = 738.1). Since the carbonyl group at the 5-position of PQQ has high reactivity toward nucleophilic attacks and furthermore the reactivity is enhanced

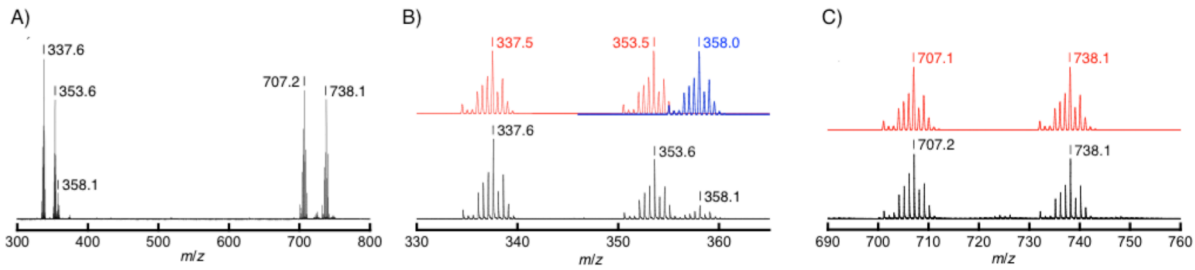

Figure 2-3. ESI-TOF-MS spectrum of **2** in MeCN and the simulation (upper colored spectra in (B) and (C)). The *m/z* range: A) 300-800, B) 330-370, and C) 690-760.

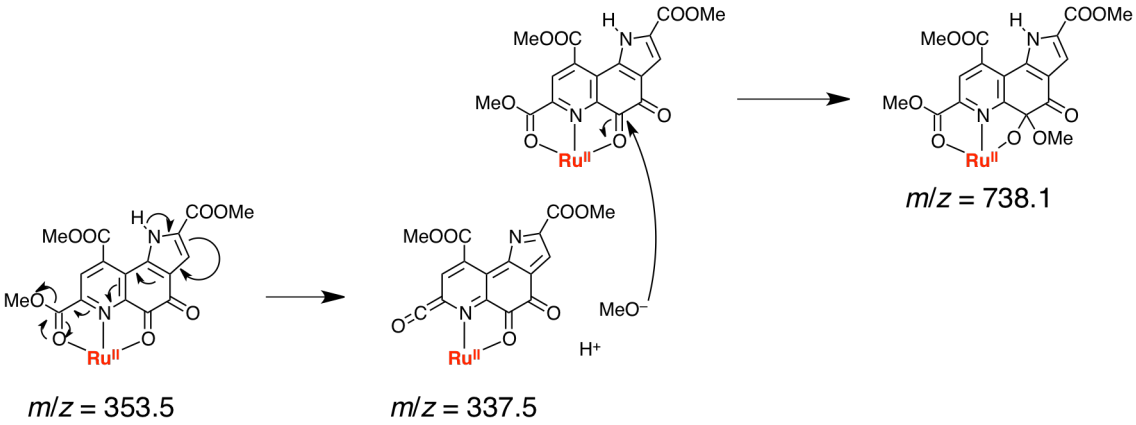

Figure 2-4. A proposed reaction mechanism of the cleavage between the oxygen atom of the methoxy group and the carbon atom of the carbonyl group at 7'-position of the PQQTME to form a putative ketene (m/z = 337.5) and the subsequent nucleophilic attack of a methoxide ion toward the carbonyl group of 5-position of the PQQTME ligand of another molecule to afford the methoxide adduct (m/z = 738.1), occurring upon ionization for ESI-TOF-MS measurements.

by metal coordination in **2**, the methoxy group is probably added at the carbonyl carbon of the 5-position of the PQQTME moiety during the ionization.[6g, 25]

Based on the ^{1}H NMR and mass spectroscopic data (See above), it is concluded that complex **1** loses the Ag^I ion in a coordinating solvent such as MeCN to give complex **2**, but no further reaction occurs including solvent coordination to the Ru^{II} center (Scheme 2-1).

The ESI-TOF-MS spectrum of **4** in a mixed solvent of MeCN and water (2:3 v/v) gave a peak cluster at m/z = 964.95 and the isotope distribution indicates that the detected ion contains both of ruthenium and silver atoms (Figure 2-5). The computer simulation enabled the assignment of the peak cluster as $[(terpy)Ru^{II}(PQQTME^{\bullet-})Ag^{I}(OTf)]^+$ (calcd: m/z = 964.92). The PQQTME ligand was probably reduced to be a semiquinone radical form in the course of the ionization. The detection of $[(terpy)Ru^{II}(PQQTME^{\bullet-})Ag^{I}(OTf)]^+$ in the ESI-TOF-MS measurement of **4** suggests that, in contrast to the case of dissolving **1**, even after dissolving in MeCN, complex **4** does not lose the silver ion, which is directly coordinated to PQQTME ligand, to give a hetero-dinuclear complex, **5** (Scheme 2-1). This difference in the stability of Ag^I coordination can be attributed to the number of coordinating atoms: PQQTME in **1** behaves

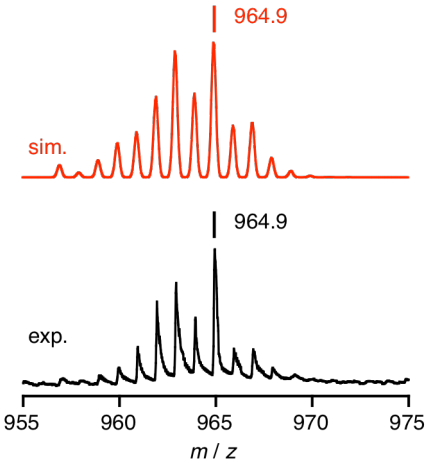

Figure 2-5. ESI-TOF-MS spectrum of **5** in MeCN-H_2O mixed solvent (2:3 v/v); experimental (black, below), simulated for [(terpy)Ru(μ-PQQTME)Ag(OTf)] (red, above)

as a bidentate ligand to the Ag^{I} ion, whereas that in **5** acts as a tridentate one.

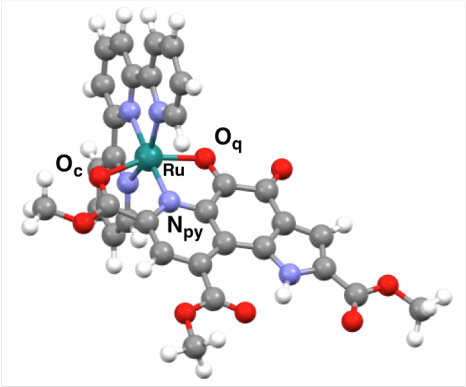

Figure 2-6. DFT-optimized structure of **2** at the B3LYP level. O_q, O_c, and N_{py} denote the Ru-bound quinone oxygen, the Ru-bound carbonyl oxygen, and the Ru-bound pyridine nitrogen of the PQQTME ligand, respectively.

2–3–3 DFT Calculations on 2 and 5

Density functional theory (DFT) calculations were conducted on **2** and **5** to shed light on the geometrical and electronic structures. The optimized structure of **2** is shown in Figure 2-6. The bond lengths of Ru-O_q, Ru-O_c, and Ru-N_p were calculated to be 2.078 Å, 2.189 Å, and 1.975 Å, respectively. The LUMO of **2** was revealed to be a π^* orbital of the quinone moiety of the PQQTME ligand as shown in Figure 2-7. In comparison with the LUMO of **5**, there are only slight differences between the LUMOs of **2** and **5** and both the LUMOs are π^* orbitals of the PQQTME ligand.

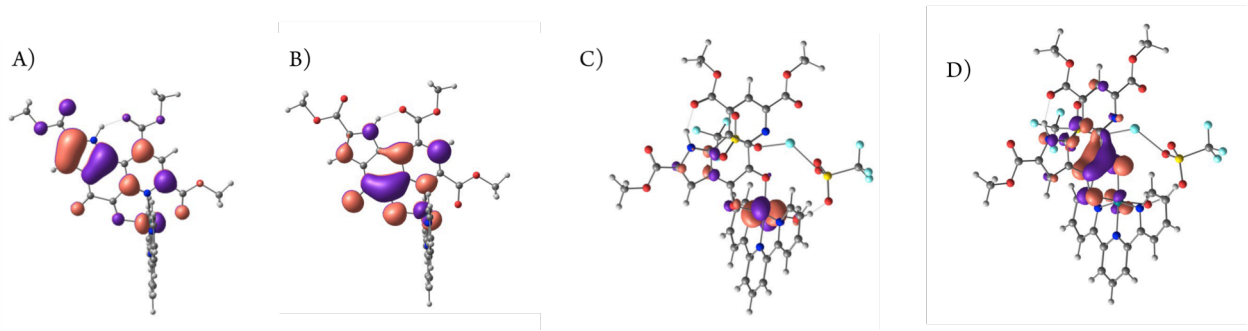

Figure 2-7. The frontier orbitals of **2** and **5** calculated at the B3LYP level. HOMO (A) and LUMO (B) of **2**, and HOMO (C) and LUMO (D) of **5**.

DFT calculations were also conducted on a free PQQTME molecule to discuss π-back bonding from the Ru^{II} center to PQQTME in **2** through comparison of the lengths of coordinating carbonyl C–O double bond between free PQQTME and **2**. In optimized structure of free PQQTME, the lengths of the C=O double bonds of the two carbonyl groups, which coordinate to the Ru^{II} center in **2**, are 1.211 Å (quinone) and 1.210 Å (ester), respectively. On the other hand, the corresponding lengths in the optimized structure of **2** are 1.262 Å (quinone) and 1.257 Å (ester). The difference in the bond lengths indicates the π-back bonding from the Ru^{II} center to the PQQTME ligand in **2**.

2–3–4 Crystal Structure of $3\cdot(PF_6)_2$

Slow concentration of a solution of **2** in acetonitrile containing $TBAPF_6$ in the presence of diffused $CHCl_3$ vapor gave a green crystal suitable for X-ray crystallography. The crystal contains two independent cation parts of $[Ru^{II}(terpy)(\eta^2\text{-PQQTME})(MeCN)]^{2+}$ (**3**), which exhibits dissociation of the methoxycarbonyl group at the 7' position from the Ru^{II} center and has a coordinated acetonitrile molecule to the Ru^{II} center (Scheme 2-1), and four hexafluorophosphate anions. The structure of one of the cations is depicted in Figure 2-8 with selected atom labeling. The cation parts are chemically equivalent, except slight structural differences caused by the crystal packing. Since the replacement of the methoxycarbonyl group in **2** to an MeCN molecule was not observed in the ^1H NMR spectra of **2** measured at a few hours later after dissolving **2** in CD_3CN, the author assumed that the substitution slowly occurred during the crystallization taking over ten days.

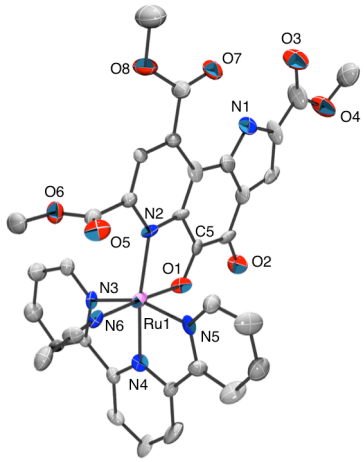

Figure 2-8. An ORTEP drawing of **3** with selected atom labeling. All the thermal ellipsoids are drawn with 30% probability.

Here, details of the crystal structure of **3** are discussed using one of the two independent cation parts, containing Ru1 atom. The geometry around the Ru^{II} ion in **3** is a distorted octahedron having terpy as a tridentate ligand and the PQQTME ligand binds to the Ru^{II} center as a neutral bidentate ligand, where the N(pyridine) and O(quinone) coordinates to the Ru^{II} center. An MeCN molecule occupies the last coordination site of the Ru^{II} center, by substituting the methoxycarbonyl O atom at the 7'-position of the PQQTME ligand. The dissociation of the carbonyl O atom should be due to the weak coordination as reported for a Cu^{I}-PQQTME complex, in which the coordination bond length has been reported to be the longest (2.579(4) Å) among other coordination bonds involved.[17] As mentioned above, the DFT-optimized structure of **2** (Figure 2-5) also showed the longest bond length for Ru-O_c (2.189 Å) to support the possibility of the dissociation of the methoxycarbonyl oxygen atom toward the coordination of MeCN, which should bind strongly to a Ru^{II} center.[26] In addition, the longer bond length of the metal-coordinating carbonyl bond (C5–O1: 1.27(1) Å) was observed than those of the Cu^{I}-PQQTME complex (1.222(8) Å)[17] and those of natural methanol dehydrogenases (1.24 Å, defined as the semiquinone radical forms).[10d] This result suggests certain contribution of π-back bonding from the $d\pi$ orbitals of the Ru^{II} center to the π^* orbitals of the PQQTME moiety, which resides mainly on the quinone moiety including the C=O double bond (Figure 2-7). The smaller bond angle of N2–Ru1–N4 (168.4(3)°) relative to that of O1–Ru1–N6 (176.9(3)°) indicates steric repulsion between the methoxycarbonyl group at the 7'-position of the PQQTME moiety and the

coordinating acetonitrile, which results in the lean of the PQQTME ligand to the direction of the O1 side. In addition, an intramolecular hydrogen bond was found between N1-H···O7 with 2.61(1) Å for N1···O7 separation.

2–3–5 Crystal Structure of 4

The explicit structural determination of **4** was done by X-ray crystallography on a single crystal obtained by crystallization from the dichloroethane solution of the reaction mixture (Figure 2-9). Complex **4** involves a PQQTME unit as a ligand in the asymmetric unit and the Ru^{II}(terpy) moiety coordinated to the *ortho*-quinone moiety of PQQTME. The bond distances between the Ru center and the terpy and PQQTME ligands are 1.975(6) Å for Ru-O1, 2.025(6) Å for Ru-O2, 2.059(10) Å for Ru-N3, 1.951(9) Å for Ru-N4, 2.051(10) Å for Ru-N5, respectively. The distances strongly indicate that the electronic state of the Ru center is +2. The last coordination site of the Ru^{II} center was occupied by an oxygen atom with the bond distance of Ru-O10 (2.081(9) Å), suggesting that the oxygen atom is not a hydroxo but an aqua-ligand.[27] An Ag(OTf) unit, which was derived from the excessive Ag^{I}(OTf) employed to remove the chloride ligands of [$Ru^{III}Cl_3$(terpy)], was found to bind to the meridional tridentate part (ONO-moiety) of PQQTME. This is the first example of a PQQ-bridged heterometallic complex, whose crystal structure has been determined. The Ag center resided in a distorted trigonal-bipyramidal coordination environment and the trigonal-equatorial plane consisted of two oxygen atoms (O12 and O14) of two OTf^- ions and a nitrogen atom (N2) at the 6-position of the PQQTME ligand and the two axial positions were occupied by two oxygen atoms derived from the 5-oxo (O2) and 7'-ester-carbonyl oxo (O5) ligands. The 5-oxo ligand (O2) was shared with both the Ru^{II} and Ag^{I} centers as a bridging ligand. The bond lengths are 2.615(6) Å for Ag1-O2, 2.493(9) Å for Ag1-O5, 2.683(13) Å for Ag1-O12, 2.361(10) Å for Ag1-O14, and 2.343(10) Å for Ag1-N2, respectively. Comparison of the bond lengths with the reported corresponding value[28] allowed the author to conclude that

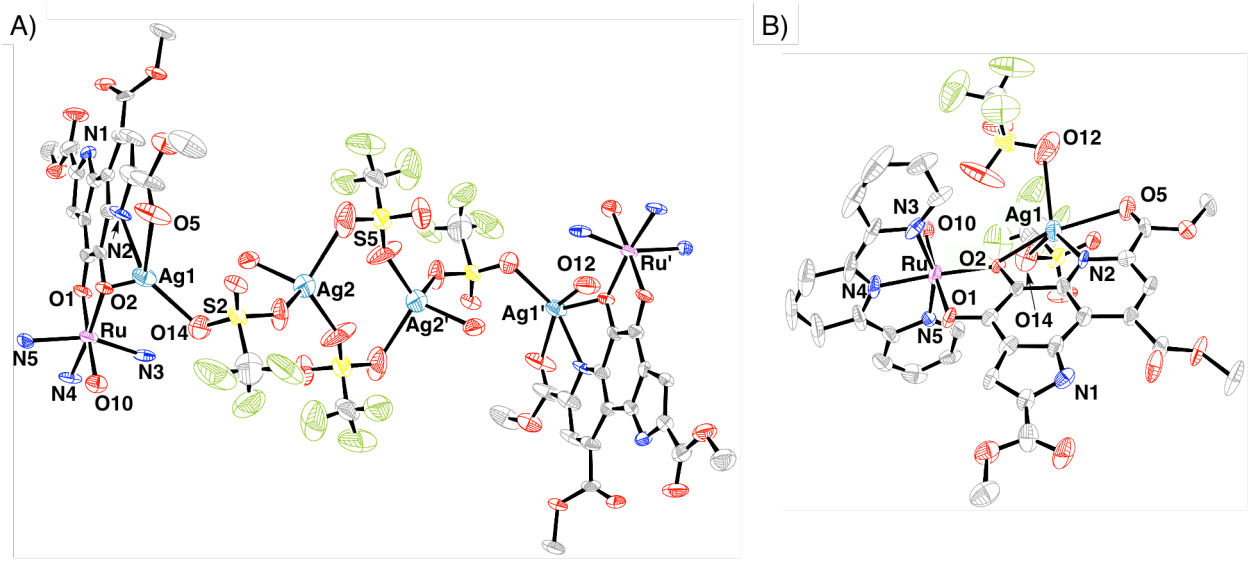

Figure 2-9. ORTEP drawings of the crystal structure of **4** with selected atom labeling. (A) The whole structure of **4**, in which the carbon atoms of the terpy ligand, trifluoromethyl groups and uncoordinating oxygen atoms of OTf^- ions, and hydrogen atoms were omitted for clarity. Each atom is drawn with the thermal ellipsoid at the 30% probability. (B) The hetero-dinuclear unit of **4**.

the oxidation state of the Ag ion was revealed to be +1. The ion radii of Ag^{I} and Ca^{2+} ions are similar to each other, and the bond lengths between the Ag1 ion and the PQQ ligand in **4** were very close to the corresponding lengths between a Ca^{2+} ion and the PQQ cofactor in quino-proteins; for instance, 2.55 Å for Ca^{2+}-to-5-oxo, 2.40 Å for Ca^{2+}-to-6-nitrogen, 2.24 Å for Ca^{2+}-to-carboxylate-oxygen, respectively, found in a crystal structure of methanol dehydrogenase.[12] In addition, two $[Ag^{I}(OTf)_2]^{-}$ units formed a eight-membered ring, which bridged two $[(terpy)(OH_2)Ru^{II}(PQQTME)Ag^{I}(OTf)]^{+}$ moieties (Figure 2-9 and Figure 2-10). In the crystal, the PQQTME ligand was found to interact with another PQQTME ligand of an adjacent molecule to form a π-π stacking pair with the inter-plane distance of 3.47 Å (Figure 2-11A and B). Concomitantly, the terpy ligand also formed a π-π stacking pair with another terpy ligand in a neighboring molecule with the inter-plane distance of 3.42 Å (Figure 2-11C and D). The intermolecular π-π interactions hold the crystal packing of **4**.

The crystal structure of **4** exhibits a completely different coordination mode of PQQTME from that in **3**; complex **4** has one Ru^{II} ion at the O(methoxycarbonyl)-N(pyridine)-O(quinone) coordination site and one Ag^{I} ion at the *o*-quinone coordination site of the PQQTME moiety (Scheme 2-1).

2–3–6 Electrochemical Measurements to Investigate Electron Acceptability of PQQ Complexes

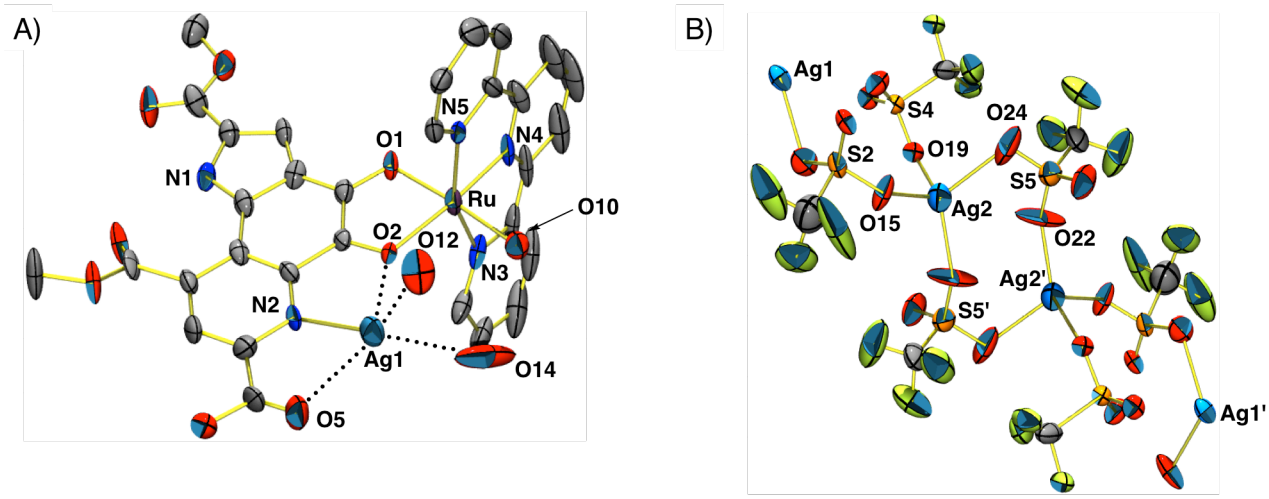

Figure 2-10. ORTEP diagrams of partial crystal structures of **4**. (A) PQQTME and the coordination environments of Ru and Ag1 centers, and (B) the bridging metallacycle. Each atom is drawn with a thermal ellipsoid at the 30% probability level.

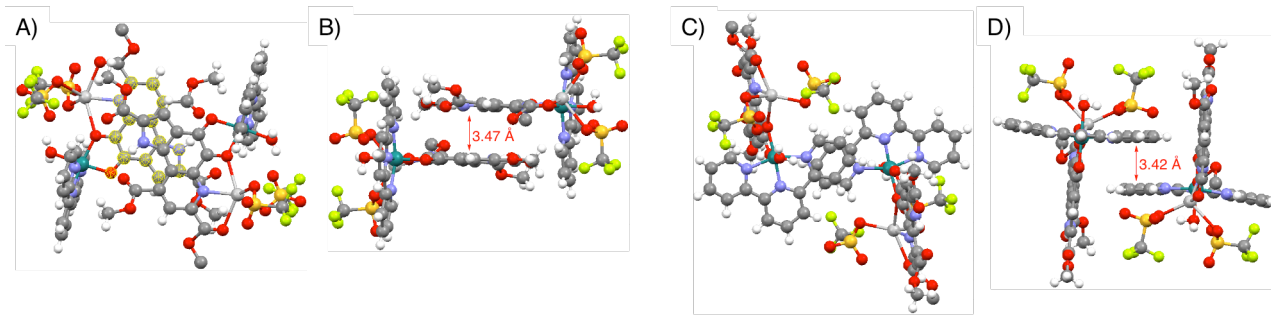

Figure 2-11. π-π stacking manners in the crystal structure of **4**. A stacking pair of PQQTME ligands (A, B) and that of terpy ligands (C, D).

Cyclic and differential-pulse voltammograms (CV and DPV, respectively) of **2** and **5** were measured in THF containing 0.1 M $TBAPF_6$ as a supporting electrolyte at room temperature under Ar atmosphere. In the measurements of **2**, the rest potential was found to be +0.77 V vs SCE and complex **2** exhibited a reversible reduction wave at +0.28 V vs SCE with a peak separation value ($E_{pc} - E_{pa}$) of 64 mV (Figure 2-12). On the other hand, CV of **5** in THF showed one irreversible reduction wave at E_{pc} = +0.42 V vs SCE, and the reduction potential was determined to be +0.50 V vs SCE using the peak potential of DPV, which is higher than that of **2** by 0.22 V. The waves can be assigned to $1e^-$ reduction of the quinone moiety of the PQQTME ligand in **2** and **5**, based on the absorption spectra of chemically reduced **2** (see below), and the DFT calculations also suggest that the LUMO of **2** and **5** is a π^* molecular orbital of the PQQTME ligand (Figure 2-7B and 2-7D). The reduction potentials exhibited a larger positive shift from that of free PQQTME (E_{red} = −0.53 V vs SCE in MeCN)[14] and even larger than that observed for a mononuclear Cu^I-PQQTME complex ($E_{1/2}$ = −0.02 V vs SCE),[17] because of the high electron acceptability of the Ru^{II}-terpy unit. As for the Ru^{II} center, no redox processes could be observed in the potential window of the MeCN solution of **2** and **5** (up to *ca*. +1.6 V). Since the redox potential of Ru^{II}/Ru^{III} couple for $[Ru^{II}(terpy)_2]^{2+}$ has been reported to be +1.38 V (vs SCE),[29] the PQQTME ligand should act as a stronger π-acceptor than terpy in the Ru^{II} coordination sphere. The difference of the redox potentials between **2** and **5** can be ascribed to the number of metal ions binding to the PQQTME ligand and also difference of the coordination modes as depicted in Figure 2-13.

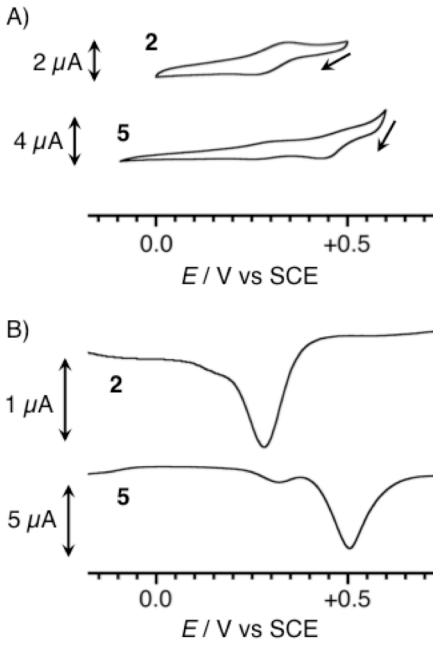

Figure 2-12. (A) Cyclic and (B) differential-pulse voltammograms of **2** (1.0 mM) and **5** (2.0 mM) in THF containing 0.1 M $TBAPF_6$ at room temperature.

Complex **2** has one Ru^{II} ion at the ONO coordination site of the PQQTME ligand, which is not fully conjugated with the quinone moiety that acts as the electron-accepting site for the reduction process. In contrast, complex **5** holds two transition metal cations at the quinone moiety, one of which is a Ag^I ion at the ONO coordination site in a monodentate fashion and the other is a Ru^{II} ion at the quinone moiety in a bidentate mode. DFT calculations indicated that the LUMO levels of **2** (–9.11 eV) was comparable to that of

$[Ru^{II}(terpy)(PQQTME)(H_2O)]^{2+}$ (–9.07 eV), which is a model compound of **5** without the $[Ag^{I}(OTf)_2]^{-}$ unit. This result suggests that, without Ag^{I} binding, the reduction potential of **5** should be comparable to that of **2**, in sharp contrast to the fact described above. Note that the OTf^{-} ions bound to Ag^{I} should be prone to be substituted by THF molecules in the THF solution used for the electrochemical measurements. Therefore, the higher reduction potential should be derived from the binding of Ag^{I} ion as a Lewis acid to support the Ag^{I} binding in the proposed structure of **5** as depicted in Scheme 2-1 and Figure 2-13. Thus, we conclude that the Ag^{I} binding to the ONO moiety of PQQTME has a strong impact on the rise of the reduction potential of PQQTME.

The difference of reversibility in the reduction waves between **2** and **5** also can be explained by difference in the coordination modes. Since the Ru^{II} ion in **2** is bound at the ONO coordination site of the PQQTME ligand, the coordination bonds should be strong because of the tridentate chelation and the strong π-acceptability of PQQTME. On the other hand, the Ru^{II} ion of **5** is bonded only with the two quinone-O atoms in a bidentate mode. Although the $1e^{-}$ reduction of **5** strengthen σ-donation from the carbonyl oxygen atoms of the reduced quinone moiety to the Ru^{II} center, the effect should be compensated by reduction of the π-acceptability of the quinone moiety. Thus, the effect of this strengthened σ-donation on reversibility of the redox process is probably limited. Therefore, the reason for the irreversibility of the reduction wave observed for **5** can be ascribed to weakness of the coordination bonds between the Ru(II) center and PQQTME in **5**. In consequence, the difference in the coordination modes between **2** and **5** causes not only difference in the reduction potentials but also that in stability of $1e^{-}$-reduced forms of **2** and **5**.

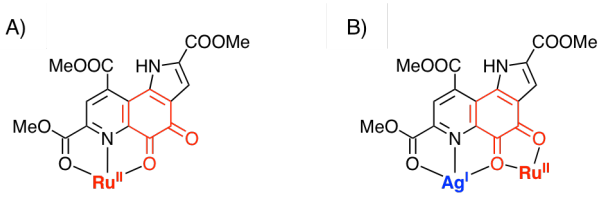

Figure 2-13. Schematic description of the difference of coordination modes between **2** (A) and **5** (B).

2–3–7 UV-Vis Spectra of 2 and 5 to Discuss their Electronic Structures

Complex **2** dissolved in DMF at –20 °C showed absorption bands at 705, 476, 377, and 338 nm (Figure 2-14). The first and the third absorption bands can be assigned to MLCT bands from $d\pi$ orbitals of the Ru^{II} ion to the PQQTME ligand (705 and 377 nm), and the second one can be assigned to another MLCT transition from the Ru^{II} center to the π^* orbitals of the terpy ligand (476 nm), based on comparison with UV-vis absorption bands of **5** (*vide infra*).

UV-Vis spectrum of **5** in DMF at –50 °C showed similar absorption bands to those of **2** at 723, 484, 376, and 318 nm (Figure 2-14). Based on the time-dependent density functional theory (Figure 2-15) calculations of **5**, the first and the third absorption bands can be assigned to MLCT transitions from the Ru^{II} center to the PQQTME ligand (723 and 376 nm) and the second one is ascribed to another MLCT transition from the Ru^{II} center to the terpy ligand (484 nm).[30] The low-energy MLCT absorption band of the Ru^{II}-PQQTME complex indicates the highly stabilized π^* orbital of the PQQTME ligand.

Since the absorption band of **2** in cooled DMF at 377 nm is not intense and hard to be separated from other overlapped absorption bands, the MLCT absorption bands at longer wavelength around 700 nm was used for discussion on the electronic structures of PQQTME in the complexes **2** and **5**. The MLCT band due to the transition from the Ru^{II} center to the PQQTME ligand in **5** around 700 nm (λ_{max} = 723 nm) is red-shifted relative to that of **2** (705 nm), and this tendency is consistent with the order of the electron acceptability of the PQQTME ligand between complexes **2** and **5**. In complex **5**, PQQTME coordinates to not only the Ru^{II} ion but also to the Ag^{I} ion, and thus, the PQQTME ligand in **5** has higher electron acceptability (+0.50 V vs SCE) than that of **2** (+0.28 V vs SCE) as mentioned above. A higher electron acceptability of PQQTME suggests that the PQQTME has a lower LUMO level, and the PQQTME having a lower LUMO level should show lower-energy MLCT absorption bands in the UV-Vis spectra. As mentioned in this section, not only results of electrochemical measurements but also those of UV-Vis measurements indicate that the metal coordination of PQQTME significantly enhances the electron-acceptability of the PQQTME ligand.

2–3–8 Chemical Reduction of 2

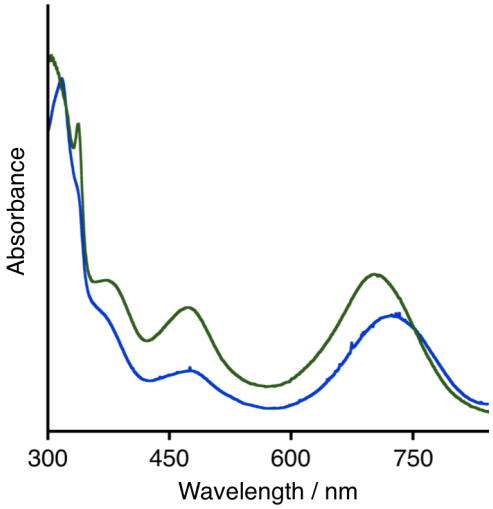

Figure 2-14. Absorption spectra of **2** (at –20 °C, green line) and **5** (at –50 °C, blue line) in DMF.

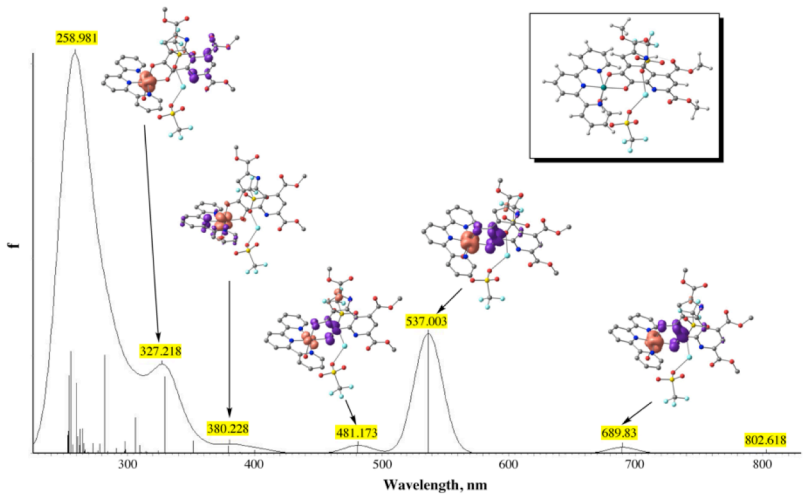

Figure 2-15. A TD-DFT calculated spectrum of **5** (solid line), the calculated excitation energies and oscillator strengths (vertical lines), and the corresponding orbitals related to each absorption band. The assigned transition occurs from a brown-colored orbital to a purple-colored one. Inset: The DFT optimized structure of **5** with an aqua ligand.

To elucidate the characteristics of $1e^-$-reduced **2**, which showed fairly good reversibility in the reduction process (Figure 2-12), the absorption spectra of **2** were measured upon addition of decamethylferrocene (E_{ox} = –0.08 V vs SCE in MeCN) as a reductant.[31] The absorption spectrum of **2** in MeCN at 0 °C under Ar atmosphere exhibited a similar spectrum to that of **2** in DMF and showed the absorption maxima at 374, 441, and 691 nm. The latter two absorption bands are assigned to the MLCT bands from $d\pi$ orbitals of the Ru^{II} ion to the π^* orbitals of the terpy ligand (441 nm) and the PQQTME ligand (691 nm). Upon addition of 1 equiv of decamethylferrocene into the solution of **2** in MeCN at 0 °C, the MLCT band of the Ru^{II} center to the terpy ligand, originally observed at 441 nm, was shifted to 475 nm, and the MLCT bands due to CT from the Ru^{II} center to the PQQTME ligand at 691 nm disappeared, with showing isosbestic points at 405, 458, and 584 nm (Figure 2-16A). Additionally, the original spectrum was recovered by adding tris(4-bromophenyl)-aminium hexachloroantimonate as a $1e^-$ oxidant to the solution of $1e^-$-reduced **2** (Figure 2-16B), indicating that the redox process is highly reversible as expected from the CV of **2** (Figure 2-12). It is assumed that the disappearance of the longer MLCT band should be caused by large rise in the energy level of the LUMO on the $1e^-$-reduced PQQTME ligand. It is also suggested that the $1e^-$ reduction of the PQQTME moiety destabilizes the $d\pi$ level of the Ru^{II} center to cause the red shift of the MLCT band from the Ru^{II} center to the terpy ligand.

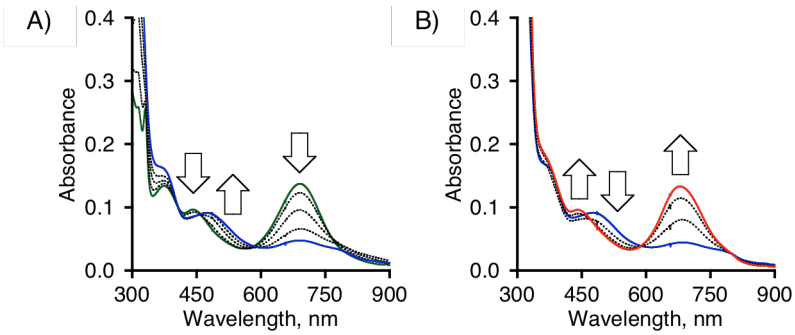

Figure 2-16. UV–vis spectral changes of **2** upon reduction in MeCN at 0 °C. (A) Titration of DecFc (0 (green) – 1 eq (blue)) and (B) re-oxidation with addition of tris(4-bromophenyl)aminium hexachloroantimonate (0 (blue) – 1 eq (red)).

2–3–9 ESR Measurements on Chemically Reduced 2 and 5

The electronic structure of the $1e^-$-reduced species of **2** was investigated by ESR sceptroscopy at 95 K in the frozen MeCN solution, which was prepared by treatment of **2** with decamethylferrocene as a reductant (Figure 2-17A). In the ESR spectrum, a signal was observed at g = 2.006, indicating the formation of a Ru^{II}-bound organic radical, that is, $PQQTME^{\bullet-}$. Kaim and co-workers have reported that the ESR spectrum of a $1e^-$-reduced Ru^{II}-PQQ complex.[17,18] The $1e^-$-reduced **2** showed a similar ESR signal to that of the Kaim's complex and the ESR spectrum of $1e^-$-reduced **2** was also very similar to that of $1e^-$-reduced **5** in frozen THF, also formed by the reaction of **5** with decamethylferrocene as a reductant (Figure 2-17B). Thus, it is concluded that the $1e^-$ reductions of **2** and **5** afford the identical electronic structure, that is, a semiquinone radical anion state of the Ru^{II}-bound PQQTME ligand.

DFT calculations were performed on $1e^-$-reduced **2** to elucidate the electronic structure of the reduced species and the redox properties of the PQQTME ligand in **2**. The calculations suggest that the SOMO of $1e^-$

-reduced **2** shows π^* character and delocalizes over the PQQTME moiety (Figure 2-18A). This result indicates that $1e^-$ reduction of **2** occurs on the PQQTME ligand similarly to that of **5** (Figure 2-18B). The similarity of the SOMOs of **2** and **5** is well matched to the results of the ESR measurements of $1e^-$-reduced **2** and **5**, in which the signals observed are very similar to each other. These results indicate that the difference in coordination modes between **2** and **5** does not affect the electronic structures of the $PQQTME^{\bullet-}$ ligand, despite the fact that it affects the stability of the $1e^-$-reduced species and the electron acceptability, that is, redox potentials of the PQQTME ligand.

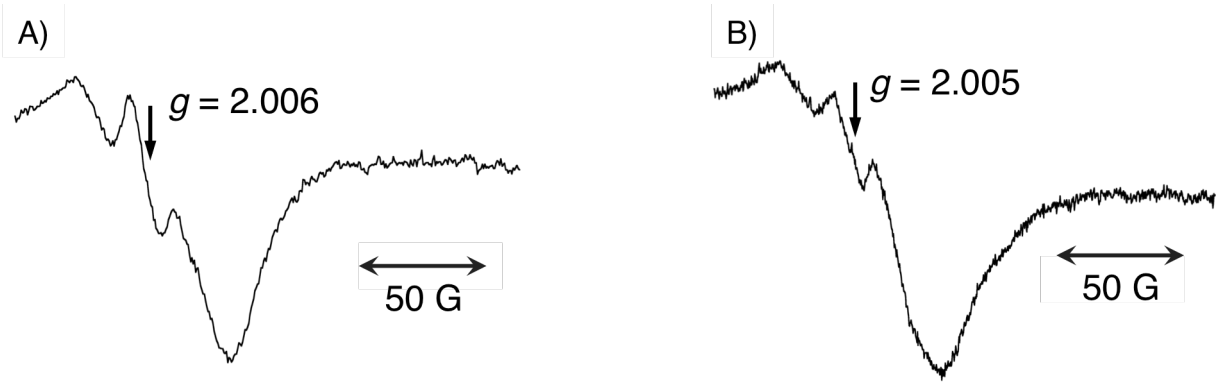

Figure 2-17. (A) An ESR spectrum of $1e^-$-reduced **2**, generated by the chemical reduction of **2** with 1 equiv decamethylferrocene in frozen MeCN at 95 K. (B) An ESR spectrum of $1e^-$-reduced **5**, generated by the chemical reduction of **5** with 1 equiv decamethylferrocene in frozen THF containing 0.1 M $TBAPF_6$ at 140 K.

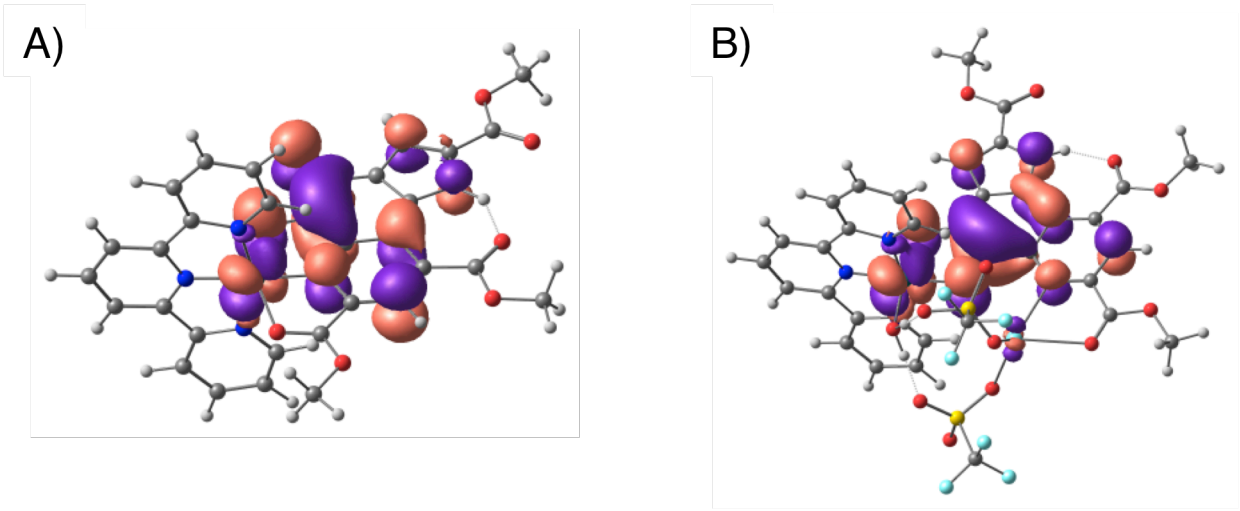

Figure 2-18. DFT-calculated SOMO of $1e^-$ reduced **2** (A) and **5** (B).

2–4 Reactivity of Ruthenium(II)-PQQTME-terpy Complexes

Oxidation reactivity of **2** was investigated in MeCN with use of organic substrates, known to be oxidized by free PQQTME. Benzylamine was added into a green solution of **2** in CD_3CN, and the color of the solution changed immediately to red-brown. However, in the ^1H NMR measurements of the red solution, only signals derived from benzylamine were observed and signals of **2** or other PQQ species did not appear

even in the paramagnetic region (Figure 2-19), and the signals completely agreed with those of the authentic sample of benzylamine in CD_3CN. Hence, under the conditions, it was concluded that only decomposition of **2** occurred and oxidation of benzylamine with **2** was not achieved.

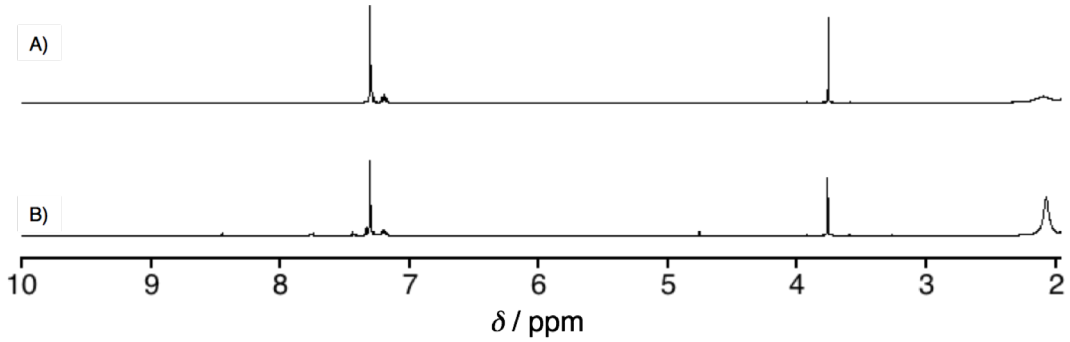

Figure 2-19. ^{1}H NMR spectra of benzylamine (A) and a reaction mixture with **2** and benzylamine (B) in CD_3CN.

When a large excess amount of ethanol (thousands eq) was added to a CD_3CN solution of **2**, no change was observed in the color of the solution and the ^{1}H NMR signals of **2** were intact after stirring the solution for 48 h at room temperature (Figure 2-20). PQQ has been known to form an adduct with an alcohol such as methanol and ethanol; in the adduct the C=O moiety at the 5-position of PQQ undergoes a nucleophilic attack of the alcoholic OH group to form a covalent C-O bond as depicted in Figure 2-4. Since the free PQQTME shows a very small association constant (K = 0.20 M^{-1}) in the adduct formation with ethanol,[6g, 25] it may be reasonable that the adduct formation between **2** and ethanol is not observed. In the PQQTME-calcium complexes, the necessity of the presence of a strong base is known for oxidizing alcohols, and thus DBU (= 1,8-diazabicyclo[5.4.0]undec-7-ene) was added as a strong base into the CD_3CN solution of **2** and ethanol; however, only upfield shifts of the ^{1}H NMR signals of **2** was observed due to deprotonation of its PQQTME ligand from the pyrrolic N-H moiety, and no change appeared in the ^{1}H NMR signals of ethanol (Figure 2-21). Even after a long period of time, the signals of ethanol did not change and the only change observed was derived from slow decomposition of deprotonated **2**. In attempts at the photochemical

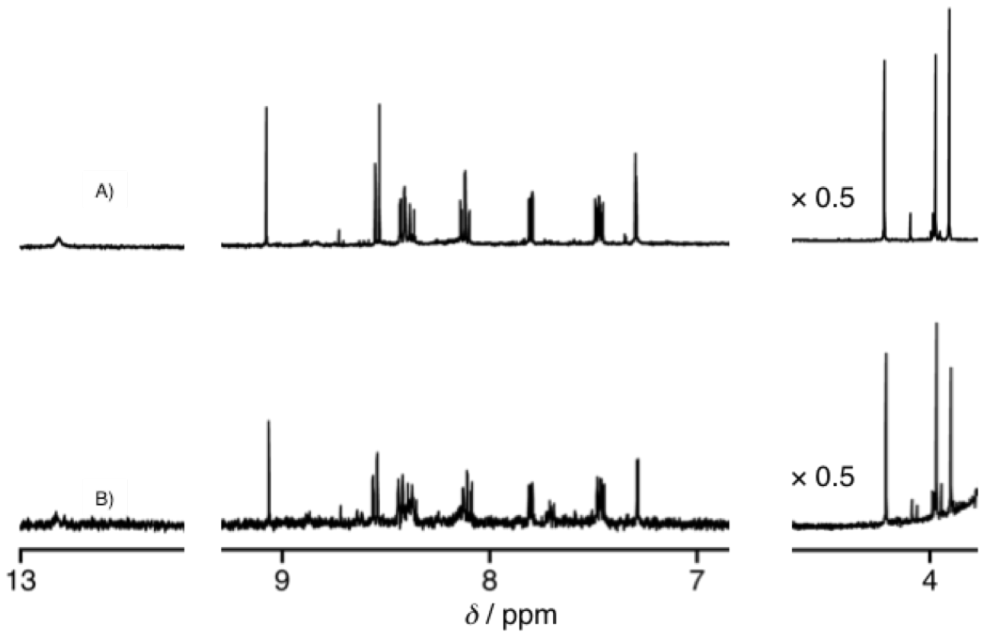

Figure 2-20. ^{1}H NMR spectra of **2** in CD_3CN before (A) and after addition of EtOH (~9000 equiv) (B).

oxidation reactions with **2** under photoirradiation with use of 4-methoxybenzyl alcohol as a substrate, 4-methoxybenzaldehyde was detected as the oxidation product; based on the amounts of the product and complex **2**, the reaction probably proceeded catalytically. However, free PQQTME and $[Ru^{II}(terpy)(MeCN)_3]^{2+}$ were observed in the ^1H NMR and ESI-TOF-MS measurements of the solution after the reaction, and most of **2** decomposed due to photoirradiation for the long time. Hence, it is plausible that the substrate oxidation observed is mainly conducted by the free PQQTME, which is photochemically released from **2**. As described above, complex **2** has never shown clear reactivity for oxidation reactions of organic substrates to date.

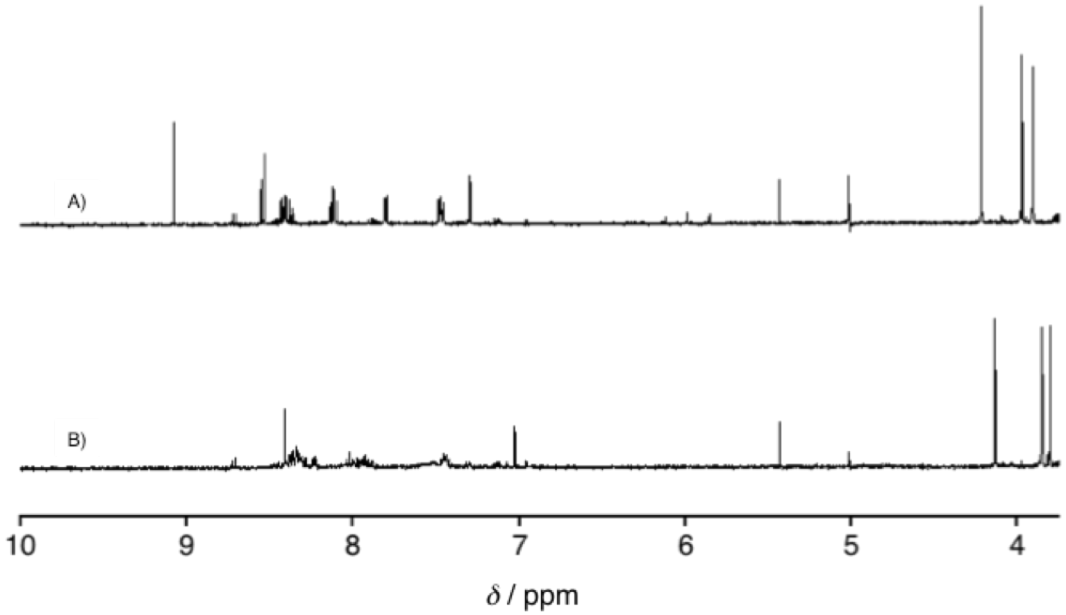

Figure 2-21. ^1H NMR spectra of the mixture of **2** and EtOH (~6000 eq) in CD_3CN before (A) and after addition of DBU (~1000 equiv) (B).

On the other hand, slow oxidation reaction of ethanol proceeded, when DBU and ethanol were added into an CD_3CN solution containing free PQQTME and $[Ru^{II}(terpy)(MeCN)_3]^{2+}$ obtained from thermal decomposition of **2**. In the reaction, a larger amount of acetaldehyde as the oxidation product was observed by ^1H NMR measurements (Figure 2-22) in comparison with the initial amount of **2**, indicating that free PQQTME generated by decomposition of **2** is capable of oxidizing alcohols catalytically even under conditions where substrate oxidation with **2** is not observed. Therefore, the coordination of PQQTME to a ruthenium(II) ion deprives the PQQTME in **2** of reactivity in oxidation of organic substrates.

In light of the results of kinetic analyses reported by Itoh and co-workers,[6] it is assumed that substrate oxidation with PQQ does not proceed through the hydride-transfer mechanism, but through the addition-elimination mechanism, and electrophilicity of the PQQ carbonyl group is necessary for substrate oxidation. As an alternative oxidation reaction pathway, PCET reaction can be considered;[32] however, the electron-acceptability of **2** (+0.28 V vs SCE) is too low to oxidize organic substrates even through a PCET mechanism. Hence there are two possible explanations why the oxidation reactivity of PQQ is lost by its coordination to a ruthenium(II) ion. One is the steric hindrance caused by the terpy ligand to hamper the nucleophilic attacks of substrates on the carbonyl groups of PQQTME. The adduct formation between free

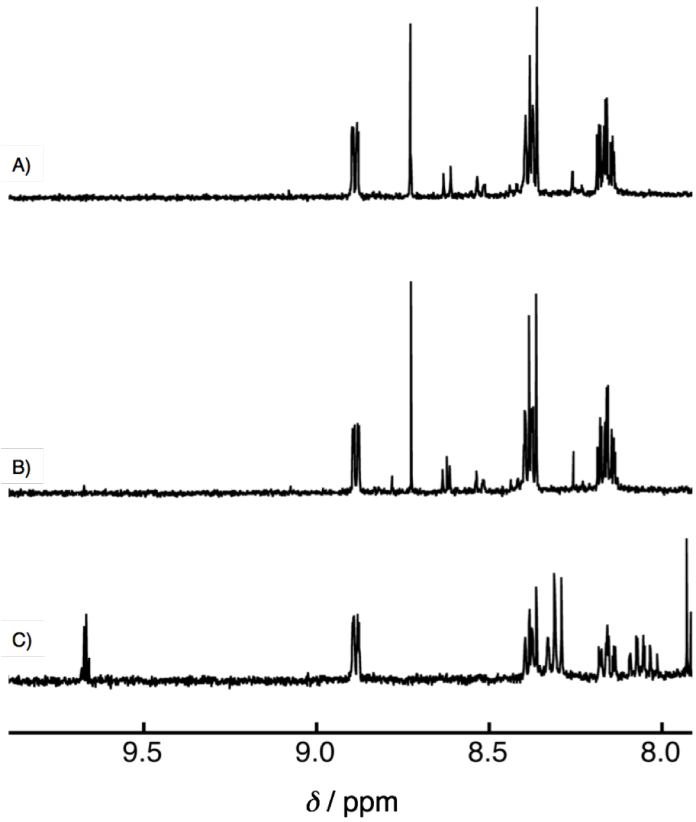

Figure 2-22. ^{1}H NMR spectra of CD_3CN solution containing free PQQTME and $[Ru^{II}(terpy)(MeCN)_3]^{2+}$ obtained from thermal decomposition of **2** (A), after addition of EtOH (~3400 eq) into the solution in A (B), and 6 h later after subsequent addition of DBU (~1000 eq) to the solution in B (C).

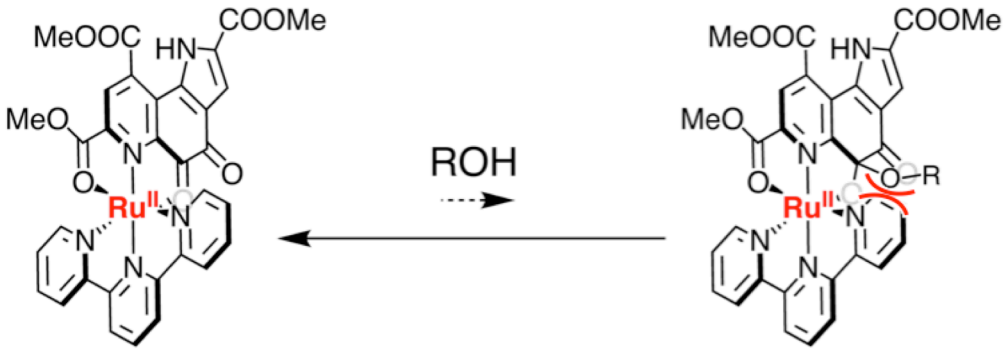

Figure 2-23. Steric hindrance to prevent adduct formation between alcohol and **2** caused by the terpy ligand around the carbonyl groups at the 5-position of the PQQTME ligand in **2**.

PQQTME and substrates is not so favorable; for example, the largest *K* value reported so far is 3.6 M^{-1} for the adduct between the PQQTME-calcium complex and methanol.[6g] Due to the very small *K* values, the substrate oxidation by PQQTME should be essentially very slow. Thus, the steric hindrance caused by the terpy ligand around the carbonyl groups at the 5-position of the PQQTME ligand completely prevents the formation of a covalently bound PQQTME-alcohol adduct (Figure 2-23). Another possible explanation for the inertness of **2** in substrate oxidation is the effect of π-back donation from the ruthenium(II) center to the PQQTME ligand. The π-back donation from the ruthenium(II) center to the π^* orbital on the carbonyl bond reduces the electrophilicity of the carbonyl group, and thus, nucleophilic addition of substrates to the carbonyl group of PQQTME becomes difficult (Figure 2-24). This effect can prevent oxidation reactions by the PQQTME ligand through the addition-elimination mechanism. It is assumed that the second hypothesis

Figure 2-24. (A) π-back donation from ruthenium(II) center to π^* orbital on the carbonyl bond of PQQTME ligand and (B) weakened double bond character of the carbonyl bond by the π-back donation from ruthenium(II) center.

is more rational, because Suzuki and coworkers have reported that their copper(II)-PQQ-terpy complex can oxidize benzylamine catalytically;[15b] this promotion of the oxidation is probably due to the fact that a copper(II) ion is much less effective in π-back donation to π-acidic ligands than a ruthenium(II) ion.

To a solution of **5** in THF containing 0.1 M $TBAPF_6$ was added methanol, and then MLCT band of **5** disappeared in the UV-Vis measurement. However, the difficulty in synthesis of **4** prevents the author from detailed investigation into the color change, thus the reactivity of **5** with methanol has yet to be clarified.

2–5 Conclusion

In this Chapter, the author has described the synthesis and characterization of Ru^{II}-PQQTME complexes. In complexes **1**, **2**, and **3**, the Ru^{II} ion is bound to the PQQTME ligand through the ONO coordination site, whereas the Ru^{II} ion coordinates to the *o*-quinone moiety of the PQQTME ligand in **4** and **5**. The PQQTME ligand in **2** and **5** exhibited higher reduction potentials in comparison with those of PQQ cofactors in natural enzymes and also those of reported metal-PQQ complexes, reflecting the high electron-acceptability of the Ru^{II}-terpy unit. The difference in coordination modes between **2** and **5** causes differences of the physical properties between the complexes. For instance, the difference in the coordination mode causes the difference in stability of the reduced form of **2** and **5**. In addition, the PQQTME moiety in **5** shows a higher reduction potential than that in **2**, despite having the similar electronic structures in their $1e^-$-reduced forms. The difference in the reduction potentials has been revealed to be mainly derived from the Ag^I-ion binding to the tridentate ONO-bay moiety of the PQQTME ligand in **5** as a Lewis acid. This finding is fully consistent with the Ca^{2+}-binding to the same position in the natural enzymes such as methanol dehydrogenases. Unfortunately, complex **2** did not show any reactivity in oxidation of organic substrates such as methanol.

Reference and Notes

(1) Hauge, J. G. *J. Biol. Chem.* **1964**, *239*, 3630.

(2) (a) Mangnusson, O. T.; Toyama, H.; Saeki, M.; Schwarzenbacher R.; Klinman, J. P. *J. Am. Chem. Soc.* **2004**, *126*, 5342. (b) Mangnusson, O. T.; RoseFigura, J. M.; Toyama, H.; Schwarzenbacher, R.; Klinman, J. P. *Biochemistry* **2007**, *46*, 7174. (c) RoseFigura, J. M.; Puehringer, S.: Schwarzenbacher, R.; Toyama H.; Klinman, J. P. *Biochemistry* **2011**, *50*, 1556. (d) Shen, Y.-O.; Bonnot, F.; Imsand, E. M.; RoseFigura, J. M.; Sjölander K.; Klinman, J. P. *Biochemistry*, **2012**, *51*, 2265. (e) Bonnot, F.; Iavarone, A. T.; Klinman, J. P. *Biochemistry* **2013**, *52*, 4667. (f) Klinman, J. P.; Bonnot, F. *Chem. Rev.*, **2014**, *114*, 4343.

(3) Anthony, C. *Biochem. J.* **1996**, *320*, 697.

(4) (a) Davidson, V. L.; Kumar, M. A.; Wu, J. *Biochemistry* **1992**, *31*, 1504. (b) Harris, T. K.; Davidson, V. L. *Biochemistry* **1993**, *32*, 4362. (c) Harris, T. K.; Davidson, V. L. *Biochemistry* **1993**, *32*, 14145. (d) Harris, T. K.; Davidson, V. L.; Chen, L.; Mathews, F. S.; Xia, Z.-X. *Biochemistry* **1994**, *33*, 12600. (e) Davidson, V. L. *Acc. Chem. Res.* **2000**, *33*, 87. (f) Davidson, V. L. *Arch. Biochem. Biophys.* **2004**, *428*, 32.

(5) (a) Oubrie, A.; Rozeboom, H. J.; Kalk, K. H.; Olsthoorn, A. J. J.; Duine, J. A.; Dijkstra, B. W. *EMBO J.* **1999**, *18*, 5187. (d) Oubrie, A.; Dijkstra, B. W. *Protein Science* **2000**, *9*, 1265.

(6) (a) Ohshiro, Y.; Itoh, S.; Kurokawa, K.; Kato, J.; Hirao, T.; Agawa, T. *Tetrahedron Lett.* **1983**, *24*, 3465. (b) Itoh, S.; Kato, N.; Ohshiro, Y.; Agawa, T. *Tetrahedron Lett.* **1984**, *25*, 4753. (c) Itoh, S.; Kato, N.; Mure, M.; Ohshiro, Y. *Bull. Chem. Soc. Jpn.* **1987**, *60*, 420. (d) Itoh, S.; Mure, M.; Ohshiro, Y. *J. Chem. Soc., Chem. Commun.* **1987**, 1580. (e) Itoh, S.; Mure, M.; Ogino, M.: Ohshiro, Y. *J. Org. Chem.* **1991**, *56*, 6857. (f) Itoh, S.; Kawakami, H.; Fukuzumi, S. *J. Am. Chem. Soc.* **1997**, *119*, 439. (g) Itoh, S.; Kawakami, H.; Fukuzumi, S. *Biochemistry* **1998**, *37*, 6562. (h) Itoh, S.; Kawakami, H.; Fukuzumi, S. *J. Mol. Catal. B: Enzymatic* **2000**, *8*, 85.

(7) (a) Rodriguez, E. J.; Bruice, T. C. *J. Am. Chem. Soc.* **1989**, *111*, 7947. (b) Eckert, T. S.; Bruice, T. C. *J. Am. Chem. Soc.* **1983**, *105*, 4431. (c) Zheng, Y.-J.; Xia, Z.-X.; Chen, Z.-W.; Mathews, F. S.; Bruice, T. C. *Proc. Natl. Acad. Sci. USA* **2001**, *98*, 432. (d) Reddy, S. Y.; Bruice, T. C. *J. Am. Chem. Soc.* **2003**, *125*, 8141.

(8) Fukuzumi, S.; Itoh, S.; Komori, T.; Suenobu, T.; Ishida, A.; Fujitsuka, M.; Ito, O. *J. Am. Chem. Soc.* **2000**, *122*, 8435.

(9) Leopoldini, M.; Russo, N.; Toscano, M. *Chem.–Eur. J.* **2007**, *13*, 2109.

(10) (a) White, S.; Boyd, G.; Mathews, F. S.; Xia, Z.-X.; Dai, W.-W.; Zhang Y.-F.; Davidson, V. L. *Biochemistry* **1993**, *32*, 12955. (b) Xia, Z.-X.; Dai, W.-W.; Zhang, Y.-F.; White, S. A.; Boyd, G. D.; Mathews, F. S. *J. Mol. Biol.* **1996**, *259*, 480. (c) Xia, Z.-X.; He, Y.-N.; Dai, W.-W.; White, S. A.; Boyd, G. D.; Mathews, F. S. *Biochemistry* **1999**, *38*, 1214. (d) Ghosh, M.; Anthony, C.; Harlos, K.; Goodwin, M. G.; Blake, C. *Structure* **1995**, *3*, 177.

(11) Oubrie, A.; Rozeboom, H. J.; Dijkstra, B. W. *Proc. Natl. Acad. Sci. USA* **1999**, *96*, 11787.

(12) Oubrie, A.; Rozeboom, H. J.; Kalk, K. H.; Huizinga, E. G.; Dijkstra, B. W. *J. Biol. Chem.* **2002**, *277*, 3727.

(13) Richardson, I. W.; Anthony, C. *Biochem. J.* **1992**, *287*, 709.

(14) Itoh, S.; Kawakami, H.; Fukuzumi, S. *J. Am. Chem. Soc.* **1998**, *120*, 7271.

(15) (a) Suzuki, S.; Sakurai, T.; Itoh, S.; Ohshiro, Y. *Chem*. *Lett*. **1988**, 777. (b) Suzuki, S.; Sakurai, T.; Itoh, S.; Ohshiro, T. *Inorg*. *Chem*. **1988**, *27*, 591.

(16) Nakamura, N.; Kohzuma, T.; Kuma, H.; Suzuki, S. *Inorg*. *Chem*. **1994**, *33*, 1594.

(17) Wanner, M.; Sixt, T.; Klinkhammer, K.-W.; Kaim, W. *Inorg*. *Chem*. **1999**, *38*, 2753.

(18) Schwederski, B.; Kasack, V.; Kaim, W.; Roth, E.; Jordanov, J. *Angew*. *Chem*., *Int*. *Ed*. *Engl*. **1990**, *29*, 78.

(19) (a) Adeyemi, S. A.; Dovletoglou, A.; Guadalupe, A. R.; Meyer, T. J. *Inorg. Chem*. **1992**, *31*, 1375. (b) Katz, N. D. L. D.; Fagalde, F.; Katz, N. E. *Polyhedron* **1995**, *14*, 3111. (c) Czap, A.; Heinemann, F. W.; van Eldik, R. *Inorg. Chem*. **2004**, *43*, 7832.

(20) MacKenzie, A. R.; Moody, C. J.; Roes, C. W. *Tetrahedron* **1986**, *42*, 3259.

(21) Glansdorp, F. G.; Spandl, R. J.; Swatton, J. E.; Loiseleur, O.; Welch, M.; Spring, D. R. *Org*. *Biomol*. *Chem*. **2008**, *6*, 4120.

(22) Carrigan, C. N.; Bartlett, R. D.; Esslinger, C. S.; Cybulski, K. A.; Tongcharoensirikul, P.; Bridges, R. J.; Thompson, C. M. *J. Med*. *Chem*. **2002**, 45, 2260.

(23) Alewood, P. F.; Hussian, S. A.; Jenkins, T. C.; Perkins, M. J.; Sharma, A. H.; Siew N. P. Y.; Ward, P. *J. Chem*. *Soc*., *Perkin Trans. 1* **1978**, 1066.

(24) Taher, D.; Thibault, M. E.; Mondo, D. D.; Jennings, M.; Schlaf, M. *Chem*.*–Eur*. *J*. **2009**, *15*, 10132.

(25) Itoh, S.; Ogino, M.; Fukui, Y.; Murano, H.; Komatsu, M.; Ohshiro, Y.; Inoue, T.; Kai, Y.; Kasai, N. *J. Am*. *Chem*. *Soc*. **1993**, *115*, 9960.

(26) (a) Kojima, T.; Hayashi, K.; Tachi, Y.; Naruta, Y.; Suzuki, T.; Uezu, K.; Shiota, Y.; Yoshizawa, K. *Bull. Chem. Soc. Jpn.* **2005**, *78*, 2152. (b) Kojima, T.; Morimoto, T.; Sakamoto, T.; Miyazaki, S.; Fukuzumi, S. *Chem.–Eur. J.* **2008**, *14*, 8904.

(27) The averages of bond distances of Ru^{II}-OH_2 and Ru^{II}-OH are in the range of 2.10 – 2.16 Å and 1.94 – 2.01 Å, respectively. Selected references: (a) Kobayashi, K.; Ohtsu, H.; Wada, T.; Kato, T.; Tanaka, K. *J. Am. Chem. Soc.* **2003**, *125*, 6729. (b) Yang, X.-J.; Drepper, F.; Wu, B.; Sun, W.-H.; Haehnel, W.; Janiak, C. *Dalton Trans.* **2005**, 256. (c) Durham, B.; Wilson, S. R.; Hodgson, D. J.; Meyer, T. J. *J. Am. Chem. Soc.* **1980**, *102*, 600.

(28) Wen, M.; Munakata, M.; Li, Y.-Z.; Suenaga, Y.; Kuroda-Sowa, T.; Maekawa, M.; Anahata, M. *Polyhedron* **2007**, *26*. 2455.

(29) Liu, Y.; Hammitt, R.; Lutterman, D. A.; Thummel, R. P.; Turro, C. *Inorg. Chem*. **2007**, *46*, 6011.

(30) Suen, H.-F.; Wilson, S. W.; Pomerantz, M.; Walsh, J. L. *Inorg. Chem.* **1989**, *28*, 786.

(31) Fourie, E.; Swarts, J. C.; Chambrier, I.; Cook, M. J. *Dalton Trans.* **2009**, 1145.

(32) PCET reactions are explained in detail in Chapter 1-4 and Chapter 4. See also (a) Culier, C.; Nocera, D. G. *Annu. Rev. Phys. Chem.* **1998**. *49*, 337. (b) Huynh, M. H. V.; Meyer, T. J. *Chem. Rev.* **2007**, *107*, 5004.

Chapter 3 Syntheses and Characterization of Ruthenium(II)- and Rhodium(III)-Pterin Complexes Having Polypyridyl Ligands

3–1 Introduction

Pterins (Figure 3-1A) are redox-active heteroaromatic coenzymes and they perform several biological functions including catalytically active sites in substrate oxidation reactions with use of dioxygen as a sacrificial oxidant.[1] In the oxidation reactions, tetrahydropterin, which is 4e⁻-reduced form of a pterin, at the vicinity of a metal center reacts with dioxygen and a substrate to produce 4a-hydroxy-dihydropterin and oxygenated products of the substrate (Figure 3-1B). In the course of the reaction, dioxygen is 4e⁻-reduced, and the tetrahydropterin and the substrate are 2e⁻-oxidized, respectively. The oxidized pterin,

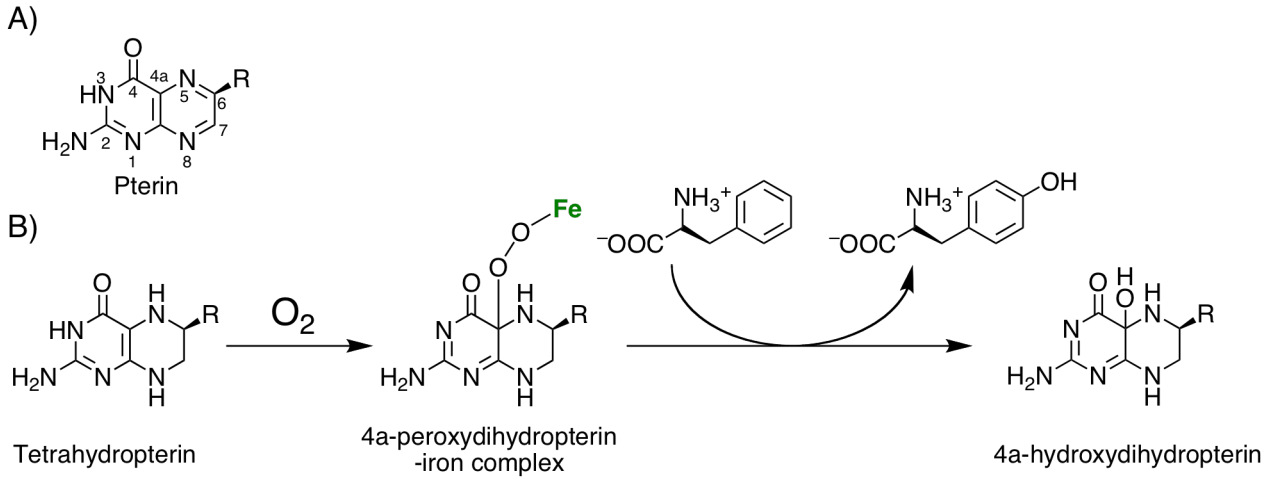

Figure 3-1. Structure of a pterin (A), and one of the proposed reaction mechanisms in the substrate oxidation at the active center of phenylalanine hydroxylase (B).[1]

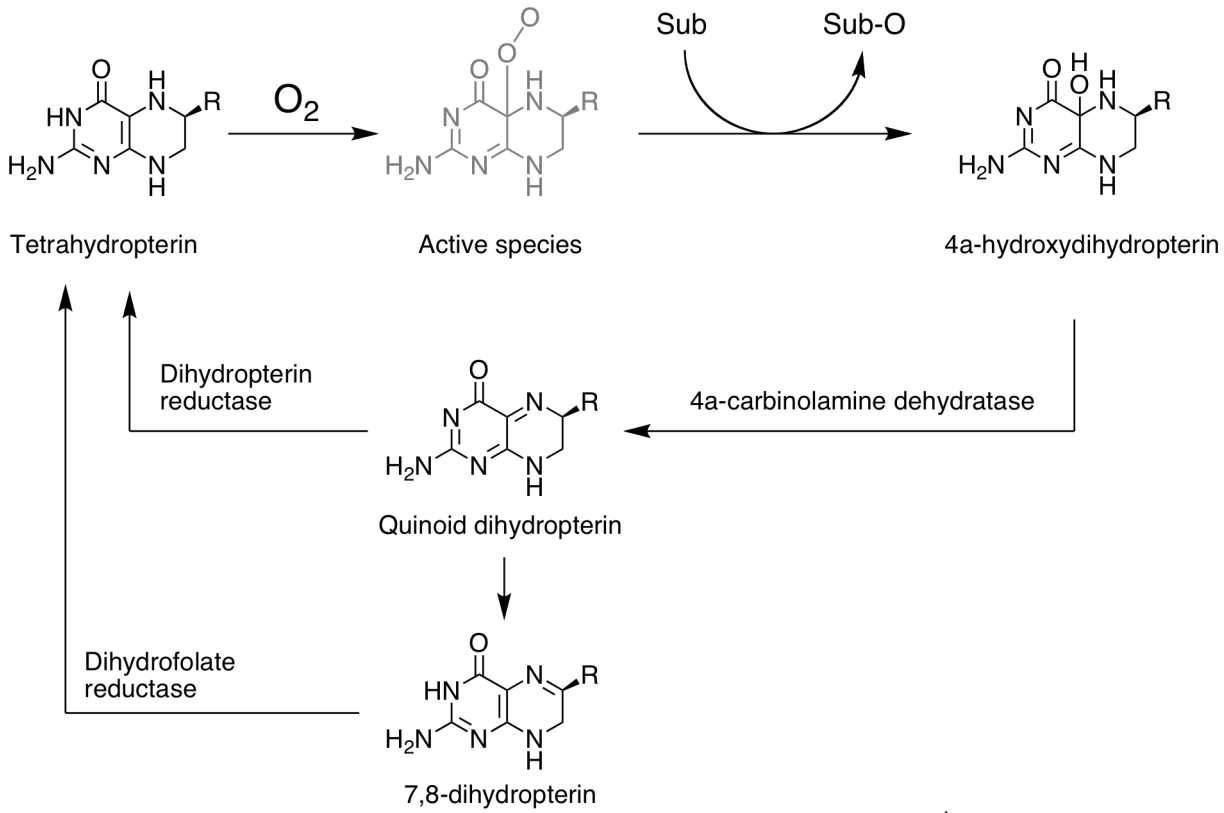

Figure 3-2. A plausible catalytic cycle of substrate oxidation with tetrahydropterin as the catalyst.[1]

4a-hydroxydihydropterin, is dehydrated by enzymes such as pterin-4-α-carbinolamine dehydratase[2] to form a dihydropterin. The generated dihydropterin is directly reduced to regenerate the tetrahydropterin by dihydropterin reductase,[3] or tautomerized to 7,8-dihydropterin. 7,8-Dihydropterin obtained is reduced by dihydrofolate reductase to regenerate the tetrahydropterin (Figure 3-2).[4]

In tetrahydropterin-dependent hydroxylases such as tryptophan hydroxylase,[5] phenylalanine hydroxylase,[6] tyrosine hydroxylase,[7,8] tetrahydropterin in combination with transition-metal ions catalyzes oxidation of aliphatic and aromatic C-H bonds to form C-O bonds, using dioxygen as a sacrificial oxidant. The oxidation reactions catalyzed by tetrahydropterins are frequently used to obtain vital molecules such as serotonin,[5] tyrosine,[6] L-DOPA (= (*S*)-2-amino-3-(3,4-dihydroxyphenyl)propanoic acid),[7] and so on.[8] Despite the fact that the oxidation of non-activated aromatic C-H bonds to C-O bonds is very difficult to achieve in artificial systems, the enzymes perform the oxidation with splendid efficiency, selectivity, and turnover numbers under mild conditions. In the oxidation reactions performed by both heme and non-heme phenylalanine hydroxylase, a pterin-OO-iron complex, in which a peroxide linkage bridges between the 4a position of the pterin and an iron center, is proposed as the most plausible candidate of the active species for

Scheme 3-1. A plausible reaction scheme to obtain target species, a pterin-OO-metal complex.

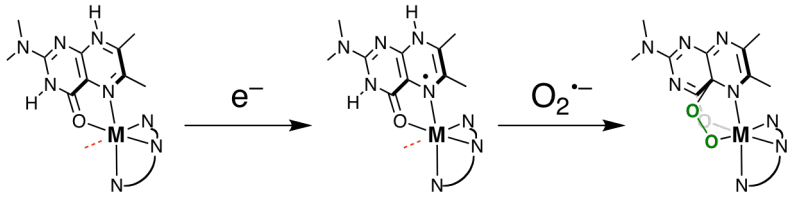

the oxidation reactions based on the detection of 4a-hydroxopterin.[9] The reaction mechanisms of pterin-dependent hydroxylation have yet to be fully elucidated, due to the lack of knowledge on the intermediates. Thus, applications of the oxidation power of pterin-dependent hydroxylases to artificial catalytic oxidation systems have been hardly achieved in spite of its splendid reactivity.

In this chapter, the author describes protonation and PCET processes of ruthenium(II) and rhodium(III) complexes of a pterin derivative (Hdmdmp = 2-(*N*,*N*-dimethyl)-6,7- dimethylpterin), toward the detection and isolation of pterin-OO-metal species. For this purpose, $1e^-$ reduction of protonated pterin complexes and subsequent addition of an $O_2^{\bullet-}$ salt were examined (Scheme 3-1).

3–2 Syntheses of Precursor Complexes and Pterin Complexes

Here, metal-pyridylamine units were adopted as platforms of the deprotonated $dmdmp^-$ ligand, because Kojima and coworkers reported that a ruthenium(II)-TPA-pterin complex has been demonstrated to exhibit high stability upon $1e^-$-reduction of the pterin ligand and clear PCET processes.[10] The TPA ligand, however, does not allow the metal center to form a tridentate peroxo-pterin ligand by a reaction of a bidentate pterin ligand with O_2 or its reduced species; because all of the coordination sites around the six-coordinate metal center are occupied by the tetradentate TPA and the bidentate pterin ligands. Hence, two tridentate polypyridyl ligands, MeBPA (= *N*-methyl-*N*,*N*-bis(pyridylmethyl)amine) and TPMOM (= tris(2-pyridyl)-methoxy-methane) have been employed as ancillary ligands (Figure 3-3) in place of the TPA

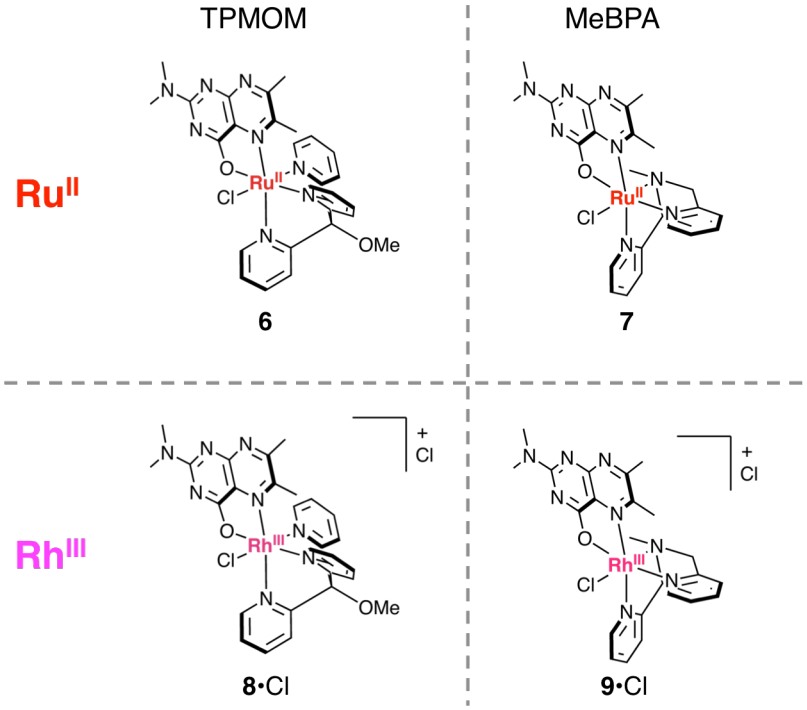

Figure 3-3. Structures of ruthenium(II)- and rhodium(III)-pterin complexes as their non-protonated forms.

ligand to provide a coordination site for accepting the peroxo ligand, as depicted in Scheme 3-1. The pyridine rings of the two ligands have π-acceptability to stabilize the reduced species of the pterin complexes. Additionally, a rhodium(III) ion was also employed as a metal center with an anticipation for stabilization of $1e^-$-reduced pterin by virtue of its higher charge (+3) than that of ruthenium(II).

$[Ru^{III}Cl_3(TPMOM)]$[11] and $[Ru^{III}Cl_3(MeBPA)]$[12] were synthesized based on reported procedures, as precursors to synthesize Ru^{II}-pterin complexes. To obtain precursors for Rh^{III}-pterin complexes, $[Rh^{III}Cl_3(TPMOM)]$ and $[Rh^{III}Cl_3(MeBPA)]$, $Rh^{III}Cl_3 \cdot nH_2O$ and TPMOM or MeBPA were heated in EtOH at reflux; as a result, the crude target complex was obtained in a high yield. The impurities included in the crude products of $[Rh^{III}Cl_3(TPMOM)]$ and $[Rh^{III}Cl_3(MeBPA)]$ were mainly a rhodium salt and the bis-chelate complex, and thus, recrystallization of the crude product from its DMSO solution with addition of 2-propanol as a poor solvent gave pure target rhodium(III) complexes, and the purities of the complexes were confirmed by their elemental analyses and ^{1}H NMR measurements.

Pterin complexes, $[Ru^{II}Cl(TPMOM)(Hdmdmp)]^+$ (**6**-H^+), $[Ru^{II}Cl(MeBPA)(Hdmdmp)]^+$ (**7**-H^+), $[Rh^{III}(dmdmp)Cl(TPMOM)]^+$ (**8**), $[Rh^{III}(dmdmp)Cl(MeBPA)]^+$ (**9**) (Figure 3-3), were synthesized in a procedure as follows; one of the precursor metal complexes, $[MCl_3(L)]$ (M = Ru^{III} or Rh^{III}, L = TPMOM or MeBPA), and Hdmdmp were heated in aqueous EtOH (water : EtOH = 1 : 4 v/v) at reflux overnight. The Ru^{II} complexes, **6** and **7**, were obtained as their protonated forms, whereas the Rh^{III} complexes, **8** and **9**, were isolated as the neutral forms.

3–3 Characterization of Ruthenium(II)- and Rhodium(III)-Pterin-Polypyridyl Complexes

3–3–1 Spectroscopic Analysis on Protonation-Deprotonation Behavior of Pterin Complexes

Ru^{II}-complex **6**-H^+ mainly shows two absorption bands in the UV-Vis region in MeCN and the absorption maxima were observed at 359 and 547 nm (Figure 3-4A, green line). The absorption band at 359 nm is attributed to the MLCT transition from the Ru^{II} center to the pyridine rings, on the basis of past reports on Ru^{II}-TPA complexes: λ_{MLCT} for $[Ru^{II}Cl(TPA)]_2^{2+}$ = 355 nm,[13] λ_{MLCT} for $[Ru^{II}(dmp)(TPA)]^+$ = 383 nm (Hdmp = 6,7-dimethylpterin).[10] Addition of 1 equiv Et_3N as a base into a **6**-H^+ solution in MeCN caused decrease of the absorbance both at 359 and 547 nm, and increase of those at 390 and 489 nm, indicating the formation of **6** by deprotonation (Figure 3-4A). The longer absorption bands of **6**-H^+ and **6**, observed at 547 and 489 nm, respectively, can be assigned to the MLCT transition from the Ru^{II} center to the pterin ligand, because deprotonation of the pterin ligand raises the energy level of the π^* orbital lying on the pterin ligand, and increases the energy required for the MLCT transition. Similar spectral changes derived from deprotonation, where the shorter MLCT band was red-shifted and the longer MLCT band was blue-shifted, were also observed upon deprotonation of $[Ru(Hdmp)(TPA)]^{2+}$ in its MeCN solution.[10]

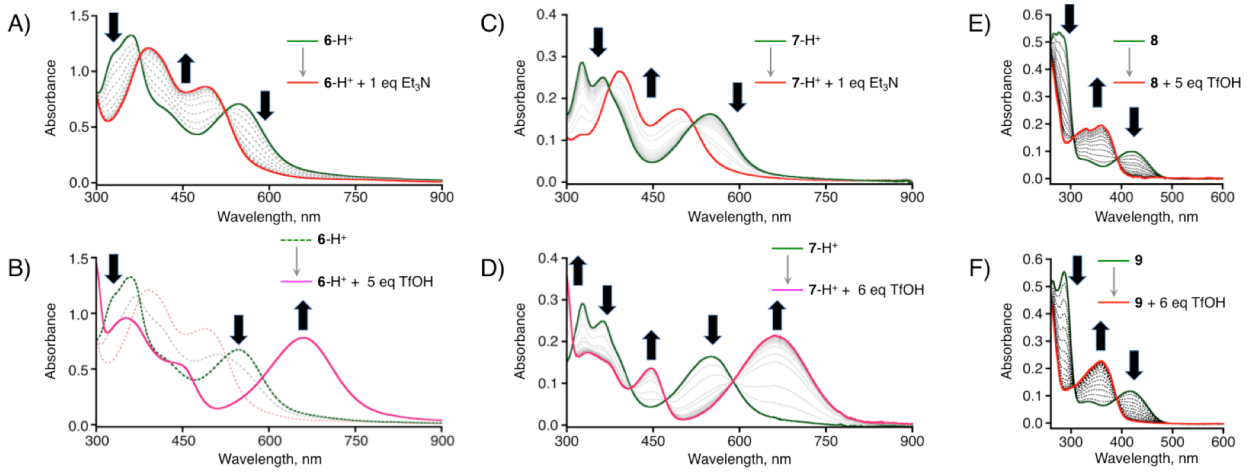

Figure 3-4. Absorption spectral changes in the course of base and acid titration of ruthenium(II)- and rhodium(III)- complexes in MeCN at 296 K: (A) deprotonation of **6**-H^+ upon addition of Et_3N, (B) protonation of **6**-H^+ upon addition of TfOH, (C) deprotonation of **7**-H^+ upon addition of Me_3Py, (D) protonation of **7**-H^+ (17.4 μM) upon addition of TfOH, (E) protonation of **8** upon addition of TfOH, and (F) protonation of **9** upon addition of TfOH.

The absorption spectrum of **6**-H^+ was recovered with addition of 1 equiv of TfOH (= trifluoromethanesulfonic acid) as a strong acid into the solution of **6** in MeCN, which indicates reversibility of the protonation-deprotonation process of **6**. With excessive addition of TfOH, further spectral change was observed; decrease in the absorption bands of **6**-H^+ and increase of the absorbance at 660 nm (Figure 3-4B). The large red-shift of the MLCT band from 547 to 660 nm indicates the formation of **6**-$2H^+$, because the large shift is consistent with lowering the energy level of the π^* orbital lying on the neutral pterin ligand in **6**-H^+ due to its further protonation. The reversibility of the protonation-deprotonation behavior between **6**-H^+ and **6**-$2H^+$ was also confirmed with addition of Et_3N as a base; however, complex **6**-$2H^+$ is relatively unstable in comparison with **6**-H^+. Keeping an MeCN solution of **6**-$2H^+$ at room temperature overnight gave a colorless solution, indicating decomposition of the ruthenium(II)-pterin complex. This instability may arise from the fact that the TPMOM ligand binds to the Ru^{II} center using three π-accepting pyridine moieties to reduce the π-back boding from the Ru^{II} center to the protonated pterin ligand, rather than the fact that the monocationic H_2dmdmp^+ ligand should cause electrostatic repulsion against binding to the monocationic

$[Ru^{II}(Cl)(TPMOM)]^+$ unit. The pK_a value of **6**-H^+ in MeCN was determined by UV-vis titration, in which an MeCN solution of **6**-H^+ was titrated by using 2,4,6-trimethylpyridine (Me_3Py, pK_a of Me_3Py-H^+ = 14.98)[14] as a weaker base than Et_3N (pK_a of Et_3NH^+ = 18.6)[15]. The pK_a value of the first protonation step to form **6**-H^+ was determined to be 15.4 by fitting analysis of the absorbance change at 560 nm (Figure 3-5A). The pK_a values of **6**-$2H^+$ was also determined to be 1.8 base on fitting analysis of the absorbance change at 660 nm in the course the of addition of TfOH (pK_a = 2.60)[16] (Figure 3-4B, 3-5B).

In MeCN, Ru^{II}-complexes **7**, **7**-H^+, and **7**-$2H^+$ show similar protonation-deprotonation behaviors to those of **6** and its protonated derivatives upon addition of acids and bases. Since the basicity of **7** and **7**-H^+ in MeCN are important for discussion on the PCET reaction with $1e^-$-oxidized **7** (See Chapter 4), those were determined by titration experiments with acid or base. The pK_a value of **7**-H^+ in MeCN was also determined by UV-vis titration to an MeCN solution of **7**-H^+, prepared by addition of 1 eq of TfOH into a solution of **7**,

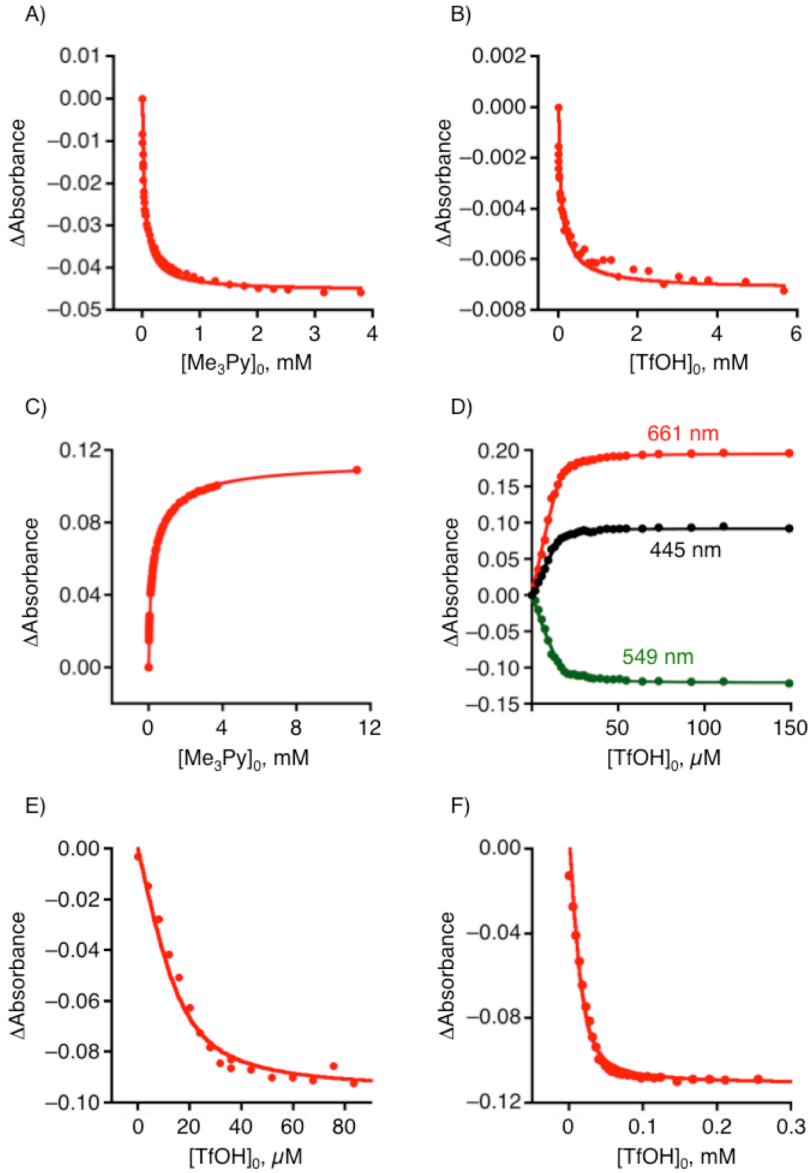

Figure 3-5. Absorbance changes at selected wavelengths in the course of acid-base titration of ruthenium- or rhodium-pterin complexes in MeCN at 296 K and the curve fittings: (A) the deprotonation behavior of **6**-H^+ upon addition of Me_3Py (560 nm), (B) the protonation step of **6**-H^+ upon addition of TfOH (660 nm), (C) the deprotonation behavior of **7**-H^+ upon addition of Me_3Py (530 nm), (D) the protonation step of **7**-H^+ upon addition of TfOH (red: 661 nm, black: 445 nm, green: 549 nm), (E) the protonation step of **8** upon addition of TfOH (420 nm) and (F) the protonation step of **9** upon addition of TfOH (411 nm).

with Me_3Py as a base (Figure 3-4C). In the course of the base titration, the absorption spectrum of **7**-H^+ changed into that of **7**; that is, increase in the absorbance at 392 and 495 nm and decrease in those at 326, 363, and 549 nm were observed with two isosbestic points at 373 and 519 nm, as shown in Figure 3-4C. Additionally, the spectrum of **7** turned back to that of **7**-H^+ again with addition of TfOH as an acid. The pK_a value of the first protonation step to form **7**-H^+ was determined to be 16.4 by fitting analysis of the absorbance change at 530 nm (Figure 3-5C). The UV-vis titration for further protonation of **7**-H^+ was performed with use of TfOH (pK_a = 2.60)[16] as one of the strongest acids in MeCN. The second protonation showed another spectral change with increase in the absorbance at 300, 446 and 663 nm and simultaneous decrease in the absorbance at 326, 363 and 549 nm, implying further protonation of **7**-H^+ (Figure 3-4D). Four isosbestic points were observed at 311, 412, 473 and 588 nm during the second protonation process and reversibility of the change was also confirmed by addition of Et_3N. The pK_a value of the second protonation step of **7** to form the diprotonated form, **7**-$2H^+$, was determined to be 3.9, by fitting analysis of the absorbance change at 594 nm (Figure 3-5D). One of the differences between **6** and **7** is the fact that the diprotonated form of **7** (**7**-$2H^+$) is stable as compared to **6**-$2H^+$. Decomposition of **7**-$2H^+$ was not observed in its MeCN solution even after keeping it for a month. This stability can be attributed to the higher electron density at the ruthenium(II) center in **7** (*vide infra*) than that in **6**. The higher electron density at the ruthenium(II) center in **7** than that of **6** due to the strongly σ-donating tertiary amino group of the MeBPA ligand can compensate the weakened σ-donation from the diprotonated dmdmp ligand, through the π-back donation from the ruthenium(II) center to the H_2dmdmp$^+$ ligand, which should be strengthened by the higher electron density at the ruthenium(II) center. As a result, coordination bonds between the ruthenium(II) center and H_2dmdmp cation are more stabilized in **7**-$2H^+$ relative to those in **6**-$2H^+$. The difference among the acidities of the ruthenium-pterin complexes also can be attributed to the difference of the electron density at the metal center due to that in the coordination environments, three π-accepting pyridines in **6** and two π-accepting pyridines and one σ-donating tertiary amino group in **7**. The pK_a values of ruthenium-MeBPA-pterin complexes (**7**-$2H^+$, 3.9; **7**-H^+, 16.4) are higher than its corresponding ruthenium-TPMOM-pterin complexes (**6**-$2H^+$, 1.8; **6**-H^+, 15.4): The lower electron density at metal center in protonated species of **6** than those of **7** should cause lowering the electron density on the pterin ligand, and the pterin ligand having lower electron density in **6** shows higher acidity than that in **7**.

Protonation behaviors of rhodium(III)-pterin complexes differ from those of ruthenium(II) complexes. Rh^{III}-complex **8** shows an absorption band at 421 nm in MeCN, and addition of 1 equiv of TfOH hardly causes spectral changes. Upon addition of excess amount of TfOH, decease in absorbance at 421 nm was observed, and new absorption bands appeared at 330 and 361 nm (Figure 3-4E). This spectral change exhibited two isosbestic points at 392 and 306 nm and continued until addition of 4 equiv of TfOH. Thus, in comparison with the cases of **6** and **7**, protonation of **8** is hard to proceed; The pK_a value of **8**-H^+ was determined to be 2.8, much lower value than those of **6**-H^+ and **7**-H^+, based on fitting analysis of the absorbance change at 420 nm in the course of the addition of TfOH into **8** solution in MeCN (Figure 3-5E). As a further difference from the ruthenium(II) complexes, complex **8**-H^+ cannot be protonated to obtain the diprotonated complex even in the presence of a large excess amount of TfOH, which is regarded as one of the strongest acid in MeCN (pK_a = 2.60).[16] Complex **9** shows similar protonation behaviors to those observed

for **8** in MeCN; addition of an excess amount of TfOH into a solution of **9** in MeCN causes decrease in absorbance at 411 nm and increase in that at 359 nm, accompanying with two isosbestic points at 307 and 390 nm (Figure 3-4F), and complex **9**-$2H^+$ also cannot be formed even in the presence of a large excess amount of TfOH. The pK_a value of **9**-H^+ was also determined to be 3.4 by fitting analysis of the absorbance change at 411 nm in the course of the addition of TfOH (Figure 3-5F). In the same way as ruthenium-pterin complexes (**6** and **7**), the protonated MeBPA complexes, **9**-H^+, shows higher pK_a value than that of the protonated TPMOM complex, **8**-H^+, indicating that the rhodium center with MeBPA ligand has higher electron density than that of the rhodium center with TPMOM ligand. The differences in the protonation behaviors among ruthenium(II)- and rhodium(III)-pterin complexes can be attributed to the difference in the valence numbers of the metal centers. The rhodium(III) complexes **8** and **9,** which cannot be diprotonated, have a larger valence number at the metal center than that of **6** and **7**, which should interrupt protonation of the Rh^{III}-bound $dmdmp^-$ ligand by decrease in the pK_a value of the pterin ligand. One of other differences between ruthenium(II)- and rhodium(III)-pterin complexes is found in their total charges; complexes **6** and **7** have no charge, whereas complexes **8** and **9** have +1 charge. However, this difference should not be a cause of the difference in their protonation behaviors among the complexes, because $[Ru(dmp)(TPA)]^+$ [10] and $[Ru(dmdmp)(TPA)]^+$ (**10**)[10] can be diprotonated by TfOH in MeCN in spite of their +1 total charges.

3–3–2 ^{1}H NMR Spectra of the Pterin Complexes

In the ^{1}H NMR measurements of the pterin complexes except **7** and its protonated complexes, the pterin

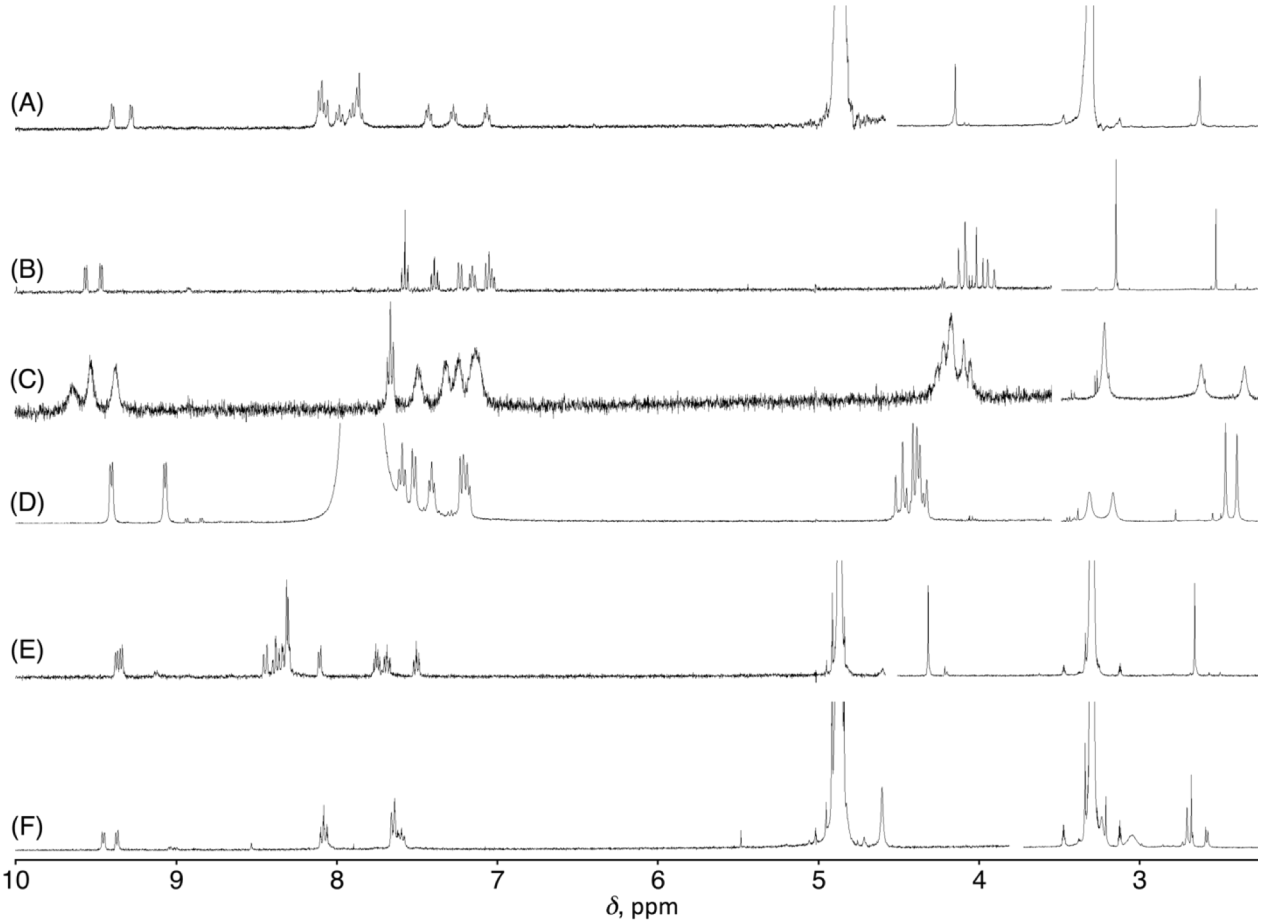

Figure 3-6. ^{1}H NMR spectra of (A) **6**-H^+, (B) **7** with K_2CO_3, (C) **7**-H^+ with $MgSO_4$, and (D) **7**-$2H^+$ with excess amount of TfOH, in CD_3CN and those of (E) **8** and (F) **9** in CD_3OD. The spectrum of **7**-$2H^+$ shows a large and broadened signal around 7.8 ppm, derived from the large amount of the acid added to the solution.

complexes showed distinctive signals in the diamagnetic region, which indicated that the metal centers of these complexes were in the d^6 low-spin state of Ru^{II} or Rh^{III} complexes (Figure 3-6). Except those of **7**-H^+, the ^{1}H NMR signals were assigned by ^{1}H-^{1}H COSY measurements.

In the ^{1}H NMR spectrum of **6**-H^+, a singlet signal was observed at δ 4.15 ppm in the typical range of chemical shifts for methoxy groups, and four doublet and eight triplet signals were observed in the aromatic region (Figure 3-6A). The latter twelve signals were assigned to the signals of three non-equivalent pyridine rings of TPMOM, and this assignment was supported by ^{1}H-^{1}H COSY measurements, and thus, formation of the TPMOM complexes was confirmed. Since signals of four methyl groups of dmdmp were observed in the aliphatic region with expected integration ratios, coordination of the Hdmdmp ligand was also verified. Additionally, the hydrogen atom at the 6-position of one of the pyridine rings in **6**-H^+, which occupied the *trans*-position to the chloride ligand, was shielded by the dmdmp ligand (Figure 3-3), and the ^{1}H NMR signal was highly upfield shifted (δ 7.87 ppm) relative to those of the other two 6-position protons (δ 9.28 and 9.40 ppm), supporting formation of the target structure of **6**-H^+.

Diprotonated complex, **7**-$2H^+$, also showed distinctive signal in the ^{1}H NMR measurement, which was measured by addition of excess amount of TfOH (Figure 3-6D), whereas the ^{1}H NMR signals of **7** and **7**-H^+ were heavily broadened because of a proton exchange at the diprotonated pterin ligand in the presence of moisture from the atmosphere. To solve the broadening problem, anhydrous basic K_2CO_3 as a desiccant was added to the CD_3CN solution of **7** for elimination of water or other protic species (Figure 3-6B). Addition of anhydrous neutral $MgSO_4$ to the solution of **7**-H^+ was also performed for the ^{1}H NMR measurements to give much sharper signals in comparison of those without addition of $MgSO_4$; however, complete sharpness of the signals was not achieved for **7**-H^+ (Figure 3-6C). The ^{1}H NMR signals of pyridine protons in **7** showed downfield shifts by protonation, because the reduction of the electron donation from the pterin ligand by protonation should cause reduction of the electron density at the ruthenium(II) center; the reduction of the electron density at the metal center induces enhancement of donation of the electron density from the MeBPA ligand to cause its deshielding (Figure 3-6). The lowest two signals, however, were upfield-shifted with protonation (**7**: 9.46 and 9.56, **7**-H^+: 9.37 and 9.53, and **7**-$2H^+$: 9.07 and 9.41 ppm). The signals can be assigned to the hydrogen atoms at the 6-position of the pyridine rings in the MeBPA ligand, and the upfield shifts by protonation can be explained by the existence of hydrogen bonding between the chloride ligand and the hydrogen atoms at the 6-position of the pyridine rings. The ^{1}H NMR signals of the hydrogen atoms at the 6-position of the pyridine ring in **7** and its protonated forms showed downfield shifts relative to those at the corresponding positions in other complexes, due to the hydrogen bonding. The protonation at the pterin ligands should induce reduction of the electron density at the Ru^{II} center, and the Ru^{II} center should attract the chloride ligand more closely to compensate the reduction of the electron density, as reflected on the

Scheme 3-2. Effect of protonation on the chemical shifts of the 6-H protons of the MeBPA ligand in **7**

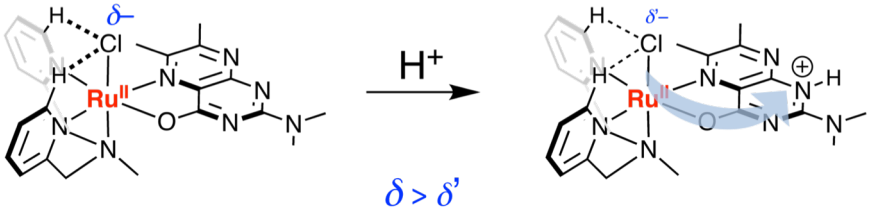

change of the Ru-Cl bond lengths in the crystal structures (Ru-Cl for **7**: 2.437(2) Å, Ru-Cl for **7**-H^+: 2.4220(8) Å, *vide infra*). The relatively electron-poor chloride ligands are expected to form weaker hydrogen bonds with the hydrogen atoms at the 6-positions, which probably cause the upfield shifts of the ^{1}H NMR signals upon protonation of **7** (Scheme 3-2).

In the ^{1}H NMR spectrum of **8** in CD_3OD, similar features to those of **6**-H^+ were observed (Figure 3-6E). Three methyl signals of the dmdmp ligand and twelve aromatic signals of the pyridine rings were observed, and the ^{1}H NMR signal of the hydrogen atom at the 6-position for one of the pyridine rings, which probably occupied the *trans*-position to the chloride ligand, was largely upfield shifted (δ 8.11 ppm), relative to those of the other two 6-position protons (δ 9.34 and 9.37 ppm). This upfield shift is probably derived from the overlapping of the proton on the ring current of the dmdmp ligand as observed for **6**-H^+ (See below). Additionally, almost of all ^{1}H signals for **8** exhibited downfield shifts in comparison to those of **6**-H^+, which derived from increase in the valence number of the metal center from +2 (Ru^{II}) in **6** to +3 (Rh^{III}) in **8**.

The lowest two ^{1}H NMR signals of **9** observed at δ 9.37 and 9.45 ppm are much downfield shifted relative to those of Rh^{III}-polypyridyl complexes; for example, $[Rh^{III}(bpy)_3]^{3+}$ (bpy = 2,2'-bipyridyl) showed the ^{1}H NMR signals at δ 9.04 ppm for the protons at the 6-position of the pyridine rings in CD_3OD.[17] The downfield shifts for the signals of **9** indicate that the 6-position protons of **9** also form hydrogen bonding with the chloride ligand, similarly to those of **7**-H^+. From this viewpoint, the author assumed that complex **9** has the same coordinating structure as that of **7**-H^+.

3–3–3 ESI-TOF-MS Spectra of Pterin Complexes

Formation of **6**-H^+, **7**-H^+, **8**, and **9** were also confirmed by ESI-TOF-MS spectrometry as shown in Figure 3-7. Complexes **6** and **7** are neutral complexes, and thus, these species cannot be directly detected by the mass spectrometry. Complex **6**-H^+ in its acetone solution mainly showed a peak cluster at m/z = 633.2, exhibiting the distribution pattern corresponding to a species having one ruthenium and one chlorine ions (Figure 3-7A). This signal could be assigned to **6**-H^+ (calcd. for $[Ru^{II}Cl(TPMOM)(Hdmdmp)]^+$: m/z = 633.1). A weak peak cluster assignable to [**6**-Na]$^+$ (calcd. for $\{[Ru^{II}(dmdmp)Cl(TPMOM)]^0 + Na\}^+$: m/z = 655.1) was also observed at m/z = 655.1 The formation of **7**-H^+ was also supported by the ESI-TOF-MS spectrum of **7**-H^+ in acetone, which showed peak clusters at m/z = 569.1 (calcd. for [**7** + H]$^+$ ($[Ru^{II}Cl(MeBPA)(Hdmdmp)]^+$): m/z = 569.1) and at m/z = 591.1 (calcd. for [**7** + Na]$^+$ ($\{[Ru^{II}(dmdmp)Cl$-$(MeBPA)]^0 + Na\}^+$): m/z = 591.1) (Figure 3-7B).

In contrast to the ruthenium(II)-pterin complexes **6**-H^+ and **7**-H^+, the mass signals of Rh-complexes do not have characteristic distribution patterns, because Rh atom is composed of one stable isotope (^{103}Rh = 100.00%). The ESI-TOF-MS spectrum of **8** in MeOH showed only one peak cluster at m/z = 633.2, and the distribution pattern of the peak cluster indicated that the ion had one chlorine atom (Figure 3-7C). Thus, the signal can be assigned to [**8**]$^+$ (calcd. for $[Rh^{III}(dmdmp)Cl(TPMOM)]^+$: m/z = 633.1). The ESI-TOF-MS spectrum of **9** in MeOH also showed a peak cluster at m/z = 569.1, assignable to the signal of [**9**]$^+$ (cacld. for $[Rh^{III}(dmdmp)Cl(MeBPA)]^+$: m/z = 569.1) (Figure 3-7D).

3–3–4 Crystal Structures of 7 and 7-H^+

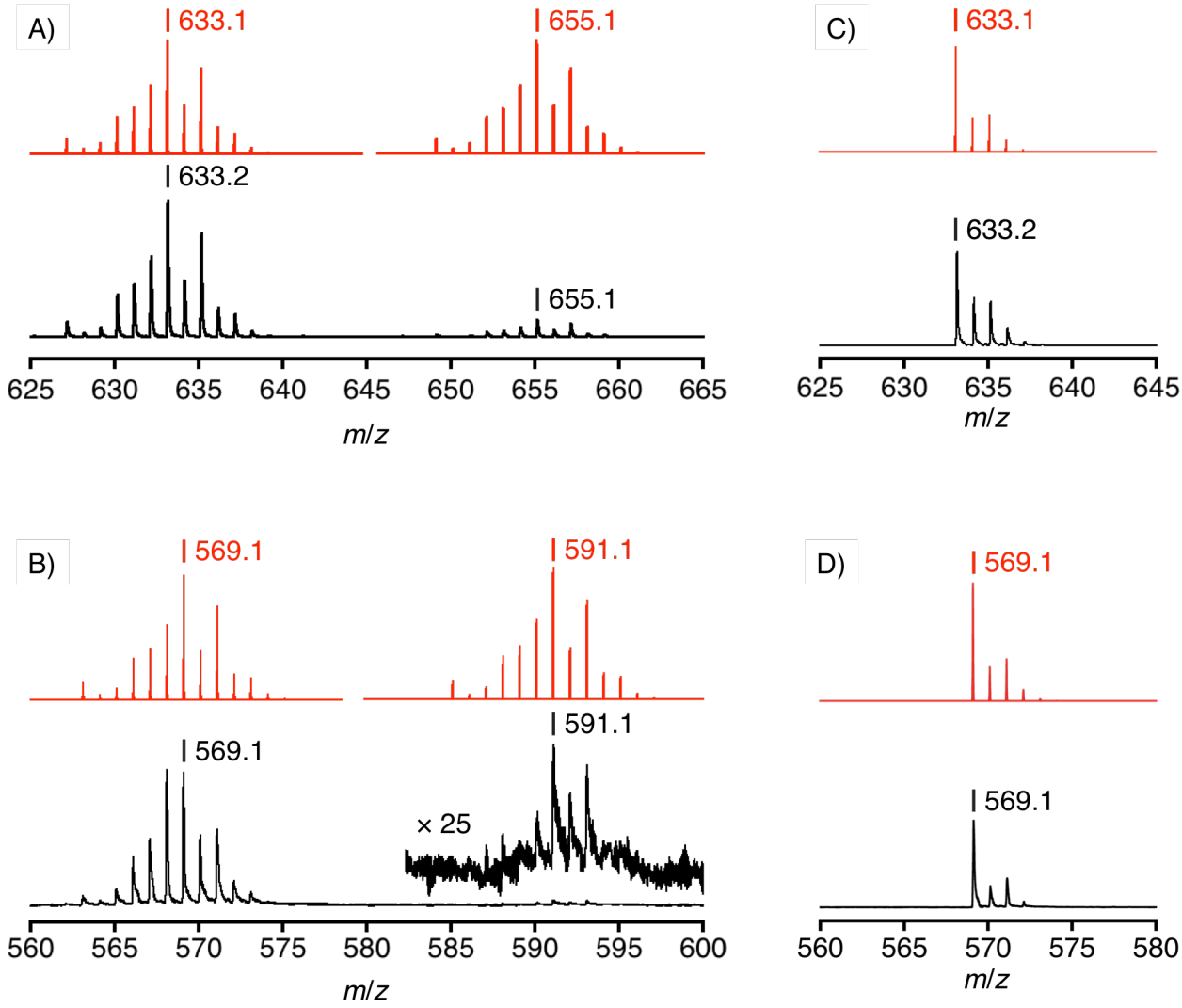

Figure 3-7. ESI-TOF-MS spectra of **6**-H^+ (A) and **7**-H^+ (B) in acetone and those of **8** (C) and **9** (D) in MeOH. Observed spectra: black traces, and their simulations: red traces.

Single crystals of **7** and (**7**-H^+)·PF_6 suitable for X-ray crystallography were obtained by slow concentration of their solutions in CD_3CN and $(CD_3)_2CO$, respectively, through vaporization of the solvents. Crystal structures of **7** and **7**-H^+ are shown in Figure 3-8 with the atom labeling. The geometries around the Ru^{II} ions of **7** and **7**-H^+ are octahedral with slight distortion as a typical coordination structure of a Ru^{II} complex bearing 5-membered chelate rings. The bond lengths around the Ru centers fall in the typical range of those of Ru^{II} complexes.[18] As described above, the pterin ligand of **7** can accept a proton relatively easily at one of the nitrogen atoms, and hence the crystal structures of **7** and **7**-H^+ were distinguished based on the number of counter anions included in the crystal structure. The crystal of **7** contained no counter ion, whereas the crystal of **7**-H^+ did one PF_6^- per one Ru-pterin-MeBPA moiety. The deprotonated dmdmp$^-$ ligand has two possible resonance forms as shown in Scheme 3-3, *amidate* and *imidate* forms. The pterin ligand of **7** can be considered as in between the *imidate* form and the *amidate* one. The bond length of C2-O1 (1.273(6) Å) is longer than those of carbonyl C=O bonds (1.20 – 1.23 Å)[19] and shorter than those of a phenolic C-O single bond (*ca.* 1.36 Å)[19] and the bond length of C2-N2 (1.343(9) Å) is shorter than those of C-N single bonds found in the MeBPA ligand (1.49 – 1.52 Å) and rather close to those found in the pyridine

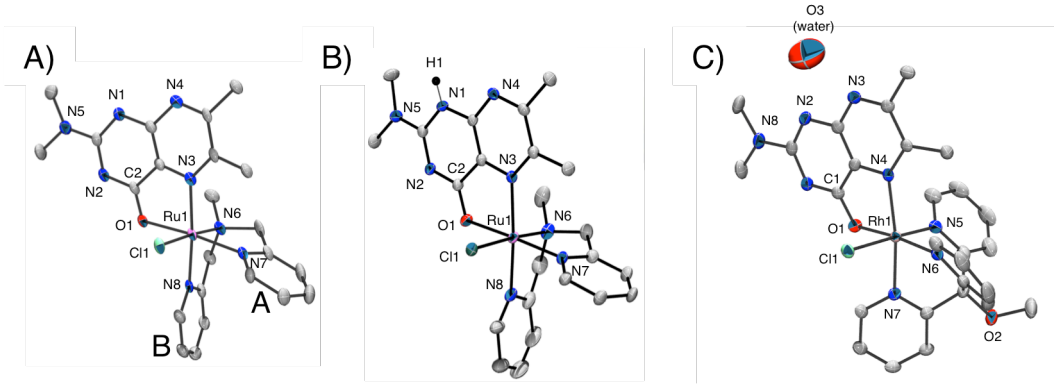

Figure 3-8. ORTEP drawings of (A) **7**, (B) **7**-H^+·PF_6 and (C) **8**·Cl with thermal ellipsoids at the 50% probability level. The hydrogen atoms in (A) – (C) and the counter ions in (B) and (C) are omitted for clarity. A hydrogen-bonded water molecule is shown in (C). Pyridine rings of **7** are labeled as "A" and "B" to clarify assignments of ^{1}H NMR signals in the experimental section. Ru-Cl for **7**: 2.437(2) Å, Ru-Cl for **7**-H^+: 2.4220(8) Å, Rh-Cl for **8**: 2.332(1) Å.

Scheme 3-3. Two resonance forms and an anion-delocalized form of Ru^{II}-dmdmp complexes

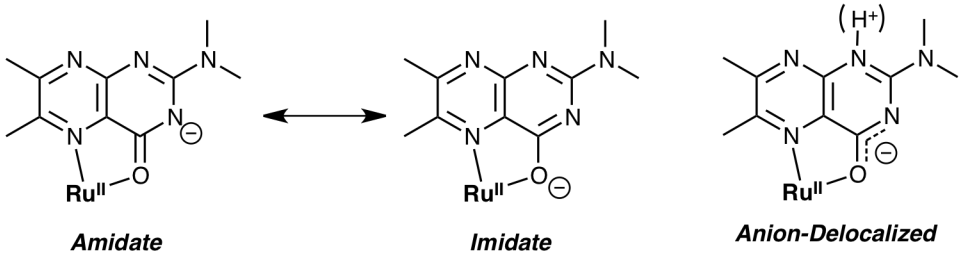

rings of MeBPA (1.34 – 1.36 Å). On the other hand, in the crystal structure of **7**-H^+, the N1 atom of a molecule and Cl1 atom of another molecule are close to each other, which indicates that there is hydrogen bonding between them (N1···Cl1: 3.285(2)Å) (Figure 3-9). Thus, the pterin ligand of **7**-H^+ in the crystal is protonated at the N1 atom (formally at the 1-position in the pteridine skeleton). The pterin ligand of **7**-H^+ was also recognized to be in between the *imidate* form and the *amidate* one as observed in **7**, on the basis of the bond lengths of C2-O1 (1.261(4) Å) and C2-N2 (1.340(3) Å). Thus, regardless of the protonation of N1 nitrogen, the pterin ligands in **7** and **7**-H^+ are in the *anion-delocalized* form as shown in Scheme 3-3.

As a difference between the crystal structures of **7** and **7**-H^+, the bond length of Ru-N3 was slightly elongated with protonation (Ru-N3 for **7**: 2.064(4) Å, Ru-N3 for **7**-H^+: 2.078(2) Å). This elongation should be derived from reduction of electron-donating ability of the pterin ligand due to its protonation, which

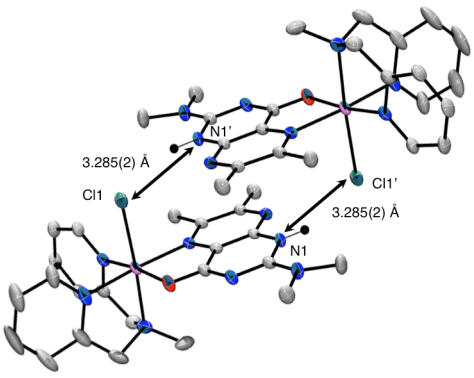

Figure 3-9. Hydrogen bonding between the chloride ligand of a cationic moiety and N1-H of another cationic moiety, observed in the crystal structure of **7**-H^+·PF_6. Counter ions were omitted for clarity.

causes the charge neutralization of the pterin ligand. In contrast, the bond length of Ru-Cl was shortened upon protonation (Ru-Cl for **7**: 2.437(2) Å, Ru-Cl for **7**-H^+: 2.4220(8) Å), because the electron donation from the pterin ligand to the Ru^{II} center was reduced due to the protonation. To compensate the reduced electron density, the Ru^{II} center attracts the chloride ligand more strongly. In both crystal structures of **7** and **7**-H^+, steric repulsion was recognized between the pyridine ring containing N7 atom in the MeBPA ligand and the methyl group at the 6-position of the pterin ligand. As a result of the steric repulsion, the bond angles of N3-Ru-N7 became larger than 90° (∠N3-Ru-N7 for **7**: 106.3(2)°, ∠N3-Ru-N7 for **7**-H^+: 103.81(9)°). Although the two donating ligands, the π-donating chloride and σ-donating tertiary-amine ligands, bind at the *trans* positions to each other in **7** and **7**-H^+, the structures should be stabilized by intramolecular hydrogen bonding among the chloride ligand and the hydrogen atoms at the 6-positions of the pyridine rings of MeBPA. In the crystals of **7** and **7**-H^+, the distances between the chloride ligand and the carbon atoms at the 6-positions of the two pyridine rings in the MeBPA ligand are 3.372(6) Å and 3.345(7) Å for **7**, and 3.337(4) Å and 3.353(3) Å for **7**-H^+, respectively. The distances are in the normal range (3.3 – 3.7 Å) of the distances between chloride and carbon atoms having non-classical hydrogen bonding.[20] The ^{1}H NMR spectra of **7** and **7**-H^+ in CD_3CN also exhibited downfield shifts due to the hydrogen bonding (see above). Additionally, in the crystal structure of $[Ru^{III}Cl_3(EtBPA)]$,[12] which resembles to the synthetic starting material of **7**, similar hydrogen bonding was observed between one of the chloride ligands, located at the *trans* position of the tertiary-amine nitrogen atom of the EtBPA ligand, and the C-H bond at the 6-position of the pyridine rings of the EtBPA ligand, judging from the C···Cl distances: 3.224(4) and 3.263(5) Å.[12] The hydrogen bonding in the Ru^{III} complex of the starting material probably makes the chloride ligand *trans* to the tertiary-amino nitrogen more inert against ligand-substitution reaction than the other two chloride ligands. Furthermore, the hydrogen bonding in **7** can cause its higher thermal stability compared to other possible isomers, having different coordination arrangements.

3–3–5 Crystal Structure of 8

A single crystal suitable of **8**·Cl for X-ray crystallography was obtained by slow concentration of its CH_2Cl_2 solution through vaporization of the solvent. A crystal structure of the cationic part of **8**·Cl with the atom labeling is shown in Figure 3-8C, which contains a hydrogen-bonded water molecule. The geometry around the Rh^{III} ion of **8** is octahedral with slight distortion as a typical coordination structure of a Rh^{III} complex bearing 5-membered chelate rings and the bond lengths around the metal center fall in the typical range of those of Rh^{III} complexes. As proposed in the ^{1}H NMR measurements of **8** (Chapter 3-3-2), a hydrogen atom at 6-position of the pyridine ring locating at the *trans* position to the chloride ligand is shielded by the dmdmp ligand, as can be seen in the crystal structure (Figure 3-8C). The N3 atom of **8** and the O3 atom of a co-crystallized water molecule form a hydrogen bond, judging from the short distance between N3 and O3 atoms (N3···O3: 3.018(9)Å) (Figure 3-8C).

The bond length of C1-O1 (1.293(4) Å) is close to the bond length of the corresponding C-O bonds in the crystal structures of **7** (1.273(6) Å) and **7**-H^+ (1.261(4) Å), and shorter than those of a phenolic C-O single bond (*ca.* 1.36 Å).[19] Judging from the C-O and C2-N1 bond lengths (1.362(5) Å), the dmdmp ligand in **8** is also in between the *imidate* form and the *amidate* one, *i. e.*, an *anion-delocalized* form as observed in

Ru^{II}-pterin complexes.[10] The bond length between the chloride ligand and the Rh^{III} center is shorter than those of the Ru^{II}-complexes, **7** (2.437(2) Å) and **7**-H^+ (2.4220(8)) Å), which is reasonable due to the smaller ionic radius of Rh^{III} than that of Ru^{II}. Comparison of bond lengths between its metal center and dmdmp ligand of **8** with those of **7** or with those of **7**-H^+ may contribute to exploration to the influence of the electron density at the metal center on the electronic structure of the pterin ligand; however, the coordination structures of the dmdmp ligands in **7** and **7**-H^+ are distorted by steric repulsion between one of the pyridine rings of MeBPA and one of the methyl groups of the dmdmp ligand (See above). Therefore, detailed discussion on the difference among these bonds lengths is not made in this study.

3–3–6 Electrochemical Measurements of the Pterin Complexes

As mentioned above, formation of $1e^-$-reduced species of the pterin complexes is necessary to obtain the target species, pterin-OO-metal complexes. Thus, electrochemical measurements of the pterin complexes were performed to reveal their reduction behaviors in MeCN containing 0.1 M $TBAPF_6$ as an electrolyte at

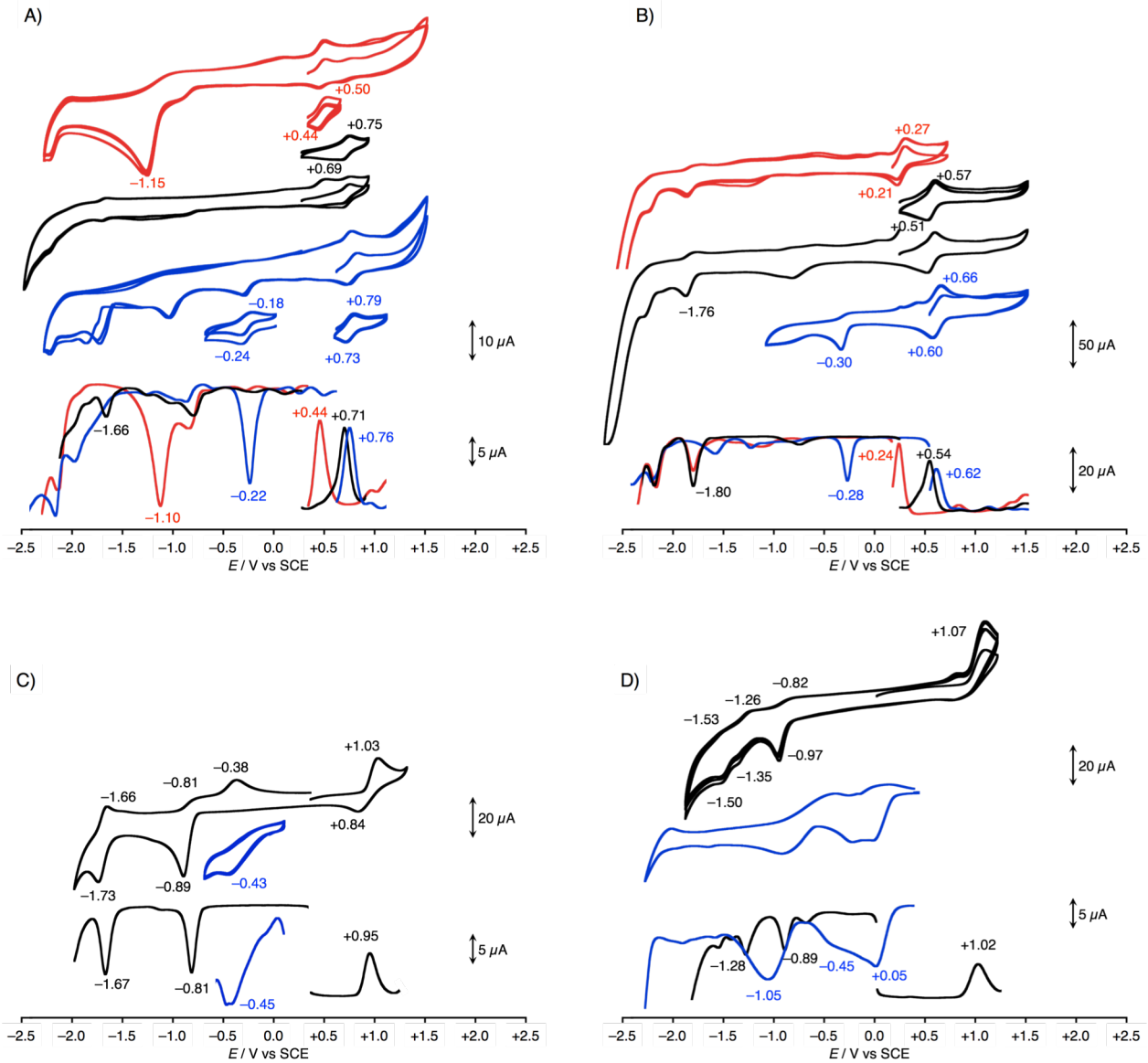

Figure 3-10. CVs and DPVs of the pterin-complexes. (A) **6** (red), **6**-H^+ (black), and **6**-$2H^+$ (blue). (B) **7** (red), **7**-H^+ (black), and **7**-$2H^+$ (blue). (C) **8** (black), and **8**-H^+ (blue); (D) **9** (black), and **9**-H^+ (blue).

room temperature.

At first, the oxidation behaviors of the Ru^{II}-pterin complexes were investigated (Figure 3-10 and Table 3-1). All of the ruthenium(II)-pterin complexes show a reversible wave, assigned to reversible $1e^-$ oxidation process at the ruthenium center for the Ru^{II}/Ru^{III} redox couple, regardless of its protonated states at the pterin ligand. In comparison of the first oxidation potentials (E_{OX}) among **6**, **7**, and their protonated complexes, and ruthenium-TPA-dmdmp complexes (**10** and its protonated forms), insights into the electronic interaction between the metal center and the pterin ligand were gained as mentioned below. The first protonation of the pterin ligand causes a large positive shift of $E_{OX}(Ru^{II}/Ru^{III})$, which indicates that the protonation of the pterin moiety reduces the electron density of the ruthenium center. The second protonation also raises the potential, but the degrees of the rise on the potentials are not so large as compared to that by the first protonation (ΔE by the first protonation, ~0.3 V; ΔE by the second protonation, < 0.1 V). The difference in the impact on $E_{OX}(Ru^{II}/Ru^{III})$ between the first and second protonation steps indicates that the first protonation more significantly reduces the electron density at the ruthenium center than the second protonation. In the UV-Vis spectra of **6**, **7**, **10** and their protonated forms, both of the first and second protonation caused red-shifts of the absorption bands due to MLCT transitions from the Ru^{II} center to the pterin ligand in similar degrees (See Chapter 3-3-1). Therefore, both of the first and second protonation lower the energy levels of π^*-orbitals of the Hdmdmp and H_2dmdmp$^+$ ligands, respectively, as compared to that of the dmdmp$^-$ ligand; however, in the case of the second protonation, the compensation of the electron density at the metal center by other ligands is probably strong, and thus, the $E_{OX}(Ru^{II}/Ru^{III})$ values are not so altered between the mono-protonated and diprotonated complexes.

Table 3-1. Redox Potentials (V vs SCE) of the Ru^{II}- or Rh^{III}-Pterin Complexes in MeCN

Complex	$E_{OX}(Ru^{II}/Ru^{III})$	E_{RED}(dmdmps)	$E_{RED}(Rh^{III}/Rh^{I})$
6	+0.44	not observed	—
6-H$^+$	+0.71	–1.66*	—
6-2H$^+$	+0.76	–0.22	—
7	+0.24	not observed	—
7-H$^+$	+0.54	–1.80*	—
7-2H$^+$	+0.62	–0.28*	—
8	—	–1.67	–0.81*
8-H$^+$	—	–0.45*	–1.05*
9	—	not observed	–0.89*
9-H$^+$	—	–1.05*	–0.39*
10 [a]	+0.66	–1.68	—
10-H$^+$ [a]	+0.92	–0.99*	—
10-2H$^+$ [a]	+0.94	–0.26	—

*: irreversible redox processes, whose potentials were determined with the DPV peaks. [a] ref. 10.

Comparing the the $E_{OX}(Ru^{II}/Ru^{III})$ values of **6**, **7** and **10** with those of the corresponding species protonated at the dmdmp ligand, the values can be arranged in the order as follows; **10** > **6** > **7**. The order of $E_{OX}(Ru^{II}/Ru^{III})$ is reasonable in the light of the coordination structures of the ruthenium-pterin complexes. Besides dmdmp$^-$, all of the three ruthenium-complexes have pyridine rings, a tertiary amine, and/or a chloride ion as ligands. Pyridine rings are a neutral ligand and known for its strong π-acceptability from the ruthenium(II) center, and a chloride ion is regarded as a strong π-donating ligand with the –1 charge. Based on the characteristics, the coordination of a tertiary amine increases the electron density at the ruthenium

center, in comparison with that of a pyridine ring, and the chloride ion much more increases the electron density at the ruthenium center with use of its π-donating character and negative charge. Hence, the electron density at the ruthenium center in **7** is higher relative to that in **6**, because complex **7** has a tertiary amino nitrogen coordinating to the Ru^{II} center instead of a pyridine ring in comparison to the structure of **6**. On the other hand, the electron density at the ruthenium center in **6** is higher relative to that in **10**, because complex **6** has a chloride ligand coordinating to the Ru^{II} center instead of a tertiary amino nitrogen in comparison to the structure of **10**. In consequence, the order of $E_{OX}(Ru^{II}/Ru^{III})$ among **6**, **7** and **10** is recognized as mentioned above. In the electrochemical measurements of the rhodium-pterin complexes, no oxidation waves were observed except for that of oxidation of the Cl^- ion serving as a counter ion for **8** and **9**.

To obtain the target compound, a pterin-OO-metal species, a reversible reduction process of the pterin ligand is indispensable, because the target species can be obtained with the reaction of the $1e^-$-reduced pterin species with a $O_2^{\bullet-}$ ion (Scheme 3-1). In the previous report,[10] the first reduction processes of the pterin ligands in **10** and its diprotonated forms were revealed to be reversible, whereas $1e^-$-reduction of the monoprotonated complex of **10** was irreversible due to a proton-shift from the N1 position to the N8 position in the pterin framework, induced by the reduction.[21] However, except **6**-$2H^+$, all of the pterin complexes synthesized in this research, having one of the tridentate ligands, did not show reversible reduction behaviors. Non-protonated Ru^{II} complexes, **6** and **7**, and the monoprotonated complexes, **6**-H^+ and **7**-H^+, showed irreversible reduction waves in their electrochemical measurements (Figure 3-10). One of the most important differences found among **6**, **7**, and **10** is the electron density at the ruthenium(II) center, as exemplified by the $E_{OX}(Ru^{II}/Ru^{III})$ values; **6**: +0.44 V, **7**: +0.24 V, **10**: +0.66 V vs SCE. This difference probably gives impacts on the stability of the reduced pterin species; as mentioned in Chapter 1-5, the positive charge of the metal center stabilizes the reduced form of the pterin ligands. Therefore, due to their higher electron densities at the ruthenium(II) centers in **6** and **7** than that in **10**, the ruthenium(II) centers of **6** and **7** cannot sufficiently cancel out the negative charge of $1e^-$-reduced pterin species and cannot stabilize them.

The diprotonated complex **7**-$2H^+$ also did not show any reversible reduction processes on the pterin ligand, whereas complex **6**-$2H^+$ showed a reversible reduction process at –0.22 V in the CV measurement as shown in Figure 3-10A (blue trace). This difference in the reversibility of the reduction process between **6**-$2H^+$ and **7**-$2H^+$ can be also attributed to the difference in the electron density at the ruthenium center between **6**-$2H^+$ and **7**-$2H^+$; the $E_{OX}(Ru^{II}/Ru^{III})$ values of **6**-$2H^+$ (+0.76 V vs SCE) and **7**-$2H^+$ (+0.62) indicate that the electron density at the ruthenium center in **6**-$2H^+$ is lower than that in **7**-$2H^+$. As mentioned in Chapter 1-5 and in discussion about the irreversibility in the reduction processes of **6** and **7** (see above), the positive charge at the metal center is expected to cancel the negative charge of the reduced ligand and resultantly stabilize the ligand-reduced species. Therefore, the electron density at the ruthenium center in **6**-$2H^+$ is assumed to be low enough to stabilize the reduced pterin species in the coordination sphere, while that in **7**-$2H^+$ is too high to stabilize the reduced pterin species.[22]

On the other hand, in electrochemical measurements of the non-protonated rhodium(III) complexes, **8** and **9**, in MeCN, the rhodium(III) center is firstly reduced and the process is highly irreversible as a typical behavior of rhodium(III) complexes.[25] The irreversibility of the redox process at the Rh^{III} center prevents discussion on the reduction process of the Rh^{III}-pterin complexes in detail. Even after protonation of **9**, the

first reduction proceeded not on the dmdmp ligand but at the rhodium(III) center (Table 1). For the electrochemical measurement of **8**-H^+, a reduction wave was observed at –0.45 V vs MeCN. A reduction process of rhodium(III)/rhodium(I) in rhodium(III)-polypyridyl complexes is known to generally show a typical wave shape in the CV;[25] however, the reduction wave observed in the electrochemical measurements with **8**-H^+ was different from the typical shape. Additionally, the reduction potential of the process (–0.45 V) is higher relative to those reported for reduction processes of rhodium(III) centers; for example, $[Rh^{III}Cl_2(bpy)_2]^+$ shows its $E_{red}(Rh^{III}/Rh^{I})$ value of –0.92 V vs SCE in DMF.[26] Therefore, the reduction wave of **8**-H^+ at –0.45 V vs SCE can be assigned to the reduction process of the pterin ligand. However, the first reduction wave of **8**-H^+ is irreversible and thus any Rh^{III} complexes involving the reduced pterin species are hard to be obtained from chemical reduction of **8**-H^+. In consequence, the reversibility in the reduction process and the high E_{RED} value indicate that complex **6**-$2H^+$ can be reduced with chemical reductants under ambient conditions, and thus, complex **6**-$2H^+$ can be regarded as the best candidate for the precursor complex among the pterin complexes studied here to obtain the target pterin-OO-metal species.

3–4 Attempt at Formation of Ru^{II}-(H_2dmdmp-O_2) Species

As mentioned above, formation of the target pterin-OO-metal species was attempted as described in the Scheme 3-1: $1e^-$ reduction of **6**-$2H^+$ and the subsequent reaction with $O_2^{\bullet-}$. In this study, cobaltocene (E_{OX} = –0.9 V vs SCE in MeCN)[27] was employed as a reductant and KO_2 was employed as a $O_2^{\bullet-}$ source in the presence of 18-crown-6 as a K^+ trapping reagent. TfOH was chosen as a proton source to produce **6**-$2H^+$, because of its almost the highest acidity in MeCN and good stability; in contrast, $HClO_4$ has high acidity comparable to that of TfOH but not so stable in aprotic solvents. To the solution of **6**-$2H^+$, obtained from addition of excess TfOH into a solution of **6**-H^+ in MeCN, was added cobaltocene, and UV-vis spectral change was observed (Figure 3-11). However, the obtained spectrum after addition of cobaltocene was reminiscent of that of **6**-H^+ and production of **6**-H^+ was also confirmed by ESI-TOF-MS measurements. This result suggests that, although the diprotonation of **6** requires presence of an excess amount of a strong acid, cobaltocene may reduce proton derived from a strong acid such as TfOH in MeCN, decreasing the proton concentration to afford **6**-H^+.

To avoid decomposition of a strong acid, the reactions were attempted in propionitrile at 0 °C or at –

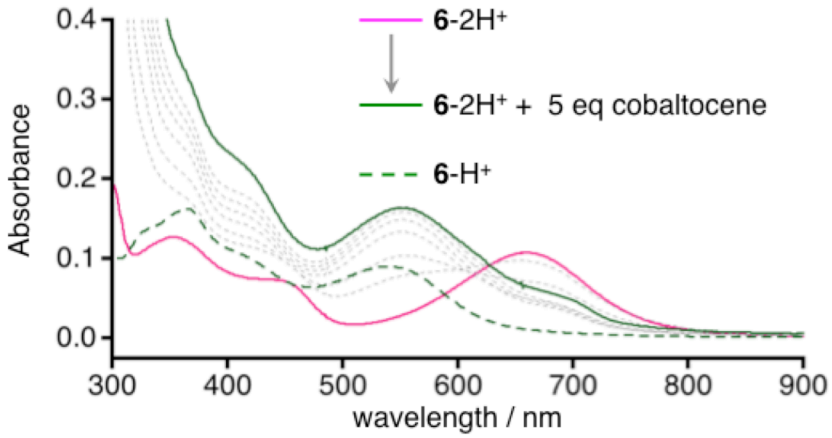

Figure 3-11. UV-Vis spectral change in the course of addition of cobaltocene into the solution of **6**-$2H^+$ in MeCN at room temperature in the presence of 6 equiv TfOH, and UV-vis spectrum of **6**-H^+ in MeCN.

85 °C, the latter of which was the lowest temperature limit of the cooling apparatus in propionitrile (m.p.: –92 °C). However, at low temperature, complex **6**-H^+ was not diprotonated to form **6**-$2H^+$ even in the presence of 5 equiv of TfOH, whereas complex **6**-H^+ was almost completely diprotonated with the same amount of TfOH at room temperature. The diprotonation of **6** is not favorable even at room temperature, and thus, the equilibrium constant on the protonation reactions of **6**-H^+ with TfOH probably decreases at low temperature to interrupt further protonation of **6**-H^+. Hence, ~1000 equiv TfOH was added into a solution of **6** in MeCN to produce **6**-$2H^+$ at –85 °C, and then, the formation of **6**-$2H^+$ was spectroscopically confirmed (Figure 3-12, orange line). The large mount of TfOH, however, caused problems; for example, cobaltocene as reductants reacted with TfOH even at low temperature due to increase in the amount of TfOH, and resultantly, ~12 equiv cobaltocene was necessary to complete the UV-Vis spectral change (Figure 3-12A). To the solution of **6**-$2H^+$ after reaction with 12 equiv cobaltocene at –85 °C, KO_2 was added, together with 0.5 equiv of 18-crown-6, to form the target species; however, excess amount of KO_2 was required to complete the spectral change and in the final spectrum, no absorption bands were observed over 400 nm, indicating decomposition of the Ru^{II} complexes. Hence, to confirm the reversibility of the reduction process of **6**-$2H^+$ with 12 equiv cobaltocene at –85 °C, tris(4-bromophenyl)aminium hexachloroantimonate (TBAH) was added as a $1e^-$ oxidant into the reaction mixture before addition of KO_2. As a result, in the course of reoxidation, a new absorption band at ~850 nm was observed (Figure 3-12B), indicating that a non-desired side reaction proceeded. The severe reaction conditions including use of a large amount of the strong acid, dry and deaerated atomosphre, and operation at low temperature, interrupted additional measurements such as ESI-TOF-MS spectrometry, NMR spectrosocopy, and so on. Therefore, the cause of the spectral changes with increase in the absorbance around 850 nm has yet to be clarified; note that $1e^-$-reduced **6**-$2H^+$ was probably not obtained in the experiment.

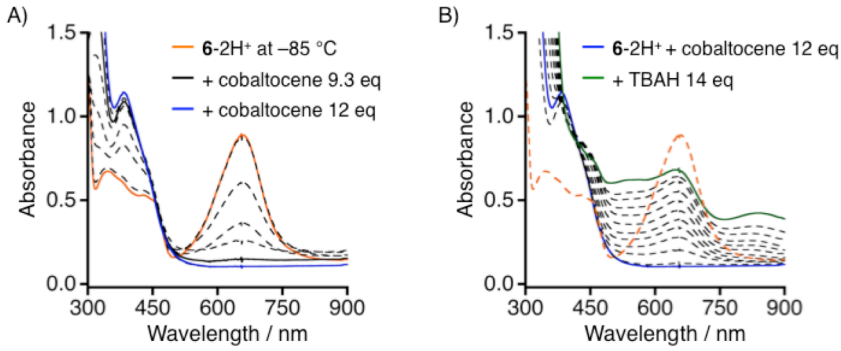

Figure 3-12. UV-Vis spectral change in the course of addition of a reductant and an oxidant into the solution of **6**-$2H^+$ in propionitrile at –85 °C in the presence of 870 eq TfOH; (A) addition of cobaltocene and (B) subsequent addition of TBAH.

3–5 Summary

To gain insights into the substrate oxidation by pterin-dependent hydroxylases in nature, the author attempted to obtain a pterin-OO-metal species, which is assumed to be the most plausible candidate of the active species in the oxidation reactions with the pterin-dependent enzymes. For this purpose, novel ruthenium(II)- and rhodium(III)-pterin complexes were synthesized and characterized especially with the electrochemical methods. The electrochemical and UV-vis measurements of the pterin complexes indicated

that selection of the metal center and ligands to prepare the pterin complexes is quite important for stabilization of the $1e^-$-reduced pterin ligand. The diprotonated ruthenium(II)-pterin complex, **6**-$2H^+$, was regarded as the best candidate for a precursor to the target pterin-OO-species, and thus, attempts to prepare the target peroxo complexes were performed by chemical reduction of **6**-$2H^+$ and subsequent addition of $O_2^{\bullet-}$ to solutions containing the reduced **6**-$2H^+$. However, the severe reaction conditions such as addition of a large amount of a strong acid interrupted formation of the target species.

In spite of efforts to search for appropriate reaction conditions including temperature, solvent, reductant, and acid, chemical reduction of **6**-$2H^+$ was not successful. Consequently, reconsideration on the design and synthesis of novel pterin complexes should be necessary to obtain the target peroxo species. The problems found for the $dmdmp^-$ complexes in this work are low protonation efficiency and irreversibility of the reduction processes. The irreversibility of the reduction processes for the monoprotonated pterin complexes can be derived from the proton-shift behaviors during the reduction process (Figure 3-13A).[21] To solve these problems, utilization of *N*-alkyl-pterin complexes,[28] which have alkylated N atom(s) instead of protonated N atom(s) in the pterin ligand, is one of the alternatives, because the *N*-alkyl-pterin ligand is equivalent to the monoprotonated pterin ligand in terms of the electronic structures, and thus, a high reduction potential of the reduction process comparable to that of the monoprotonated complexes can be expected. Moreover, the alkyl groups are probably not eliminated nor shifted during the reduction processes, and thus, high reversibility of the reduction process can be expected (Figure 3-13B).

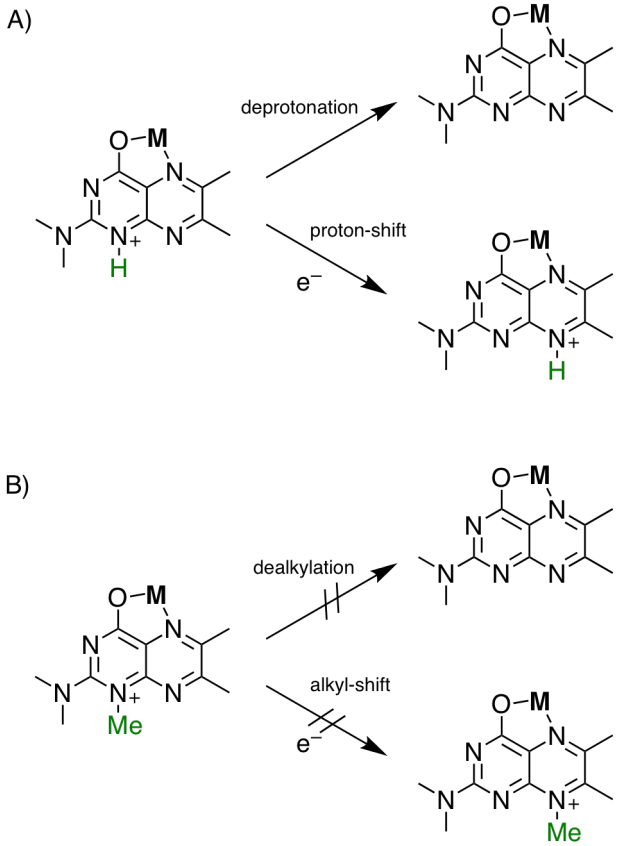

Figure 3-13. (A) Deprotonation and proton-shift of a protonated dmdmp complex and (B) dealkylation and alkyl-shift behaviors of alkylated dmdmp complex.

Reference and Notes

(1) Kappock T. J.; Caradonna, J. P. *Chem*. *Rev*. **1996**, *96*, 2659.

(2) Milatovich, A.; Mendel, D. B.; Crabtree, G. R.; Francke, U. *Genomics* **1993**, *16*, 292.

(3) Hasegawa, H. *J. Biochem*. **1977**, *81*, 169.

(4) Chen, M.-J.; Shimada, T.; Moulton, A. D.; Harrison, M.; Nienhuis, A. *Proc*. *Natl*. *Acad*. *Sci*. *USA* **1982**, *79*, 7435.

(5) McKinney, J.; Teigen, K.; Frøystein, N. Å.; Salaün, C.; Knappskog, P. M.; Haavik, J.; Martínez, A. *Biochemistry* **2001**, *40*, 15591. (b) Wang, L.; Erlandsen, H.; Haavik, J.; Knappskog, P. N.; Stevens, R. C. *Biochemistry* **2002**, *41*, 12569. (c) Windahl, M. S.; Petersen, C. R.; Christensen, H. E. M.; Harris, P. *Biochemistry* **2008**, *47*, 12087.

(6) (a) Flydal, M. I.; Martinez, A. *IUBMB Life* **2013**, *65*, 341. (b) Andersen, O. A.; Flatmark, T.; Hough, E. *J. Mol*. *Biol*. **2001**, *314*, 279. (c) Erlandsen, H.; Bjørgo, E.; Flatmark, T.; Stevens, R. C. *Biochemistry* **2000**, *39*, 2208. (d) Andersen, O. A.; Flatmark, T.; Hough, E. *J. Mol. Biol.* **2002**, *320*, 1095.

(7) (a) Tekin, I.; Roskoski, R., Jr.; Carkaci-Salli, N.; Vrana, K. E. *J. Neural Transm*. **2014**, *121*, 1451. (b) Haavik, J.; Toska, K. *Mol*. *Neurobiol*. **1998**, *16*, 285. (c) Goodwill, K. E.; Sabatier, C.; Stevens, R. C. *Biochemistry* **1998**, *37*, 13437. (d) Zhang, S.; Huang, T.; Ilangovan, U.; Hinck, A. P.; Fitzpatrick. P. F. *J. Mol. Biol.* **2014**, *426*, 1483.

(8) (a) Pfleger, R. C.; Piantadosi, C.; Snyder, F. *Biochim. Biophys. Acta* **1967**, *144*, 633. (b) Bhat, S. G.; Vaidyanathan, C. S. *Arch*. *Biochem*. *Biophys*. **1976**, *176*, 314. (c) Reddy, C. C.; Vaidyanathan, C. S. *Biochim*. *Biophys*. *Acta* **1975**, *384*, 46. (d) Reddy, C. C.; Vaidyanathan, C. S. *Arch*. *Biochem*. *Biophys*. **1976**, *177*, 488. (e) Sreeleela, N. S.; SubbaRao, P. V.; Premkumar, R.; Vaidyanathan, C. S. *J. Biol*. *Chem*. **1969**, *244*, 2293.

(9) (a) Dix, T. A.; Bollag, G. E.; Domanico, P. L.; Benkovic, S. J. *Biochemistry* **1985**, *24*, 2955. (b) Benkovic, S.; Wallick, D.; Bloom, L.; Gaffney, B. J.; Domanico, P.; Dix, T.; Pember, S. *Biochem. Soc. Trans.* **1985**, *13*, 436. (c) Lazarus, R. A.; Wallick, D. E.; Dietrich, R. F.; Gottschall, D. W.; Benkovic, S. J.; Gaffney, B. J.; Shiman, R. *Fed. Proc., Fed. Am. Soc. Exp. Biol.* **1982**, *41*, 2605.

(10) Miyazaki, S.; Kojima, T.; Sakamoto, T.; Matsumoto, T.; Ohkubo, K.; Fukuzumi, S. *Inorg*. *Chem*. **2008**, *47*, 333.

(11) Huynh, M. H. V.; Lasker, J. M.; Wetzler, M.; Mort, B.; Szezepura, L. F.; Witham, L. M.; Cintron, J. M.; Marschilok, A. C.; Ackerman, L. J.; Castellano, R. K.; Jameson, D. L.; Churchill, M. R.; Jircitano, A. J.; Takeuchi, K. J. *J*. *Am*. *Chem*. *Soc*. **2001**, *123*, 8780.

(12) Shimizu, Y.; Fukui, S.; Oi, T.; Nagao, H. *Bull*. *Chem*. *Soc*. *Jpn*. **2008**, *81*, 1285.

(13) Kojima, T.; Amano, T.; Ishii, Y.; Ohba, M.; Okaue, Y.; Matsuda, Y. *Inorg*. *Chem*. **1998**, *37*, 4076.

(14) Kaljurand, I.; Kütt, A.; Sooväli, L.; Rodima, T.; Mäemets, V.; Leito. I.; Koppel, I. A. *J. Org. Chem.* **2005**, *70*, 1019.

(15) *Kagaku Binran, Kiso-hen II (The Chemical Data Book)*; Chemical Society of Japan, Ed.; Maruzen: Tokyo, 1984; p 343.

(16) Izutsu, K. *Acid-Base Dissociation Constants in Dipolar Aprotic Solvents*; Blackwell Scientific: Boston, MA, 1990.

(17) Cline, E. D.; Adamson, S. E.; Bernhard, S. *Inorg. Chem.* **2008**, *47*, 10378.

(18) (a) Wu, A.; Masland, J.; Swartz, R. D.; Kaminsky, W.; Mayer, J. M. *Inorg. Chem.* **2007**, *46*, 11190. (b) Schulze, B.; Escudero, D.; Friebe, C.; Siebert, R.; Görls, H.; Sinn, S.; Thomas, T.; Mai, S.; Popp, J.; Dietzek, B.; González, L.; Schubert, U. S. *Chem. Eur.–J.* **2012**, *18*, 4010. (c) Taher, D.; Thibault, M. E.; Mondo, D. D.; Jennings, M.; Schlaf, M. *Chem.–Eur. J.* **2009**, *15*, 10132. (d) Nagao, H.; Mizukawa, T.; Tanaka, K. *Inorg. Chem.* **1994**, *33*, 3415.

(19) *CRC Handbook of Chemistry and Physics*, *82nd Ed.*: CRC Press, Boca Raton, USA, 2001; Section 9.

(20) (a) Aakeröy, C. B.; Evans, T. A.; Seddon, K. R.; Pálinko, I. *New J. Chem.* **1999**, *23*, 145. (b) Jones, P. G.; Ahrens, P. *Chem. Commun.* **1998**, 2307.

(21) Miyazaki, S.; Ohkubo, K.; Kojima, T.; Fukuzumi, S. *Angew. Chem., Int. Ed.* **2008**, *47*, 9669.

(22) A similar relation between reversibility of reduction processes of metal complexes and the electron density at their metal centers was shown by Kaim and coworkers. Four DML (= 1,3-dimethyllumazine) complexes, including $[Cu^{I}(DML)(PPh_3)_2]^+$ (ref. 23), $[Ru^{II}(DML)(bpy)_2]^{2+}$ (ref. 23), $[Re^{I}(DML)(CO)_3Cl]$ (ref. 23), and $[Ir^{III}(Cp^*)Cl(DML)]^{2+}$ (ref. 24, HCp* = 1,2,3,4,5-pentamethyl-cyclopentadiene) showed different reversibility in the reduction processes of the DML ligands. $[Cu^{I}(DML)(PPh_3)_2]^+$ showed an irreversible wave in the CV, and $[Ru^{II}(DML)(bpy)_2]^{2+}$ and $[Re^{I}(DML)(CO)_3Cl]^+$ showed quasi-reversible wave with i_a/i_c = 0.4 and 0.92, respectively, whereas $[Ir^{III}(Cp^*)Cl(DML)]^{2+}$ showed a reversible wave. Kaim and coworkers also succeeded in observation of an ESR signal of the $1e^-$-reduced DML species only with $[Ir^{III}(Cp^*)Cl(DML^{\bullet-})]^+$.[24] Therefore, the higher valence number of the metal center, that is, the low electron density on the metal center, can stabilize the ligand-reduced species.

(23) Bessenbacher, C.; Vogler, C.; Kaim, W. *Inorg. Chem.* **1989**, *28*, 4645.

(24) Heilmann, O.; Hornung, F. M.; Kaim, W.; Fiedler, J. *J. Chem. Soc., Faraday Trans.* **1996**, *92*, 4233.

(25) Kew, G.; Hanck, K.; DeArmond, K. *J. Phys. Chem.* **1975**, *79*, 1828.

(26) Amarante, D.; Cherian, C.; Catapano, A.; Adams, R.; Wang, M. H.; Megehee, E. G. *Inorg. Chem.* **2005**, *44*, 8804.

(27) Mandal, S.; Shikano, S.; Yamada, Y.; Lee, Y.-M.; Nam, W.; Llobet, A.; Fukuzumi, S. *J. Am. Chem. Soc.* **2013**, *135*, 15294.

(28) Pfleiderer, W.; Mengel, R.; Hemmerich, P. *Chem. Ber.* **1971**, *104*, 2273.

Chapter 4 Oxidation of C–H bonds in Hydrocarbons by Ruthenium(III)-Pterin Complexes

4–1 Introduction

Proton-coupled electron transfer (PCET) provides an energetically feasible pathway for H-atom abstraction from a substrate with an oxidant (See Chapter 1-4).[1] In PCET reactions, an oxidant receives one electron and one proton from substrates at different sites; *i.e.*, an electron goes to an electron accepting site and a proton moves to a proton accepting site.[2] The concerted processes reduce the activation free-energy, $\Delta G^{\ddagger}$, in oxidation of hydrocarbons despite their high oxidation potentials (normally, > 2 V vs SCE).[1b] Because of this advantage, PCET reactions are widely employed not only in biological redox reactions but also in production of fine chemicals in chemical industry.[3,4] In biological systems, oxidation reactions through a PCET process are also conducted at an active center by oxidation enzymes;[5] for example, lipoxygenase,[6] methane monooxygenase,[7] ribonucleotide reductase,[8] and cytochrome P450s[9] oxidize organic substrates at the active sites including transition-metal complexes. The active sites of the enzymes are well characterized and many research groups have synthesized transition-metal complexes as functional models to gain mechanistic insights into the enzymatic oxidation reactions and to learn splendid methods for oxidation of organic molecules.[5, 10-12]

Hydrogen-atom transfer (HAT) reactions can be categorized into 4 types; (1) transfer of H atom from a substrate to a single atom such as an oxyl group in an oxidant, (2) electron transfer followed by proton transfer (ET/PT), (3) proton transfer followed by electron transfer (PT/ET), and (4) concerted proton-electron transfer (CPET).[1b] The latter three types are recognized as PCET, in which a proton and an electron are transferred from a substrate to two different sites of the oxidant as mentioned above, in terms of weak coupling between electron donor and acceptor.[13] In CPET reactions, the "oxidation power" of an oxidant can be defined by the bond dissociation enthalpy (BDE) of a $1e^{-}/1H^{+}$-reduced form of the oxidant.[14] Also, the inertness of a substrate in HAT can be judged from the BDE value of an X-H bond to be cleaved. BDE values of the reduced species obtained from oxidants are determined from the pK_a value of its conjugate acid and the redox potential ($E_{1/2}$),[15] which correspond to the Gibbs free-energy change of the PCET reaction. The BDE value can be defined by eq 1:[16-19]

$$\text{BDE (kcal mol}^{-1}) = 2.303RT(\text{p}K_a) + F(E_{1/2}) + C \qquad (1)$$

In eq 1, R, F, E_{ox} and C refer to the gas constant, the Faraday constant, one-electron oxidation potential, and a proportionality constant in a certain solvent, respectively. Thus, the high pK_a and high E_{red} values result in high BDE of the reduced species obtained from the oxidant to promote the oxidation reaction. The correlation between the oxidation reactivity of an oxidant and the BDE value of an oxidant as a hydrogen atom acceptor has been well investigated by many researchers mainly with high valent metal-oxo complex as an oxidant.[20] In high-valent metal-oxo species, the oxo group of the oxidants can behave as good proton acceptors driven by its –2 charge, and the metal center should acts as good electron acceptors by virtue of its high valency. Therefore, many researchers have used metal-oxo species in CPET reactions. As one of the reports investigating reactivity in PCET, Que, Shaik, Nam and coworkers compared reactivity among

non-heme iron(IV)-oxo complexes showing close calculated BDE values in C-H abstraction reactions, to conclude that the involvement of the quintet state of iron(IV)-oxo complexes should be important in enhancing the reactivity of H-atom abstraction.[21] As mentioned above, an important factor to determine the reactivity of an oxidant in PCET reactions is its BDE value, which can be divided into two components, *i.e.*, pK_a and $E_{1/2}$. Determination of the $E_{1/2}$ value of metal-oxo complexes is relatively easy, and thus, correlation between the $E_{1/2}$ value and the reactivity as an oxidant has been discussed for several metal-oxo complexes; for example, Que and coworkers determined the reduction potential of $[Fe^{IV}(O)(N4Py)]^{2+}$ (+0.50 V vs SCE in MeCN) by spectropotentiometry,[11] and concluded that the higher reactivity of $[Fe^{IV}(O)(N4Py)]^{2+}$ than Fe(IV)-oxo-tetramesitylporphyrin (+0.29 V)[22] and Fe(IV)-oxo-trisureaylate (–0.06 V)[23] was attributed to its high potential among the Fe^{IV}-oxo complexes.[11] On the other hand, the correlation between pK_a of oxidants and their reactivity in C-H oxidation has never been clarified yet, due to the difficulty in the determination of pK_a values of metal-oxo species, because metal-oxo complexes are generally unstable and usually not capable of accepting a proton in an acid-base reaction.

Besides the C-H oxidation by metal-oxo complexes mentioned above, no report has described systematic investigation on C-H oxidation reactions with metal complexes without oxo ligands.[24] Mayer and coworkers have reported that PCET oxidation of O-H bonds in substrates such as phenol derivatives and TEMPOH can be achieved by using Ru(III) and Fe(III) complexes having basic sites in the ligands without oxo ligands.[25,26] It should be important to develop oxidants without oxo ligands for expansion of versatility in C-H oxidation reactions and this strategy may make it possible to construct catalytic oxidation systems without using hazardous peroxides or aqua complexes as precursors, which can be used only in aqueous media.

In order to clarify controlling factors of the reactivity of oxidants in C-H bond cleavage *via* HAT, the author examined metal complexes bearing a basic site as a proton-accepting site, without oxo ligands. As a proton-accepting site, a pterin derivative was selected. Pterins are heteroaromatic coenzymes, which play crucial roles in biological redox reactions (See Chapter 1-3).[27,28] Additionally, transition-metal complexes of pterin derivatives have attracted much attention due to their unique redox behaviors (See Chapter 3).[29,30] For example, our research group has reported that the 1e$^-$-oxidized species of a Ru^{II}-pterin complex, $[Ru^{II}(dmdmp)(TPA)]^+$ (**10**: Hdmdmp = *N*,*N*-dimethyl-6,7-dimethylpterin, TPA = tris(2-pyridylmethyl)amine; see Scheme 1),[31] was revealed to perform oxidation reactions of phenol derivatives through a PCET mechanism.[32] However, H-atom abstraction reactions from C-H bonds have never been performed. In this chapter, the ruthenium(II)-pterin complex, $[Ru^{II}(dmdmp)Cl(MeBPA)]$ (**7**: MeBPA = *N*-methyl-*N*,*N*-bis(2-pyridylmethyl)amine; see Scheme 1), and complex **10** were employed. Complex **7** has a similar structure to that of **10**, except possession of a chloride ligand, instead of one pyridine ring of the TPA ligand in **10**. Note that both the complexes do not have oxo ligands in the structures. The alteration of coordination environments between the two complexes involves total charges of the cation moieties, the pK_a values of the pterin ligand and 1e$^-$-oxidation potentials of the metal centers as mentioned in Chapter 3 to regulate the reactivity of the complexes in PCET reactions. The author herein compares the reactivity of 1e$^-$-oxidized **7** and **10** in oxidation of organic substrates, involving H-atom abstraction from C-H bonds of substrates, to explore the effect of the differences in the electron-acceptability reflected on the pK_a values and the proton-acceptability reflected on the redox potentials between **7** and **10** on the substrate oxidation through a

Scheme 4-1. Structures of complexes **7** and **10**.

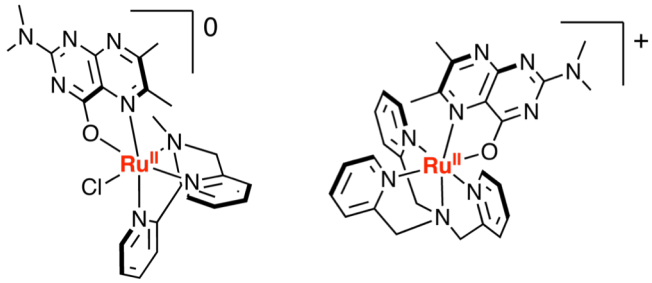

7 **10**

PCET mechanism. The purpose of this study is (1) clarification of the fact that non-metal-oxo oxidants having proton- and electron-accepting sites are capable of performing sufficient C–H bond oxidation and (2) gaining insights into impacts of proton- and electron acceptability of the oxidants on the transition states in PCET oxidation reactions of C–H bonds.

4–2 Determination of BDE values

The pK_a values of **7**-H$^+$ and **7**-2H$^+$ in MeCN were determined by UV-vis titration experiments (16.4 for **7**-H$^+$ and 3.9 for **7**-2H$^+$) as described in Chapter 3. The pK_a value of **10**-H$^+$ was also reexamined in this work by using the same method for **7**-H$^+$ as mentioned in Chapter 3; the pK_a value of **10**-H$^+$ was determined to be 14.3 using Me_3Py (pK_a of Me_3Py-H$^+$ = 14.98)[33] as a base. The pK_a values of **10**-H$^+$ (14.3) and **10**-2H$^+$ (2.0)[32] are much smaller than those of **7**-H$^+$ and **7**-2H$^+$, respectively, indicating higher acidity of **10**-H$^+$ and **10**-2H$^+$ than that of **7**-H$^+$ and **7**-2H$^+$. Therefore, the dmdmp ligand in **7** has stronger basicity than that in **10**, reflecting larger electron density of the Ru^{II} center caused by ligand alteration from a π-accepting and neutral pyridine ligand to a π-donating and anionic chloride ligand. Thus, it has been revealed that proton acceptability of **7** is much larger than that of **10** in PCET reactions.

As mentioned in Chapter 3, all of **7**, **7**-H$^+$ and **7**-2H$^+$ showed one reversible oxidation waves at +0.24, +0.54, and +0.62 V vs SCE in MeCN, respectively, which were assigned to the Ru^{II}/Ru^{III} processes (Figure 3-10 in Chapter 3). The large positive shift with the first protonation of the pterin ligand and the small positive shift with the second protonation were also observed in the measurements of **10** and the protonated forms (Table 4-1).[30d,31] In comparison of the redox potentials of the corresponding protonated species between **10** and **7**, the redox potentials of **7** and the protonated forms are lower than those of **10** and the protonated forms, due to the ligand alteration of one π-accepting and neutral pyridine ligand of the TPA ligand in **10** with the π-donating and negatively-charged chloride ligand in **7**, together with the charges of the complex cations. Combined with effects of the ligand alteration on the pK_a values (14.3 for **10** and 16.4 for **7**) of the pterin ligand as mentioned above, the change of coordination environments and the charge of the complexes brought much impact on physical properties of the pterin complexes through change of the electron density of the Ru^{II} centers.

The pK_a values and the first oxidation potentials of **7** and those of the protonated forms obtained in this work allowed the author to draw "square schemes" of PCET reactions for **7** (Scheme 4-2) and also to calculate BDEs based on eq 1.[16-19] In the case of MeCN as a solvent, the *C* value in eq 1 is estimated to be

Table 4-1. Oxidation Potentials (V vs SCE) of the Ru-pterin Complexes in MeCN

Protonation status the pterin ligand	**7**	**10**[a]
$dmdmp^-$	+0.24	+0.66
Hdmdmp	+0.54	+0.92
H_2dmdmp^+	+0.62	+0.94

[a]: these values are taken from ref. 32.

59.5 kcal mol^{-1} with use of redox potentials against the ferrocene/ferrocenium couple.[15] Also in calculations,

Scheme 4-2. Thermochemical square schemes for multistep PCET of **7** (A) and **10** (B) in MeCN.

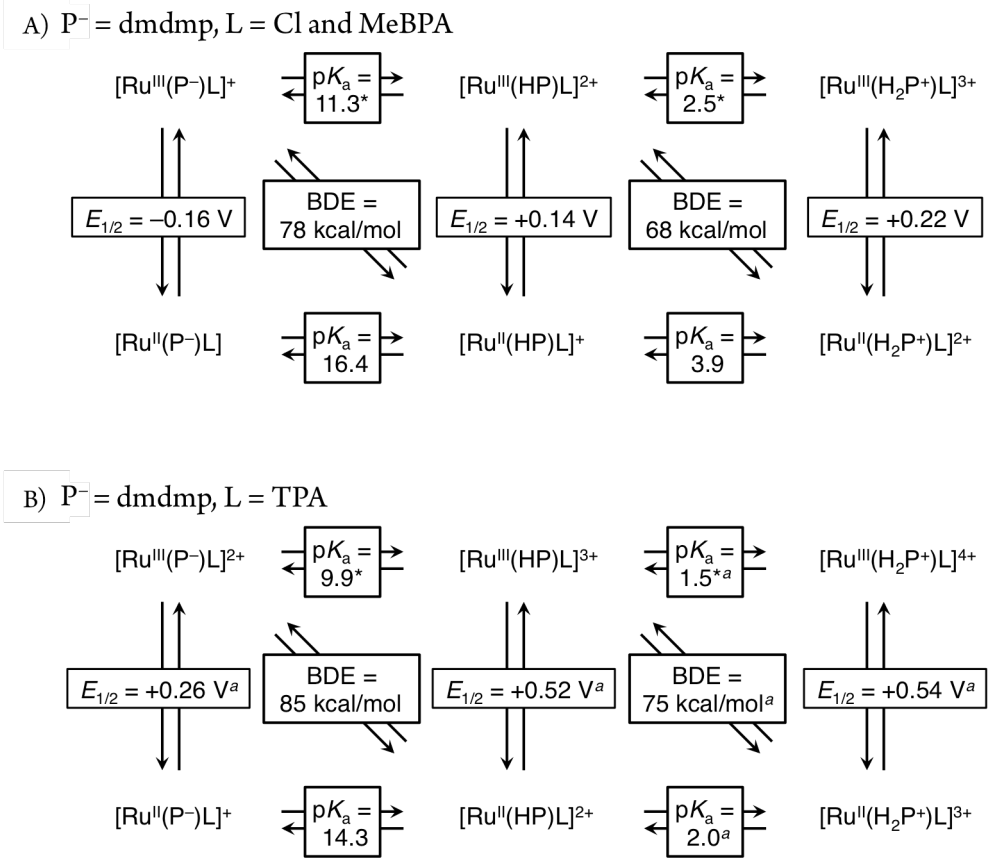

$E_{1/2}$ values are referenced to ferrocene/ferrocenium couple. *: calculated pK_a values on the basis of eq 1.
[a] Values taken from ref. 32.

the potentials vs SCE are converted to the values against ferrocene/ferrocenium couple by subtraction of 0.40 V.[34] In this study, the author adopted BDE rather than bond dissociation free-energy (BDFE),[35,36] because in this case a small contribution of the entropy term should be expected.[36,37] The BDE values for the H-atom abstraction reaction from **7**-H^+ to give $[Ru^{III}(dmdmp)Cl(MeBPA)]^+$ ($\mathbf{7}_{OX}$) was calculated to be 78 kcal mol^{-1}, and that for the reaction from **7**-$2H^+$ to give $[Ru^{III}Cl(Hdmdmp)(MeBPA)]^{2+}$ ($\mathbf{7_{ox}}$-H^+) was determined to be 68 kcal mol^{-1}. The BDE values for **7**-H^+ and **7**-$2H^+$ are slightly lower than those for the corresponding **10**-H^+ and **10**-$2H^+$ (85 and 75 kcal mol^{-1}, respectively). Thus, complex $\mathbf{7}_{OX}$ is expected to show lower reactivity in PCET reactions than $\mathbf{10}_{OX}$.

4–3 1e⁻ Oxidation of Ru^{II}-dmdmp Complexes

Complexes **7** and **10** were oxidized with addition of 1 equiv of $[Fe^{III}(bpy)_3]^{3+}$ (E_{red} = +1.10 V vs SCE)[38]

as an oxidant in MeCN in accordance with the same procedure described in the previous report of our research group.[32] The absorption spectrum of **7** in MeCN exhibited the absorption maxima at 392 and 493 nm as shown as the red trace in Figure 4-1. Upon addition of the oxidant to the MeCN solution of **7**, the spectrum of **7** changed with showing two isosbestic points at 372 and 510 nm as depicted in Figure 4-1A. In the course of the reaction, the increase of absorbance at 520 nm was observed due to the formation of $[Fe^{II}(bpy)_3]^{2+}$. The absorption spectrum of the 1e$^-$-oxidized form of **7**, $\mathbf{7}_{OX}$, was obtained by subtraction of the

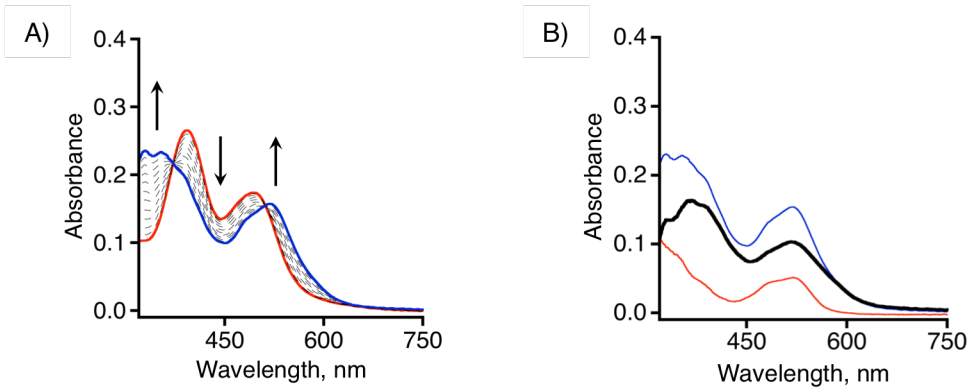

Figure 4-1. (A) UV-Vis spectral change in the course of the addition of $[Fe^{III}(bpy)_3](PF_6)_3$ as a 1e$^-$-oxidant into the solution of **7** (17.4 μM, red trace) up to 1 equiv in MeCN at room temperature. (B) UV-vis spectrum of the reaction mixture of **7** (17.4 μM) and $[Fe^{III}(bpy)_3]^{2+}$ (blue trace), that of $[Fe^{II}(bpy)_3]^{2+}$ (17.4 μM, red trace) and (c) a differential spectrum of the former two traces (black trace) in MeCN at room temperature.

spectrum of $[Fe^{II}(bpy)_3]^{2+}$ from the final spectrum (black line in Figure 4-1B) and the spectrum of $\mathbf{7}_{OX}$ exhibited the absorption maxima at 366 and 517 nm.

4–4 Oxidation Reactivity of $\mathbf{7}_{OX}$ and $\mathbf{10}_{OX}$ toward C–H bonds of Hydrocarbons

The 1e$^-$-oxidized species of **7** and **10** ($\mathbf{7}_{OX}$ and $\mathbf{10}_{OX}$) reacted with substrates such as hydrocarbons. The oxidation reactions of organic substrates with $\mathbf{7}_{OX}$ and $\mathbf{10}_{OX}$ were monitored with a stopped-flow apparatus using a double-mixing mode. In the reaction of $\mathbf{7}_{OX}$ with 9,10-dihydroanthracene (DHA) as a substrate, the absorbance at 528 nm due to **7**-H$^+$ increased as shown in Figure 4-2A. In the reaction of $\mathbf{10}_{OX}$ with DHA, the absorbance at 497 nm, which was assigned to that of **10**-H$^+$,[32] increased as can be seen in Figure 4-2B. The spectral changes indicate the formation of **7**-H$^+$ or **10**-H$^+$ in the course of the reaction of $\mathbf{7}_{OX}$ or $\mathbf{10}_{OX}$ with

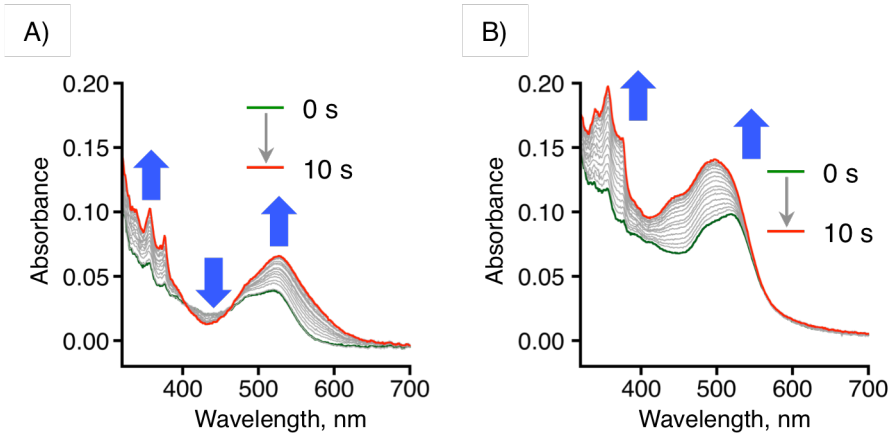

Figure 4-2. Absorption spectral changes in the course of the reactions of DHA with $\mathbf{7}_{OX}$ (A) and $\mathbf{10}_{OX}$ (B) (0 – 10 s after addition of DHA), monitored by a stopped-flow spectrometer in MeCN at 296 K. [Ru] = 15 μM, [DHA] = 2.4 mM.

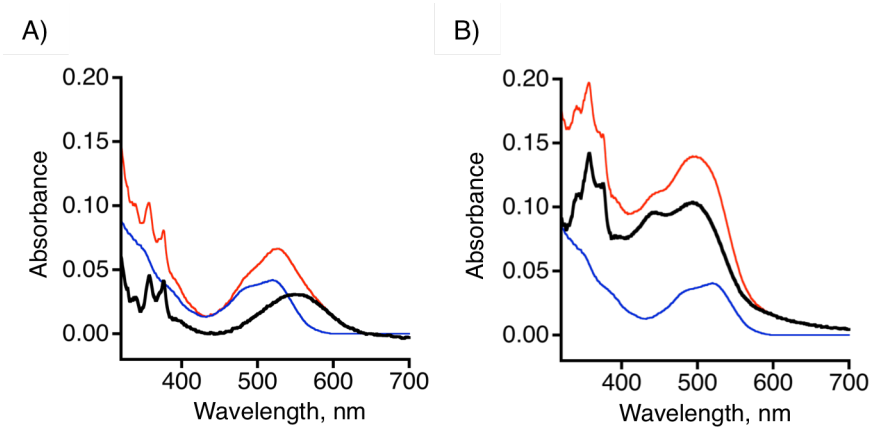

Figure 4-3. Differential spectra obtained for the reactions of DHA with $\mathbf{7}_{OX}$ (A) and $\mathbf{10}_{OX}$ (B) in MeCN. The final spectra of the reactions: red, the spectrum of $[Fe^{II}(bpy)_3]^{2+}$ (15 μM): blue, the spectra obtained by (red) – (blue): black.

DHA. In both cases, characteristic absorption bands of anthracene as the product increased in the range of λ < 400 nm with a vibronic feature (Figure 4-2).[39] In order to clarify the final products derived from $\mathbf{7}_{OX}$ and $\mathbf{10}_{OX}$ in the DHA oxidation, the differential spectra were obtained by the subtraction of the spectrum of $[Fe(bpy)_3]^{2+}$ (15 μM in MeCN) from the final spectra of the reaction mixtures (Figure 4-3). The spectra of the products, shown as the black traces in Figure 4-3, are identical to the spectrum of $\mathbf{10}$-H^+ as represented by the absorptions at 443 and 493 nm[40] and that of $\mathbf{7}$-H^+ as supported by the absorption at 549 nm, which is consistent with the green line in Figure 4-1B. Thus, it is concluded that a proton and an electron of a C-H bond of DHA are transferred to the N-1 position of the $dmdmp^-$ ligand and to the Ru^{III} center, respectively, through a PCET mechanism as shown in Scheme 4-3.

The absorbance changes of the solution containing $\mathbf{7}_{OX}$ at 530 nm obeyed pseudo first-order kinetics in the presence of an excess amount of DHA as shown in Figure 4-4A and curve-fitting of the time-course of

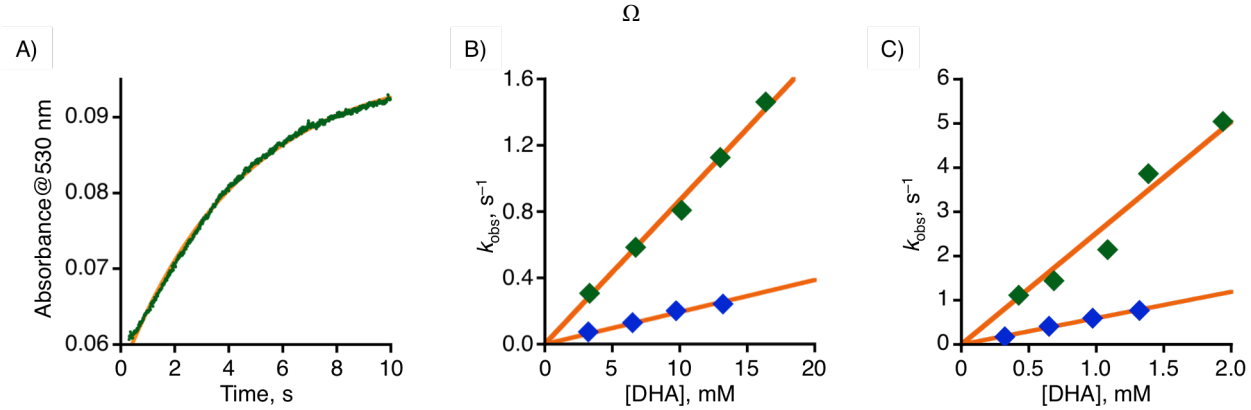

Figure 4-4. (A) The absorbance change at 530 nm (green dot) and the pesudo first-order fitting curve (orange line) in the course of the reaction of $\mathbf{7}_{OX}$ with DHA monitored by a stopped-flow spectrometer in MeCN at 296 K: [Ru] = 15 μM, [DHA] = 3.3 mM. Concentration dependence of k_{obs} for the oxidation (green squares) of DHA (green squares, DHA-d_0; blue squares, DHA-d_4) and the fitting analysis (orange solid line) with $\mathbf{7}_{OX}$ (B) or $\mathbf{10}_{OX}$ (C) at 296 K in MeCN. $[\mathbf{7}_{OX}]_0$ and $[\mathbf{10}_{OX}]_0$ = 15 μM.

Scheme 4-3. Reactions of $\mathbf{7}_{OX}$ with a substrate

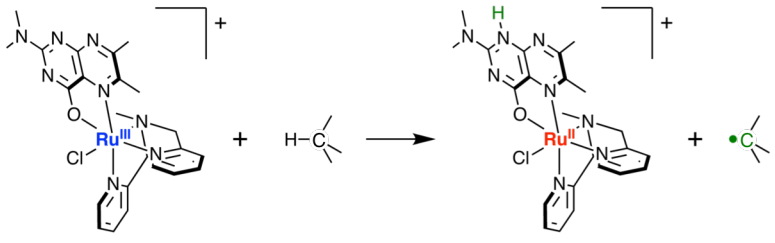

Table 4-2. Oxidation Potentials, pK_a and BDE Values of Hydrocarbons, and Second-Order Rate Constants of C-H Oxidation Reactions by $\mathbf{7}_{OX}$ or $\mathbf{10}_{OX}$ in MeCN at 296 K

substrate	E_{ox}, V vs SCE	pK_a	BDE, kcal mol^{-1}	k, M^{-1} s^{-1}	
				$\mathbf{7}_{OX}$	$\mathbf{10}_{OX}$
xanthene	+1.56[a]	41.0[b]	75.5[c]	$(8.7 \pm 0.4) \times 10^2$	$(1.32 \pm 0.05) \times 10^3$
DHA	+2.13[a]	41.1[b]	76.3[c]	87 ± 2	$(2.5 \pm 0.1) \times 10^2$
HCp*	+0.95[a]	37.1[b]	77[c]	$(5.7 \pm 0.2) \times 10^2$	$(6.0 \pm 0.2) \times 10^4$
fluorene	+1.58[a]	33.6[b]	82[c]	1.42 ± 0.02	35.5 ± 0.6
indene	+1.54[a]	31.1[b]	83[c]	0.24 ± 0.01	13 ± 1
EtPh	+2.41[a]	—	85.4[c]	too slow	0.50 ± 0.02

[a] Determined by second-harmonic alternating current voltammetry (SHACV) in MeCN. [b] Values measured in DMSO (Ref. 41) and extrapolated to those in MeCN using the equation: p$K_{a(C\text{-}H)}$ (in MeCN) = 11 + p$K_{a(C\text{-}H)}$ (in DMSO) (Ref. 17). [c] Ref. 42.

the absorbance at 530 nm allowed the author to determine a pseudo-first-order rate constant (k_{obs}). On the basis of a plot of the k_{obs} values versus the concentrations of the substrate (Figure 4-4B), the author determined the second-order rate constants (k) from the slope of the linear correlation as depicted in Figure 4-4B. The k values of the DHA oxidation by $\mathbf{7}_{OX}$ and $\mathbf{10}_{OX}$ were determined to be 87 ± 2 M^{-1} s^{-1} and $(2.5 \pm 0.1) \times 10^2$ M^{-1} s^{-1}, respectively (Figure 4-4B and C). In accordance with this procedure, the k vales for C–H oxidation reactions of a series of substrates were determined in MeCN at 296 K (Figure 4-5 – 4-9). The second-order rate constants of oxidation reactions of other substrates by $\mathbf{7}_{OX}$ and $\mathbf{10}_{OX}$ are summarized in Table 4-2.

Complexes $\mathbf{7}_{OX}$ and $\mathbf{10}_{OX}$ showed similar reactivity on the oxidation reaction of xanthene, with showing comparable rate constants: $k = (8.7 \pm 0.4) \times 10^2$ M^{-1} s^{-1} for $\mathbf{7}_{OX}$ and $(1.32 \pm 0.05) \times 10^3$ M^{-1} s^{-1} for $\mathbf{10}_{OX}$. In contrast, for the C-H oxidation of other substrates, the reactivity of the two complexes were different; for example, the k value for the reaction of 1,2,3,4,5-pentamethyl-cyclopentadiene (HCp*) with $\mathbf{10}_{OX}$ was *ca.* 100 times larger than that with $\mathbf{7}_{OX}$: $k = (5.7 \pm 0.2) \times 10^2$ M^{-1} s^{-1} for $\mathbf{7}_{OX}$ and $(6.0 \pm 0.2) \times 10^4$ M^{-1} s^{-1} for

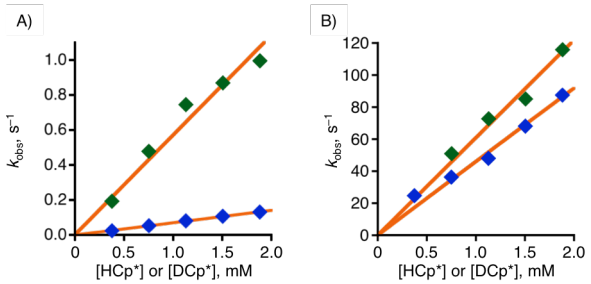

Figure 4-5. Concentration dependence of k_{obs} for the oxidation (green squares) of HCp* (green squares for HCp*-d_0, blue squares for HCp*-d_1) and the fitting analysis (orange solid line) with $\mathbf{7}_{OX}$ (A) or $\mathbf{10}_{OX}$ (B) at 296 K in MeCN. $[\mathbf{7}_{OX}]_0$ and $[\mathbf{10}_{OX}]_0$ = 15 μM.

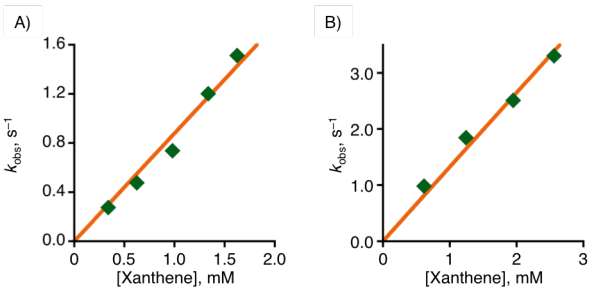

Figure 4-6. Concentration dependence of k_{obs} for the oxidation (green squares) of xanthene and the fitting analysis (orange solid line) with $\mathbf{7}_{OX}$ (A) or $\mathbf{10}_{OX}$ (B) at 296 K in MeCN. $[\mathbf{7}_{OX}]_0$ and $[\mathbf{10}_{OX}]_0$ = 15 μM.

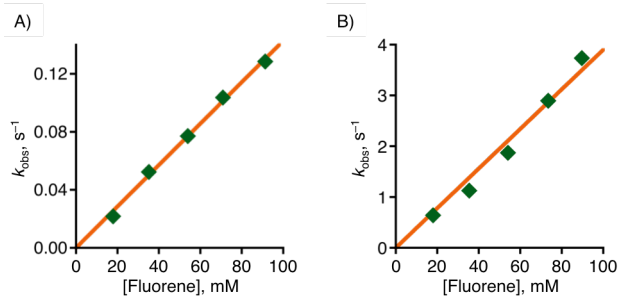

Figure 4-7. Concentration dependence of k_{obs} for the oxidation (green squares) of fluorene and the fitting analysis (orange solid line) with $\mathbf{7}_{OX}$ (A) or $\mathbf{10}_{OX}$ (B) at 296 K in MeCN. $[\mathbf{7}_{OX}]_0$ and $[\mathbf{10}_{OX}]_0$ = 15 μM.

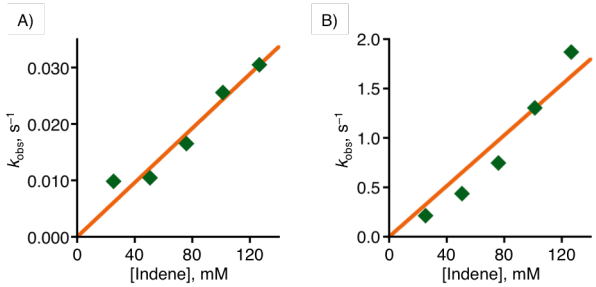

Figure 4-8. Concentration dependence of k_{obs} for the oxidation (green squares) of indene and the fitting analysis (orange solid line) with $\mathbf{7}_{OX}$ (A) or $\mathbf{10}_{OX}$ (B) at 296 K in MeCN. $[\mathbf{7}_{OX}]_0$ and $[\mathbf{10}_{OX}]_0$ = 15 μM.

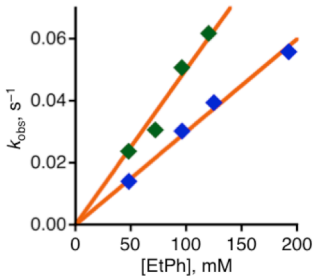

Figure 4-9. Concentration dependence of k_{obs} for the oxidation of EtPh (green squares for EtPh-d_0, blue squares for EtPh-d_{10}) and the fitting analysis (orange solid line) with $\mathbf{10}_{OX}$ at 296 K in MeCN. $[\mathbf{10}_{OX}]_0$ = 15 μM.

$\mathbf{10}_{OX}$. In addition, the k values of the indene oxidation were 0.24 ± 0.01 M^{-1} s^{-1} for $\mathbf{7}_{OX}$ and 13 ± 1 M^{-1} s^{-1} for $\mathbf{10}_{OX}$, respectively. As for ethylbenzene (EtPh, $BDE_{C\text{-}H}$ = 85.4 kcal mol^{-1}), complex $\mathbf{10}_{OX}$ showing the BDE value of 85 kcal mol^{-1} reacted slowly with the substrate at the rate constant of 0.50 ± 0.02 M^{-1} s^{-1}; however, the reaction of $\mathbf{7}_{OX}$ showing the BDE value of 78 kcal mol^{-1} with ethylbenzene did not proceed, because of the energetically uphill situation in light of the BDE values of the oxidant and the substrate. This result is consistent with the relationship of the BDE values of both complexes and the substrates, indicating that the C-H oxidation by $\mathbf{7}_{OX}$ and $\mathbf{10}_{OX}$ proceed *via* CPET.

Product analyses were conducted for the oxidation reactions of the respective substrates; the oxidation of DHA gave anthracene as mentioned above, and formation of xanthylium cation[43] was suggested by absorption around ~370 nm in the oxidation of xanthene at high concentration (Figure 4-10). Attempts to detect the products of the oxidation reactions of other substrates were performed using GC-MS; however, no signals of organic products were detected.

The indenyl radical, which is presumed to be formed from the oxidation of indene with $\mathbf{7}_{OX}$ and $\mathbf{10}_{OX}$, has been known to polymerize rapidly;[44] hence, the indenyl radical formed probably should further react rapidly to afford polymers, which are insensitive to the GC measurements. Supporting this, in SHACV

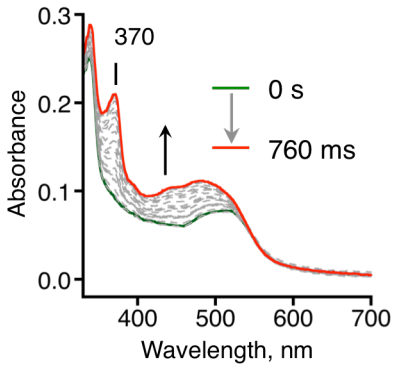

Figure 4-10. UV-Vis spectral change in the course of oxidation of xanthene with $\mathbf{10}_{OX}$ at 296 K in MeCN. [$\mathbf{10}_{OX}$] = 15 μM, [DHA] = 4.2 mM.

measurements of an indene solution in MeCN, the working electrode (glassy carbon disk) was coated with brown materials, which were assumed to be indenyl polymers. In addition, the formation of the indenyl radical was confirmed by the detection of the ESR signal of a spin adduct using 2-Methyl-2-nitrosopropane (MNP) dimer as a spin trapping reagent; a triplet of doublets (g = 2.0064, A_N = 14.7 G, A_H = 2.4 G) was observed as shown in Figure 4-11A and assigned to a carbon radical with one hydrogen atom.[45] The control experiments support that the short-lived indenyl radical should be formed in the reaction of indene with $\mathbf{10}_{OX}$, not derived from self decomposition of MNP dimer (Figure 4-11F) and other possible oxidation reactions of indene by $[Fe^{III}(bpy)_3]^{3+}$ (Figure 4-11C).

Coating of the working electrode was also observed in the measurements of an HCp* solution in MeCN, and thus, oxidized HCp* is also assumed to form its polymers. C-H abstraction from fluorine at the 9-position has been reported to afford 9*H*,9′*H*-[9,9′]bifluorenyl as a product;[46] however, the author could not detect any dimeric products.

To elucidate the C-H bond cleavage process, kinetic isotope effects (KIE) were investigated for the oxidation reactions of HCp* (HCp* and HCp*-d_1) and DHA (DHA and DHA-d_4) with $\mathbf{7}_{OX}$ or $\mathbf{10}_{OX}$, and KIE for the oxidation reaction of ethylbenzene (EtPh and EtPh-d_{10}) with $\mathbf{10}_{OX}$ was also determined. In the oxidation of DHA, both $\mathbf{7}_{OX}$ and $\mathbf{10}_{OX}$ showed relatively large KIE values: 4.5 ± 0.2 for $\mathbf{7}_{OX}$ and 4.2 ± 0.3 for $\mathbf{10}_{OX}$. For the oxidations of ethylbenzene with $\mathbf{10}_{OX}$ and HCp* by $\mathbf{7}_{OX}$, KIE values were determined to be 1.67 ± 0.08 and 8.1 ± 0.4, respectively. The four KIE values mentioned above indicated that the C-H oxidations proceed through a CPET mechanism rather than a stepwise PT/ET or ET/PT mechanism. In stark contrast, the oxidation reaction of HCp* with $\mathbf{10}_{OX}$ gave a small KIE value of 1.33 ± 0.06. Based on this small KIE value as well as the aforementioned much larger k value, the oxidation of HCp* with $\mathbf{10}_{OX}$ is proposed to proceed through an ET/PT mechanism, in which the PT step is the rate-determining step, rather than a CPET pathway. The lower E_{ox} potential of HCp* (+0.95 V vs SCE) as compared to those of other substrates (+1.5 – 2.0 V vs SCE) probably provides the ET/PT mechanism with increasing the driving force of electron transfer from HCp* to the Ru^{III}-pterin complex, $\mathbf{10}_{OX}$.

Plots of log k' (k' = k/n; n = number of equivalent hydrogen atoms to be abstracted) for C-H oxidations with $\mathbf{7}_{OX}$ and $\mathbf{10}_{OX}$ against BDE values of the C-H bonds to be cleaved were prepared to argue the difference of the mechanisms, depending on the substrates and the oxidants (Figure 4-12). In the case of $\mathbf{7}_{OX}$, the log k' values for the oxidation reactions of the five hydrocarbons showed a linear relationship with the BDE values as depicted in Figure 4-12A. In the case of $\mathbf{10}_{OX}$, in contrast to the case of $\mathbf{7}_{OX}$, a much higher k' value was

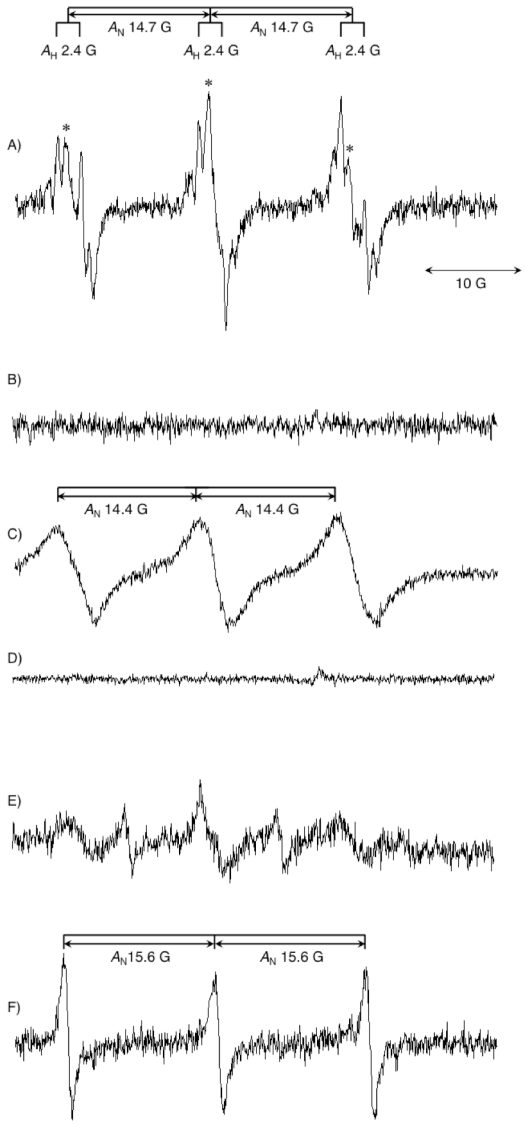

Figure 4-11. ESR spectra of spin adducts formed in trapping reactions with MNP and those of control samples observed at room temperature under Ar atmosphere. (A) $\mathbf{10}_{OX}$ in MeCN/indene/MNP dimer in the dark; (B) $\mathbf{10}_{OX}$ in MeCN/indene in the dark; (C) $[Fe^{III}(bpy)_3]^{3+}$ in MeCN/indene/MNP dimer in the dark; (D) $\mathbf{10}_{OX}$ in MeCN in the dark; (E) MNP dimer in MeCN in the dark; (F) MNP in MeCN under light irradiation (white light). ESR spectrometer conditions: micro wave power, 60 mW; modulation, 100.00 kHz, 0.50 G; scan range, 3510 ± 25 G; gain, 1.00×10^4; scans, 7. Signals with an asterisk in (A) are those of MNP monomer depicted in (F) with A_N = 15.6 G.

obtained for the aforementioned ET/PT oxidation of HCp* than those for other five substrates. Except HCp*, the log *k*' values for the other five substrates showed a linear relationship relative to the BDE values of the C-H bonds, as depicted in Figure 4-12B. The linear correlations observed for the oxidation reactions by $\mathbf{7}_{OX}$ and $\mathbf{10}_{OX}$ indicate that the reactions proceed through a common mechanism. Thus, the oxidation of HCp* by $\mathbf{10}_{OX}$ is concluded to proceed in a different mechanism, *i.e.,* an ET/PT mechanism, as mentioned above.

In general, the linear relationship between the second-order rate-constants and BDEs of the C-H bonds to be cleaved has been analyzed on the basis of the Bell-Evans-Polanyi (BEP) relation as expressed by the following equations 4 and 5:[47,48]

$$E_a = a\Delta H° + C \quad (4)$$

$$\Delta H° = \mathrm{BDE}_{\text{C–H to be cleaved}} + \mathrm{BDE}_{\text{for oxidant}} \quad (5)$$

Logarithm of rate constants of C-H oxidation reactions by high-valent metal-oxo complexes, which are excellent oxidants to oxidize organic substrates, generally obey the BEP relation to give coefficients of $\alpha \sim -0.5$.[49] In the case of a metal complex having a hydroxo ligand as a basic site as an oxidant in HAT, the α values have been reported by Stack and coworkers to be –0.1 (Mn^{III}-OH)[50] and –0.2 (Fe^{III}-OH),[51] which are smaller than those with metal-oxo complexes as oxidants. Except the oxidation of HCp* with $\mathbf{10}_{OX}$, the log k' values for oxidation reactions of hydrocarbons with $\mathbf{7}_{OX}$ and $\mathbf{10}_{OX}$ obeyed the BEP correlation and the coefficients α were determined to be –0.44 for $\mathbf{7}_{OX}$ and –0.27 for $\mathbf{10}_{OX}$, respectively (Figure 4-12). Note that the α value for the C-H oxidation by $\mathbf{10}_{OX}$ is apparently negatively smaller than that obtained for the oxidation of phenol derivatives by $\mathbf{10}_{OX}$ (–0.44).[32] The difference between the α values for $\mathbf{7}_{OX}$ and $\mathbf{10}_{OX}$ highlights distinguishable alteration of characteristics of PCET reactions by both oxidants.

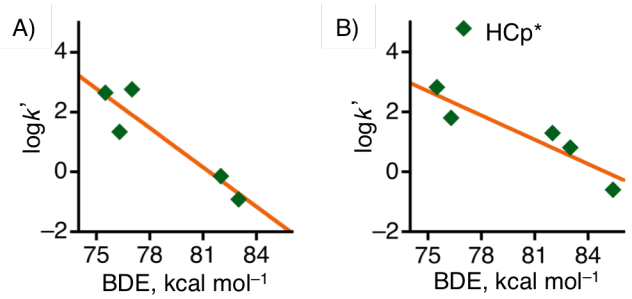

Figure 4-12. Plots of the log k' values at 296 K for oxidation of five hydrocarbon substrates with $\mathbf{7}_{OX}$ (A) and with $\mathbf{10}_{OX}$ (B) against BDE values of C-H bonds to be cleaved in the substrates. In the linear fitting for (B), the k' value for oxidation of HCp* is not included for the calculations.

Leffler advocated that the coefficient α of the BEP correlations reflected the structure of the transition state;[52] based on the Leffler's discussion, a reaction passing through the transition state with the structure reminiscent of that of the product show a negatively larger α value, whereas that passing through the transition state with the structure reminiscent of that of the starting material affords a negatively smaller α value.[50,51] From this viewpoint, the coefficient α of the oxidation reactions with $\mathbf{10}_{OX}$ suggest that the reaction proceeds *via* a transition state involving a structure close to the initial structure: The proton to be transferred should interact strongly with the attached carbon atom. On the contrary, the reactions by $\mathbf{7}_{OX}$ go through a transition state involving a structure close to the product compared to the case of $\mathbf{10}_{OX}$ and the proton should interact strongly with the N1 atom of the $dmdmp^-$ ligand than in the reaction with $\mathbf{10}_{OX}$.

The arguments can be supported by the difference of characteristics of the two complexes, in light of the redox potentials of the Ru^{II}/Ru^{III} couples (+0.24 V for $\mathbf{7}_{OX}$ and +0.66 V for $\mathbf{10}_{OX}$; see Table 4-1 and Scheme 4-2), representing the electron-acceptability at the Ru^{III} center, and the pK_a values of the Ru^{III}-bound $dmdmp^-$ ligand (11.3 for $\mathbf{7}_{OX}$ and 9.9 for $\mathbf{10}_{OX}$ see Scheme 4-2), standing for the proton-acceptability. Thus, complex $\mathbf{7}_{OX}$ has lower electron-acceptability and higher proton-acceptability, whereas complex $\mathbf{10}_{OX}$ has higher electron-acceptability and lower proton-acceptability. Thus, the more basic complex $\mathbf{7}_{OX}$ pulls a proton from the substrate to be abstracted at the early stage of the oxidation reaction based on its high basicity to compensate its low electron acceptability (Scheme 4-4, left). The "proton-pulling" arrangement in the transition state induces the rise of electron acceptability of the Ru^{III} center and lowering of the oxidation

potential of the substrate to be oxidized. On the other hand, since complex $\mathbf{10}_{OX}$ shows the higher electron-acceptability reflected on the higher redox potential, even though complex $\mathbf{10}_{OX}$ shows lower proton acceptability reflected on the lower pK_a value, the complex requires not so much proton shift toward the dmdmp$^-$ ligand to gain large polarization of the C-H bond. Thus, it is concluded that the polarization of the C-H bond in the transition state can be controlled by the basicity of the proton acceptor site, even though the apparent BDE values are comparable, and this causes the difference of the reactivity of the oxidants in C-H oxidation.

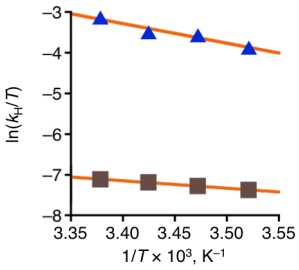

Figure 4-13. Eyring plots for the oxidation of DHA by $\mathbf{7}_{OX}$ (brown squares) and $\mathbf{10}_{OX}$ (blue triangles) in MeCN.

The activation parameters were determined from the kinetic measurements at several temperatures about oxidation of indene, DHA, xanthene, HCp*, and fluorene with $\mathbf{7}_{OX}$ and $\mathbf{10}_{OX}$ (Figure 4-13 and Table 4-3). Apart from oxidation of HCp*, complex $\mathbf{7}_{OX}$ shows negatively larger $\Delta S^{\ddagger}$ values and positively smaller $\Delta H^{\ddagger}$ values than those of $\mathbf{10}_{OX}$. The larger $\Delta S^{\ddagger}$ values of $\mathbf{7}_{OX}$ correspond to the aforementioned proposal about the transition states; *i.e.* complex $\mathbf{7}_{OX}$ preforms oxidation reactions *via* more strongly interacted transition states than that of $\mathbf{10}_{OX}$. The smaller $\Delta H^{\ddagger}$ values of $\mathbf{7}_{OX}$ also correspond to difference between $\mathbf{10}_{OX}$ and $\mathbf{7}_{OX}$; complex $\mathbf{7}_{OX}$ is expected to have higher basicity (calcd. pK_a = 11.3) than that of $\mathbf{10}_{OX}$ (calcd. pK_a = 9.9) and the higher basicity must provide stable formation of the complex between C-H bond to be cleaved and the dmdmp ligand of the oxidants in the transition state.

In oxidation of HCp* with $\mathbf{7}_{OX}$ and $\mathbf{10}_{OX}$, inverted tendency was observed in values of $\Delta S^{\ddagger}$ and $\Delta H^{\ddagger}$; complex $\mathbf{10}_{OX}$ shows negatively larger (or comparable) $\Delta S^{\ddagger}$ values and positively smaller $\Delta H^{\ddagger}$ values than these of $\mathbf{7}_{OX}$. The deviation from the tendency can be explained by the aforementioned proposal that complex $\mathbf{10}_{OX}$ oxidizes HCp* through a different process (ET/PT) from that by $\mathbf{7}_{OX}$ (CPET). This large $\Delta S^{\ddagger}$ value in the oxidation reaction of HCp* with $\mathbf{10}_{OX}$ can be attributed to the character of its transition state and the solvation. Among the oxidation reactions studied here, only that of HCp* with $\mathbf{10}_{OX}$ afforded radical cation species (HCp*$^{\bullet+}$) by ET instead of a neutral radical (Cp*$^{\bullet}$) by HAT. In outer-sphere electron transfer, reorganization of solvent molecules mainly controls the activation entropy of the reaction.[53-55] MeCN employed in this study as the solvent is expected to firmly solvate the molecules in the transition state for the

Table 4-3. Activation Parameters for Oxidation of C-H Bonds with $\mathbf{7}_{OX}$ and $\mathbf{10}_{OX}$.

	$\mathbf{7}_{OX}$		$\mathbf{10}_{OX}$	
Substrates	$\Delta S^{\ddagger}$ [a]	$\Delta H^{\ddagger}$ [b]	$\Delta S^{\ddagger}$ [a]	$\Delta H^{\ddagger}$ [b]
xanthene	–32 ± 2	4.0 ± 0.6	–21 ± 2	6.9 ± 0.7
DHA	–33 ± 3	4.8 ± 0.8	–28 ± 1	5.6 ± 0.3
HCp*	–17 ± 5	9 ± 1	–21.5 ± 0.3	4.5 ± 0.7
indene	–49.1 ± 0.5	3.6 ± 0.1	–21 ± 5	9 ± 2
fluorene	–51.2 ± 0.4	2.0 ± 0.1	–44.9 ± 0.7	1.9 ± 0.2

[a] cal K^{-1} mol^{-1} . [b] kcal mol^{-1}

Scheme 4-4. Proposed arrangements of the transition states in C-H oxidation by $\mathbf{7}_{OX}$ and $\mathbf{10}_{OX}$.

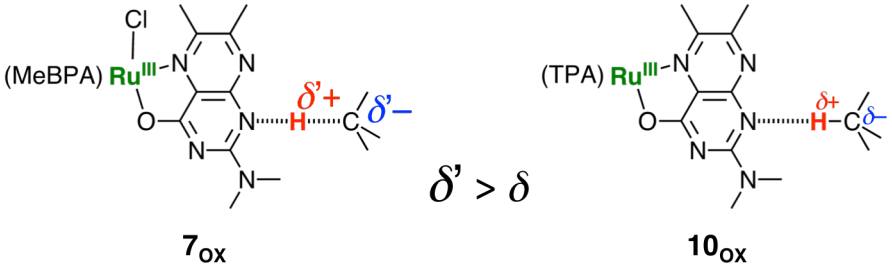

$\mathbf{7}_{ox}$ $\mathbf{10}_{ox}$

ET reaction from HCp* to $\mathbf{10}_{OX}$, and the strong solvation probably provides the relatively large $\Delta S^{\ddagger}$.

4–5 Summary

The two Ru^{II}-pterin complexes employed in this work, **7** and **10**, have similar structures to each other, and their corresponding $1e^-$-oxidized species ($\mathbf{7}_{OX}$ and $\mathbf{10}_{OX}$) show relatively comparable BDE values in the thermochemical square schemes of PCET. Complexes $\mathbf{7}_{OX}$ and $\mathbf{10}_{OX}$, however, have difference in electron- and proton-acceptability; *i.e.* complex $\mathbf{10}_{OX}$ shows higher electron-acceptability than that of **7**, whereas complex $\mathbf{7}_{OX}$ shows higher proton-acceptability than $\mathbf{10}_{OX}$. To explore the impact of the electron- and proton-acceptability of the oxidant on the oxidation activity, the substrate oxidations with $\mathbf{7}_{OX}$ and $\mathbf{10}_{OX}$ were investigated on the basis of detailed kinetic analysis. Complexes $\mathbf{7}_{OX}$ and $\mathbf{10}_{OX}$ show the same reactivity in oxidation of substrates with relatively high pK_a values such as xanthene, whereas in oxidation reactions of substrates with relatively small pK_a values such as indene, complex $\mathbf{10}_{OX}$ showed a *ca.* 50 times larger rate constant than that with $\mathbf{7}_{OX}$. BEP analysis for the oxidation reaction with $\mathbf{7}_{OX}$ and $\mathbf{10}_{OX}$ revealed that complex $\mathbf{7}_{OX}$ attracts proton from the C-H bond of a substrate to make the bond more polarized for making electron transfer from the substrate more favorable. Therefore, pK_a and E_{red} values of an oxidant are not only components of BDE, but also are significant factors to control the reactivity of the oxidant as a hydrogen-atom acceptor by affecting the transition-state structure in CPET oxidation reactions.

Reference and Notes

(1) (a) Huynh, M. H. V.; Meyer, T. J. *Chem. Rev.* **2007**, *363*, 1246. (b) Warren, J. J.; Tronic, T. A.; Mayer, J. M. *Chem. Rev.* **2010**, *110*, 6961. (c) Gagliardi, C. J.; Westlake, B. C.; Kent, C. A.; Paul, J. J.; Papanikolas, J. M.; Meyer, T. J. *Coord. Chem. Rev.* **2010**, *254*, 2459. (d) Weinberg, D. R.; Gagliardi, C. J.; Hull, J. F.; Murphy, C. F.; Kent, C. A.; Westlake, B. C.; Paul, A.; Ess, D. H.; McCafferty, D. G.; Meyer, T. J. *Chem. Rev.* **2012**, *112*, 4016.

(2) (a) Mayer, J. M. *Annu. Rev. Phys. Chem.* **2004**, *55*, 363. (b) Hammes-Schiffer, S. *Acc. Chem. Res.* **2009**, *42*, 1881. (c) Hammes-Schiffer, S.; Hatcher, E.; Ishikita, H.; Skone, J. H.; Soudackov, A. V. *Coord. Chem. Rev.* **2008**, *252*, 384.

(3) Olah, G. A.; Molnár, Á. *Hydrocarbon Chemistry*; Wiley: New York, 1995.

(4) Snider, B. B. *Chem. Rev.* **1996**, *96*, 339.

(5) Reece, S. Y.; Nocera, D. G. *Annu. Rev. Biochem.* **2009**, *78*, 673.

(6) (a) Samuelsson, B.; Dahlè, S.-E.; Lindgren, J. Å.; Rouzer, C. A.; Serhan, C. N. *Science* **1987**, *237*, 1171. (b) Gradner, H. W. *Biochim. Biophys. Acta* **1991**, *1084*, 221. (c) Clark, K. B.; Culshaw, P. N.; Griller, D.; Lossing, F. P.; Simões J. A. M.; Walton, J. C. *J. Org. Chem.* **1991**, *56*, 5535. (d) de Groot, J. J. M. C.; Veldink, G. A.; Vliegenthart, J. F. G.; Boldingh, J.; Wever, R.; van Gelder, B. F. *Biochim. Biophys. Acta* **1975**, *377*, 71. (e) Schilstra, M. J.; Veldink, G. A.; Vliegenthart, J. F. G. *Biochemistry* **1994**, *33*, 3974. (f) Nelzon, M. J. *J. Am. Chem. Soc.* **1988**, *110*, 2985.

(7) (a) Merkx, M.; Kopp, D. A.; Sazinsky, M. H.; Blazyk, J. L.; Müller, J.; Lippard, S. J. *Angew. Chem., Int. Ed.* **2001**, *40*, 2782. (b) Baik, M.-H. H.; Newcomb, M.; Friesner, R. A.; Lippard, S. J. *Chem. Rev.* **2003**, *103*, 2385.

(8) Mulliez, E.; Fontecave, M. *Chem. Ber./Recueil* **1997**, *130*, 317.

(9) Ortiz de Montellano, P. R. *Cytochrome P450 Structure, Mechanism, and Biochemistry*; Springer Science & Business Media, (a) 2nd ed. 1995; (b) 1st ed. 1985.

(10) Du Bois, J.; Mizoguchi, T. J.; Lippard, S. J. *Coord. Chem. Rev.* **2000**, *200-202*, 443.

(11) Que, L., Jr.; Dong, Y. *Acc. Chem. Res.* **1996**, *29*, 190.

(12) (a) Groves, J. T.; Nemo, T. E.; Myers, R. S. *J. Am. Chem. Soc.* **1979**, *101*, 1032. (b) Groves, J. T.; Haushalter, R. C.; Nakamura, M.; Nemo, T. E.; Evans, B. J. *J. Am. Chem. Soc.* **1981**, *103*, 2884.

(13) (a) Cukier, R. I. *Biochim. Biophys. Acta* **2004**, *1655*, 37. (b) Hammes-Schiffer, S. *Acc. Chem. Res.* **2001**, *34*, 273.

(14) McMillen, D. F.; Golden, D. M. *Annu. Rev. Phys. Chem.* **1982**, *33*, 493.

(15) Tilset, M.; Parker, V. D. *J. Am. Chem. Soc.* **1989**, *111*, 6711.

(16) Parker, V. D.; Handoo, K. L.; Roness, F.; Tilset, M. *J. Am. Chem. Soc.* **1991**, *113*, 7493.

(17) Wayner, D. D.; Parker, V. D. *Acc. Chem. Res.* **1993**, *26*, 287.

(18) Skagestad, V.; Tilset, M. *J. Am. Chem. Soc.* **1993**, *115*, 5077.

(19) Tilset, M. In *Electron Transfer in Chemistry*; Balzani, V., Ed.; Wiley-VCH: Weinheim, Germany, MA, 2001; Vol. 2, pp 677-713.

(20) (a) Mayer, J. M. *Acc. Chem. Res.* **2011**, *44*, 36. (b) Que, L., Jr. *Acc. Chem. Res.* **2007**, *40*, 493. (c) Nam, W. *Acc. Chem. Res.* **2007**, *40*, 522. (d) Fukuzumi, S. *Dalton Trans.* **2015**, *44*, 6696. (e) Ishizuka,

T.; Ohzu, S.; Kojima, T. *Synlett* **2014**, *25*, 1667.

(21) Sastri, C. V.; Lee, J.; Oh, K.; Lee, Y. J.; Lee, J.; Jackson, T. A.; Ray, K.; Hirao, H.; Shin, W.; Halfen, J. A.; Kim, J.; Que, L., Jr.; Shaik, S.; Nam, W. *Proc. Nat. Acad. Sci. USA* **2007**, *104*, 19181.

(22) Groves, J. T.; Gross, Z.; Stern, M. K. *Inorg. Chem.* **1994**, *33*, 5065.

(23) Gupta, R.; Borovik, A. S. *J. Am. Chem. Soc.* **2003**, *125*, 13234.

(24) Roth, J. P.; Mayer, J. M. *Inorg. Chem.* **1999**, *38*, 2760.

(25) Mader, E. A.; Davidson, E. R.; Mayer, J. M. *J. Am. Chem. Soc.* **2007**, *129*, 5153.

(26) (a) Manner, V. W.; DiPasquale, A. G.; Mayer, J. M. *J. Am. Chem. Soc.* **2008**, *130*, 7210. (b) Manner, V. W.; Mayer, J. M. *J. Am. Chem. Soc.* **2009**, *131*, 9874.

(27) (a) Hille, R. *Chem. Rev.* **1996**, *96*, 2757. (b) Kappock, T. J.; Caradonna, J. P. *Chem. Rev.* **1996**, *96*, 2659.

(28) (a) Benkovic, S. J.; Sammons, D.; Armarego, W. L. F.; Waring, P.; Inners, R. *J. Am. Chem. Soc.* **1985**, *107*, 3706. (b) Bobst, A. *Helv. Chim. Acta* **1967**, *50*, 2222.

(29) Kaim, W.; Schwederski, B.; Heilmann, O.; Hornung, F. M. *Coord. Chem. Rev.* **1999**, *182*, 323.

(30) (a) Abelleira, A.; Galang, R. D.; Clarke, M. J. *Inorg. Chem.* **1990**, *29*, 633. (b) Kohzuma, T.; Masuda, H.; Yamauchi, O. *J. Am. Chem. Soc.* **1989**, *111*, 3431. (c) Odani, A.; Masuda, H.; Inukai, K.; Yamauchi, O. *J. Am. Chem. Soc.* **1992**, *114*, 6294. (d) Kojima, T.; Sakamoto, T.; Matsuda, Y.; Ohkubo, K.; Fukuzumi, S. *Angew. Chem., Int. Ed.* **2003**, *42*, 4951. (e) Inui, Y.; Miyazaki, S.; Ohkubo, K.; Fukuzumi, S.; Kojima, T. *Angew. Chem., Int. Ed.* **2012**, *51*, 4623.

(31) Miyazaki, S.; Kojima, T.; Sakamoto, T.; Matsuyama, T.; Ohkubo, K.; Fukuzumi, S. *Inorg. Chem.* **2008**, *47*, 333.

(32) Miyazaki, S.; Kojima, T.; Mayer, J. M.; Fukuzumi, S. *J. Am. Chem. Soc.* **2009**, *131*, 11615.

(33) Kaljurand, I.; Kütt, A.; Sooväli, L.; Rodima, T.; Mäemets, V.; Leito. I.; Koppel, I. A. *J. Org. Chem.* **2005**, *70*, 1019.

(34) Luo, J.; Rath, N. P.; Mirica, L. M. *Inorg. Chem.* **2011**, *50*, 6152.

(35) Goldsmith, C. R.; Jonas, R. T.; Stack, T. D. P. *J. Am. Chem. Soc.* **2002**, *124*, 83.

(36) Wu, A.; Mayer, J. M. *J. Am. Chem. Soc.* **2008**, *130*, 14745.

(37) Mader, E. A.; Manner, V. W.; Markle, T. F.; Wu, A.; Franz, J.; Mayer, J. M. *J. Am. Chem. Soc.* **2009**, *131*, 4335.

(38) Rhile, J. I.; Markle, T. F.; Nagano, H.; Dipasquale, A. G.; Lam, O. P.; Lockwood, M. A.; Rotter K.; Mayer, J. M. *J. Am. Chem. Soc.* **2006**, *128*, 6075.

(39) Manna, B.; Ghosh, R.; Palit, D. K. *J. Phys. Chem. C* **2015**, *119*, 10641.

(40) The absorption spectrum of **10**-H^+ has been reported to show the absorption maxima at 490 and 441 nm. See ref. 32

(41) (a) Bordwell, F. G.; Cheng, J.-P.; Ji, G.-Z.; Satish, A. V.; Zhang, X. *J. Am. Chem. Soc.* **1991**, *113*, 9790. (b) Bordwell, F. G. *Acc. Chem. Res.* **1988**, *21*, 456.

(42) Luo, Y.-R. *Handbook of Bond Dissociation Energies in Organic Compounds*, CRC Press, Boca Raton, **2003**.

(43) Marcinek, A.; Rogowski, J.; Adamus, J.; Gębicki, J.; Platz, S. *J. Phys. Chem.* **1996**, *100*, 13539.

(44) Akbulut, U.; Khurshid, A.; Hacioğlu, B.; Toppare, L. *Polymer* **1990**, *31*, 1343.

(45) Buettner, G. R. *Free Radical Biol. Med.* **1987**, *3*, 259.

(46) Matsumoto, T.; Ohkubo, K.; Honda, K.; Yazawa, A.; Furutachi, H.; Fujinami, S.; Fukuzumi, S.; Suzuki, M. *J. Am. Chem. Soc.* **2009**, *131*, 9258.

(47) Mayer, J. M.; Stack, T. D. P. *Acc. Chem. Res.* **1998**, *31*, 441.

(48) Wang, D.; Zhang, M.; Bühlmann, P.; Que, L., Jr. *J. Am. Chem. Soc.* **2010**, *132*, 7638.

(49) Bryant, J. R.; Mayer, J. M. *J. Am. Chem. Soc.* **2003**, *125*, 10351.

(50) Goldsmith, C. R.; Cole, A. P.; Stack, T. D. P. *J. Am. Chem. Soc.* **2005**, *127*, 9904.

(51) Goldsmith, C. R.; Stack, T. D. P. *Inorg. Chem.* **2006**, *45*, 6048.

(52) (a) Leffler, J. E. *Science* **1953**, *117*, 340. (b) Murdoch, J. R. *J. Am. Chem. Soc.* **1972**, *94*, 4410.

(53) Bader, J. S.; Kuharski, R. A.; Chandler, D. *J. Chem. Phys.* **1990**, *93*, 230.

(54) (a) Garrera, H. A.; Gsponer, H. E.; Garcia, N. A.; Cosa, J. J.; Previtali, C. M. *J. Photochem.* **1986**, *33*, 257. (b) Garrera, H. A.; Cosa, J. J.; Previtali, C. M. *J. Photochem. Photobiol. A*; *Chem.* **1991**, *56*, 267.

(55) Ungar, L. W.; Newton, M. D.; Voth, G. A. *J. Phys. Chem. B* **1999**, *103*, 7367.

Chapter 5 Concluding Remarks

In this thesis, to shed lights on the characteristics of heteroaromatic coenzymes, a PQQ derivative and a pterin derivative, which are indispensable for biologically important oxidation reactions, transition-metal complexes having the heteroaromatic coenzymes as ligands have been synthesized and characterized in detail. The scope has been expanded to PCET oxidation reactions of C-H bonds of organic substrates, which have been argued on the basis of the detailed kinetic analysis to clarify the impact of the characteristic of oxidants on molecular arrangements in the transition states.

In Chapter 2, two ruthenium(II)-silver(I)-PQQTME-terpy complexes (**1** and **4**) have been synthesized, and redox processes of their derivatives (**2**, and **5**) have been investigated to reveal the influence of the metal coordination upon the electronic structures of their PQQTME ligands. The ruthenium(II) and silver(I) ions in **1** are bound to the PQQTME ligand through the ONO and OO coordination sites, respectively, while the coordination sites of the ruthenium(II) and silver(I) ions in **4** are inverted from those in **1**. Additionally, two Ru^{II}-Ag^{I}-PQQTME units in **4** are linked with a ring-structured $Ag^{I}_2(OTf)_2$ unit. By the difference in the coordination structures between **1** and **4**, the stability gain in the complexation of the silver(I) ion with the PQQTME ligand in solution are controlled. When complex **1** was dissolved into a coordinating organic solvent, it lost the silver(I) ion to give a mononuclear ruthenium(II) complex, **2**. On the other hand, when complex **4** was dissolved into a solvent such as aqueous MeCN or THF, **4** lost the $Ag^{I}_2(OTf)_2$ bridge and split into two parts, but the silver(I) ion bound at the ONO coordinating site did not dissociate to give two molecules of a Ru^{II}-Ag^{I}-heterodinuclear PQQTME complex **5**, because of the higher stability in the coordination of the Ag(I) ion at the ONO tridentate site in **4** than that at the OO bidentate site in **1**. The PQQTME ligands in **2** and **5** exhibited higher reduction potentials than those of PQQ in natural quinoproteins and free PQQTME, reflecting the high electron-acceptability of the bound ruthenium(II)-terpy unit. In addition, PQQTME in **5** showed a higher reduction potential than that in **2**, and thus, the silver(I) ion in **5** played a role as a Lewis acid to raise the reduction potential of the PQQTME ligand. In consequence, the coordination of the silver(I) ion at the ONO-coordination site in **5** significantly strengthens the electron-acceptability of the PQQTME ligand.

In Chapter 3, four pterin complexes (**6**-H^+, **7**-H^+, **8**, and **9**) have been synthesized on the purpose to obtain pterin-OO-metal species, which is regarded as a plausible candidate of the active species in pterin-dependent hydroxylases. The pterin complexes and their protonated derivatives have been characterized especially with electrochemical measurements to obtain $1e^-$-reduced pterin species, because the target species can be formed by the reaction of the accessible $1e^-$-reduced pterin species with a $O_2^{\bullet-}$ ion. Among the pterin complexes studied here, only ruthenium(II)-(diprotonated pterin)-TPMOM complex, **6**-$2H^+$, gave a reversible reduction wave for the protonated pterin ligand in the CV measured in MeCN. Judging from the higher reduction potential and the reversibility of its $1e^-$-reduction behavior, complex **6**-$2H^+$ was regarded as the best candidate among the pterin complexes for the precursor to obtain the target pterin-OO-metal species. However, the target pterin-OO-metal species could not be obtained from **6**-$2H^+$, mainly due to the low protonation efficiency of **6** and decomposition of the chemical reductant in the presence of excessive amount of a strong acid added to the solution of **6**. To solve these problems, introduction of alkyl groups to the N1

and N3 position of the pterin framework is one of the alternatives: The *N*-alkylated pterins are equivalent to the neutral or protonated pterin in terms of the electronic structures, and thus, a high reduction potential can be expected. On the other hand, the *N*-alkyl groups should be stable against the detachment in comparison with a proton, and thus, reversibility of the reduction processes is more prominent.

As described in Chapter 4, $1e^-$-oxidized species of two pterin complexes, $\mathbf{7}_{OX}$ and $\mathbf{10}_{OX}$, have been demonstrated to oxidize C-H bonds of hydrocarbons, which is rare for metal complexes having no oxo groups in the structure. In addition, Complex $\mathbf{7}_{OX}$ has higher proton-acceptability and lower electron-acceptability than $\mathbf{10}_{OX}$, and thus, comparison of the reactivity between these oxidants can reveal the impacts of the proton- and electron-acceptability of oxidants on the mechanisms of PCET oxidation reactions at C-H bonds. In this study, it has been revealed that molecular arrangements of transition states in CPET reactions are affected by proton- and electron-acceptability of oxidants; *i.e.* an oxidant with high proton-acceptability and low electron acceptability involves a transition state having relatively more polarized C-H bond of a substrate to lower the oxidation potential of the substrate.

Throughout this research, the author has revealed that ancillary ligands in transition-metal complexes of hereoaromatic coenzymes and protonation states of the coenzyme ligands severely affect reversibility of the reduction processes of the heteroaromatic coenzymes as ligands. Based on the results, the author has obtained important insights for molecular designs to form reduced coenzyme species in a metal coordination sphere. The strategy to improve the reversibility of the ligand reduction process and stabilize the ligand-reduced species by coordination to transition-metal complex moieties has been proved very effective also in this study. The studies on redox properties and reactivity of heteroaromatic enzymes will be more important to elucidate the biological functions and to gain mechanistic insights into biologically important reactions performed by enzymes using the heteroaromatic coenzymes as indispensable cofactors. Also, development of an oxidant in C-H oxidation without a metal-oxo group can provide a novel, clean, and sustainable strategy toward production of useful molecules and materials *via* energetically feasible PCET pathway.

Chapter 6 Experimental Section

6–1 General

Chemicals and solvents were used as received from Tokyo Chemical Industry (TCI) Co., Wako Chemicals, Nacalai Tesque or Sigma-Aldrich Corp. PQQTME,[1-4] [$RuCl_3$(terpy)],[5] MeBPA,[6,7] TPMOM,[8] [$RuCl_3$(TPMOM)],[9] Hdmdmp,[10] [Ru(dmdmp)(TPA)][11] were prepared by the literature procedures. [$Ru^{III}Cl_3$(MeBPA)] was prepared with a modified procedure reported by Shimizu *et al.*.[12] UV-vis spectra were collected on Shimadzu UV-3600 and Shimadzu UV-2450 spectrophotometers. ^{1}H NMR measurements were made on JEOL EX-270 and JNM-ECS 400 spectrometers at room temperature. ESI-TOF- and GC-EI-MS spectra were measured on JEOL JMS-T100CS and SHIMADZU GC-2010 Plus spectrometers, respectively. Electrochemical measurements were performed on a BAS CV-1B voltammetric analyzer and an AUTOLAB PGSTAT12 potentiometer. ESR spectra were recorded on a Bruker EMXPlus 9.5/2.7 spectrometer at 95 K, controlled by ER 4131VT and ER 4141VT temperature-control modules using liquid N_2.

6–2 Synthesis

6–2–1 [(terpy)Ru^{II}(μ-PQQTME)$Ag^{I}(OTf)_2$](OTf) (1·OTf)

At first, the chloro ligands of [$RuCl_3$(terpy)] were substituted with solvent molecules by a modified procedure of the Thibault's method;[13] to a dried Schlenk tube, [$RuCl_3$(terpy)] (3.0 mg, 6.8 μmol) and AgOTf (11.4 mg, 44.6 μmol) were charged and then degassed H_2O (5 mL) was added under argon atmosphere. The mixture was stirred at 55 °C for 60 min, cooled down to room temperature and then filtered through a membrane filter to remove AgCl formed. The brown filtrate was dried up for several hours *in vacuo* at < 40 °C to give green solid of [Ru(terpy)$(OH_2)_3$]$(OTf)_2$. To the solid was added PQQTME (2.6 mg, 7.0 μmol) and dry 1,2-dichloroethane (2.5 mL), and then heated at reflux for 3 h under argon atmosphere. The reaction mixture was cooled down to room temperature and then filtered. Concentration of the filtrate under ambient pressure for 2 weeks gave green crystals and brown solution. Collection of the green crystals gave the title compound (5.0 mg, 4.0 μmol, 59%). Anal.: Calcd. for $C_{35}H_{23}N_5O_{17}F_9S_3RuAg\cdot 2CH_2Cl_2\cdot 7H_2O$: C 28.53, H 2.65, N 4.50. Found: C 28.50, H 2.41, N 4.76. ESI-TOF-MS (MeCN): *m*/*z* = 353.6 (calcd. for [Ru^{II}(PQQTME)(terpy)]$^{2+}$: *m*/*z* = 353.5). ^{1}H NMR (CD_3CN): δ 3.91 (s, 3H, COOMe), 3.97 (s, 3H, COOMe), 4.22 (s, 3H, 7-COOMe of PQQTME), 7.30 (d, *J* = 2.2 Hz, 1H, H3 of PQQTME), 7.48 (ddd, *J* = 7.7, 5.5, 1.1 Hz, 2H, H5 of terpy), 7.81 (dd, *J* = 5.5, 1.1 Hz, 2H, H6 of terpy), 8.12 (td, *J* = 7.8, 1.1 Hz, 2H, H4 of terpy), 8.39 (d, *J* = 7.9 Hz, 1H, H4' of terpy), 8.42 (dd, *J* = 7.9, 1.1 Hz, 2H, H4 of terpy), 8.54 (d, *J* = 7.9 Hz, 2H, H3' of terpy), 9.08 (s, 1H, H8 of PQQTME), 12.82 (br s, 1H, H1 of PQQTME). UV-Vis (DMF at –20 °C): λ_{max} [nm] = 705, 476, 377, 338.

6–2–2 [Ru^{II}(η^3-PQQTME)(terpy)]$^{2+}$ (2)

Dissolving **1**·OTf in MeCN gave a green solution of **2**. ESI-TOF-MS (MeCN): *m*/*z* = 353.6 (calcd. for [Ru(PQQTME)-(terpy)]$^{2+}$: *m*/*z* = 353.5). ^{1}H NMR (CD_3CN): δ 3.91 (s, 3H, COOMe), 3.97 (s, 3H, COOMe), 4.22 (s, 3H, 7-COOMe of PQQTME), 7.30 (d, *J* = 2.2 Hz, 1H, H3 of PQQTME), 7.48 (ddd, *J* = 7.7, 5.5, 1.1 Hz, 2H, H5 of terpy), 7.81 (dd, *J* = 5.5, 1.1 Hz, 2H, H6 of terpy), 8.12 (td, *J* = 7.8, 1.1 Hz, 2H, H4 of terpy),

8.39 (d, J = 7.9 Hz, 1H, H4' of terpy), 8.42 (dd, J = 7.9, 1.1 Hz, 2H, H4 of terpy), 8.54 (d, J = 7.9 Hz, 2H, H3' of terpy), 9.08 (s, 1H, H8 of PQQTME), 12.82 (br s, 1H, H1 of PQQTME). UV-Vis (DMF at –20 °C): λ_{max} [nm] = 705, 476, 377, 338.

6–2–3 $[Ru^{II}(terpy)(\eta^2\text{-PQQTME})(MeCN)](PF_6)_2$ (3)

Dissolving **1**·OTf into an MeCN solution of $TBAPF_6$ gave a green solution of **2** as mentioned above. A single crystal of **3** was obtained by slow concentration of the solution for several days in the presence of $CHCl_3$ vapor as a poor solubility solvent. This incorporation of the poor solubility solvent into the solution could cause a reduction in the solubility of the complex and the appearance of crystals. HR-MS (MeCN): m/z = 374.0444 (calcd for $[Ru^{II}(PQQTME)(terpy)(MeCN)]^{2+}$: m/z = 374.0428). ^{1}H NMR (CD_3CN): δ 3.91 (s, 3H, COOMe), 3.99 (s, 3H, COOMe), 4.10 (s, 3H, 7-COOMe of PQQTME), 7.35 (d, J = 2.2 Hz, 1H, H3 of PQQTME), 7.48 (ddd, J = 6.6, 5.5, 2.2 Hz, 2H, H5 of terpy), 8.17 (ddd, J = 8.6, 6.6, 1.6 Hz, 2H, H4 of terpy), 8.37 (t, J = 8.2 Hz, 1H, H4′ of terpy), 8.39 (d, J = 8.6 Hz, 2H, H3 of terpy), 8.62 (d, J = 8.2 Hz, 2H, H3′ of terpy), 8.73 (s, 1H, H8 of PQQTME), 8.89 (dd, J = 5.5, 1.6 Hz, 2H, H6 of terpy).

6–2–4 $[\{(terpy)(OH_2)Ru^{II}(\mu\text{-PQQTME})Ag^{I}(OTf)(\mu\text{-OTf})\}_2\{(OTf)Ag^{I}(\mu\text{-OTf})_2Ag^{I}(OTf)\}]$ (4)

Complex **4** was synthesized by a similar procedure of complex **1**. To a dried Schlenk tube, $[RuCl_3(terpy)]$ (5.9 mg, 13 μmol) and AgOTf (27.5 mg, 100 μmol) were charged and then degassed H_2O (5 mL) was added under argon atmosphere. The mixture was stirred at 50 °C for 50 min. The mixture was cooled down to room temperature and then filtered through a membrane to remove precipitated AgCl.[13] The brown filtrate was dried up for several hours *in vacuo* at < 40 °C to give green solid of $[Ru(terpy)(OH_2)_3](OTf)_2$. To the solid was added PQQTME (5.0 mg, 13 μmol) and dry 1,2-dichloroethane (10 mL), and then heated at reflux for 11 h under argon atmosphere. The reaction mixture was cooled down to room temperature and then filtered. Concentration of the filtrate under ambient pressure for 2 weeks gave dark-green crystals and brown solution. Collection of the dark-green crystals gave the title compound (15.2 mg, 4.9 μmol, 75%). Anal.: Calcd. for $C_{72}H_{46}N_{10}O_{40}F_{24}S_8Ru_2Ag_4\cdot 2ClCH_2CH_2Cl\cdot 3H_2O$: C 27.75, H 1.84, N 4.25. Found: C 28.01, H 2.11, N 4.48. ESI-TOF-MS (MeCN/H_2O): m/z = 964.9 (calcd. for $[(terpy)Ru^{II}(PQQTME^{\bullet-})Ag^{I}(TfO^{-})]^{+}$: m/z = 964.9). UV-Vis (DMF at – 50 °C): λ_{max} [nm] = 723, 484, 376, 318.

6–2–5 $[Ru^{II}Cl(TPMOM)(Hdmdmp)](PF_6)$ (6-$H^+\bullet PF_6$)

To a mixture of $[Ru^{III}Cl_3(TPMOM)]$ (56 mg, 0.12 mmol) and Hdmdmp (24.8 mg, 113 μmol) was added a mixture of ethanol (48 mL) and water (12 mL), and the mixture was heated at reflux. Color change of the mixture from brown to dark red was observed immediately after heating, and further reflux for 8.5 h gave dark purple solution. This obtained solution was dried up and the residual solid was dissolved into MeOH. Addition of NH_4PF_6 and ether caused precipitation of title compound as dark purple powder, and that was collected by filtration. ESI-TOF-MS (acetone): m/z = 633.1 (calcd. for $\{[Ru^{II}Cl(Hdmdmp)(MeBPA)]\}^{+}$: m/z = 633.1). ^{1}H NMR (CD_3CN): δ 1.83 (s, 3H, 7-Me), 2.57 (s, 3H, 6-Me), 3.28 (s, 6H, NMe_2), 4.08 (s, 3H, OMe), 6.98 (dd, J = 7.5, 5.5 Hz, 1H, H5 of pyridine-A), 7.20 (dd, J = 8.0, 5.7 Hz, 1H, H5 of pyridine-B), 7.42 (dd, J = 8.0, 6.1 Hz, 1H, H5 of pyridine-C), 7.74 (d, J = 5.5 Hz, 1H, H6 of pyridine-A), 7.81 (td, J = 7.5, 1.4 Hz, 1H, H4 of pyridine-A), 7.84 (ddd, J = 8.0, 7.7, 1.4 Hz, 1H, H4 of pyridine-B), 7.94 (ddd, J = 8.0, 7.8, 1.3 Hz, 1H, H4 of pyridine-C), 7.97 (d, J = 7.7 Hz, 1H, H3 of pyridine-A), 8.02 (d, J = 7.7 Hz, 1H, H3 of pyridine-B), 8.03 (d, J = 7.8 Hz, 1H, H3 of pyridine-C), 9.26 (dd, J = 5.7, 1.4 Hz, 1H, H6 of pyridine-B),

9.29 (dd, J = 6.1, 1.3 Hz, 1H, H6 of pyridine-C) 9.85 (br s, 1H, NH).

6–2–6 [Ru^{II}Cl(dmdmp)(MeBPA)] (7)

To a mixture of [$Ru^{III}Cl_3$(MeBPA)] (56.6 mg, 135 μmol) and Hdmdmp (32.5 mg, 148 μmol) was added ethanol (48 mL), and then water (12 mL) was poured into the suspension. The mixture obtained was degassed and heated at reflux under argon. Color change of the mixture from brown to dark red was observed immediately after heating, and further reflux for 12 h gave dark purple solution. This solution was filtered and Et_3N (10 mL, 72 mmol) was added to the filtrate. EtOAc (150 mL) was added to the red solution obtained and the mixture was concentrated to half a volume to give brown suspension. Filtration of the suspension gave brown powder and colorless needles, the latter of which were assumed to be (Et_3NH)Cl. The solid mixture was dissolved into methanol, and the target compound was separated with column chromatography on Sephadex LH20 eluted with MeOH. The first dark-red fraction was collected, and further purification was performed with column chromatography on Sephadex LH20 eluted with MeOH. After adding EtOAc into the red fraction eluted, the solution was concentrated to give dark purple solution with brown powder. The suspension was filtered, and the obtained solid was washed with EtOAc and diethyl ether gave the target compound as brown powder (30.6 mg, 53.8 μmol, 40%). Anal.: Calcd. for $C_{23}H_{27}N_8OClRu \cdot 0.5H_2O \cdot 0.5MeOH$: C 47.59, H 5.10, N 18.89. Found: C 47.87, H 4.84, N 18.91. ESI-TOF-MS (MeOH): m/z = 591.1 (calcd. for $\{Na^+ + [Ru^{II}(dmdmp)(Cl)(MeBPA)]\}^+$: m/z = 591.2). ^{1}H NMR (CD_3CN): δ 2.12 (s, 3H, 7-Me), 2.18 (s, 3H, CH_3 of MeBPA), 2.23 (s, 3H, 6-Me), 2.52 (s, 6H, NMe_2), 3.89 – 4.12 (m, 4H, CH_2), 7.03 (ddd, J = 7.7, 5.8, 1.2 Hz, 1H, H5 of pyridine-A), 7.06 (dd, J = 7.7, 1.2 Hz, 1H, H3 of pyridine-A), 7.15 (ddd, J = 7.7, 6.3, 1.1 Hz, 1H, 5H of pyridine-B), 7.23 (dd, J = 7.2, 1.1 Hz, 1H, H3 of pyridine-B), 7.39 (td, J = 7.7, 1.2 Hz, 1H, H4 of pyridine-A), 7.57 (ddd, J = 7.7, 7.2, 1.1 Hz, 1H, H4 of pyridine-B), 9.46 (dd, J = 5.8, 1.2 Hz, 1H, H4 of pyridine-A), 9.56 (dd, J = 6.3, 1.1 Hz, 1H, H6 of pyridine-B). UV-Vis (MeCN): λ_{max} [nm] = 392, 495.

6–2–7 [Ru^{II}Cl(Hdmdmp)(MeBPA)](PF_6) (7-$H^+ \cdot PF_6$)

Recrystallization of crude **7**-H^+**,** which was prepared by the method mentioned above, from acetone/octane in the presence of NH_4PF_6 gave dark purple crystals. Anal.: Calcd. for $C_{23}H_{28}N_8OF_6PClRu$: C 38.69, H 3.95, N 15.69. Found: C 38.97, H 3.94, N 15.38. ESI-TOF-MS (MeOH): m/z = 569.1 (calcd. for $\{[Ru^{II}Cl(Hdmdmp)(MeBPA)]\}^+$: m/z = 569.1). UV-Vis (MeCN): λ_{max} [nm] = 326, 363, 549.

6–2–8 [$Rh^{III}Cl_3$(TPMOM)]

$Rh^{III}Cl_3 \cdot nH_2O$ (Rh content: 40 w/w%, 49.68 mg, 193 μmol) and TPMOM (54.9 mg, 197 μmol) were heated in EtOH (5 mL) for 10 h to give pale yellow suspension. Filtration of the suspension gave the title compound as pale yellow powder (79.8 mg, 164 μmol, 85%). Anal.: Calcd. for $C_{17}H_{15}N_3ORhCl_3$: C 41.96, H 3.11, N 8.64. Found: C 41.85, H 3.11, N 8.40. ^{1}H NMR ($(CD_3)_2SO$): δ 4.18 (s, 3H, -OMe), 7.69 (ddd, J = 8.2, 6.9, 1.6 Hz, 3H, H4 of pyridine), 8.13 (dd, J = 8.2, 1.1 Hz, 3H, H3 of pyridine), 8.20 (ddd, J = 6.9, 6.1, 1.1 Hz, 3H, H5 of pyridine), 9.23 (d, J = 6.1 Hz, 3H, H6 of pyridine).

6–2–9 [Rh^{III}(dmdmp)Cl(TPMOM)]Cl (8·Cl)

To a mixture of Hdmdmp (25.10 mg, 114 μmol) and [$Rh^{III}Cl_3$(TPMOM)] (54.30 mg, 112 μmol), were added EtOH (8 mL) and H_2O (2 mL). Obtained yellow suspension was heated at reflux for 13.5 h to obtain yellow solution, and then this solution was filtered. Concentration of the filtrate and addition of ether into the

filtrate caused precipitation of yellow solid of a crude mixture including the target compound, and the solid was collected by filtration. Purification with column chromatography on Sephadex LH 20 eluted with MeOH and recrystallization from MeOH gave the title compound as pale yellow crystal (3.32 mg, 5.0 μmol, 4%). ESI-TOF-MS (MeOH): m/z = 633.2 (calcd. for $\{[Rh^{III}(dmdmp)(Cl)(TPMOM)]\}^+$: m/z = 633.1). ^{1}H NMR ($(CD_3)_2OD$): δ 1.84 (s, 3H, 7-Me), 2.65 (s, 3H, 6-Me), 4.31 (s, 3H, -OMe), 7.51 (ddd, J = 6.1, 6.8, 1.7 Hz, 1H, H5 of pyridine-A), 7.69 (ddd, J = 8.0, 5.4, 1.6 Hz, 1H, H5 of pyridine-C), 7.75 (td, J = 6.0, 4.4, 1.6 Hz, 1H, H5 of pyridine-B), 8.11 (d, J = 6.1 Hz, 1H, H6 of pyridine A), 8.28 – 8.37 (m, 3H, H4 of pyridine-B, H3 of pyridine-A, H3 of pyridine-C), 8.38 (td, J = 8.0, 1.8 Hz, 1H, H4 of pyridine-C), 8.44 (d, J = 8.0 Hz, 1H, H3 of pyridine-B), 9.34 (dd, J = 6.0, 1.1 Hz, 1H, H6 of pyridine-B), 9.37 (dd, J = 5.4, 1.8 Hz, 1H, H6 of pyridine-C).

6–2–10 [$Rh^{III}Cl_3$(MeBPA)]

To red solution of $Rh^{III}Cl_3 \cdot nH_2O$ (Rh content: 40 w/w%, 121 mg, 470 μmol) in EtOH (10 mL) was added MeBPA (51 mg, 239 μmol), and precipitate immediately appeared in the mixture. The mixture was heated at reflux for 0.5 h and yellow suspension was obtained. The suspension was filtered, and the obtained solid was washed with H_2O, MeCN, and ether to give yellow powder (115.84 mg) as a crude product including the target compound. Recrystallization from DMSO gave yellow powder (49.40 mg, 117 μmol, 49%) of pure [$Rh^{III}Cl_3$(MeBPA)]. Anal.: Calcd. for $C_{13}H_{15}N_3RhCl_3$: C 36.95, H 3.58, N 9.94. Found: C 36.98, H 3.53, N 9.66. ^{1}H NMR ($(CD_3)_2SO$): δ 3.19 (s, 3H, -NMe), 4.58 and 4.91 (ABq, J_{AB} = 16.9 Hz, 4H, -CH_2-) 7.49 (d, J = 7.1 Hz, 2H, H3 of pyridine), 7.50 (t, J = 7.7 Hz, 2H, H5 of pyridine), 7.91 (dd, J = 7.7, 7.1 Hz, 2H, H4 of pyridine), 9.19 (d, J = 7.1 Hz, 2H, H6 of pyridine).

6–2–11 [Rh^{III}(dmdmp)Cl(MeBPA)]Cl (9·Cl)

EtOH (4 mL) and H_2O (2 mL) were added to a mixture of Hdmdmp (11.80 mg, 53.9 μmol) and [$Rh^{III}Cl_3$(MeBPA)] (12.01 mg, 28.4 μmol), and then, Et_3N (16 μL, ~110 μmol) was added. A yellow suspension obtained was heated at reflux for 18.5 h under Ar to give a yellow solution(?), and this solution was concentrated to half the volume. Addition of 1,2-dichloroethane into the solution caused separation between aqueous and organic layers, and addition of ether to the collected organic layer brought precipitation. Filtration of the suspension gave the title compound as yellowish brown powder (9.79 mg, 16.2 μmol, 57%). Anal.: Calcd. for $C_{24}H_{34}N_8O_{3.5}RhCl_2$: C 43.39, H 5.16, N 16.90. Found: C 43.26, H 5.04, N 16.61. ESI-TOF-MS (MeOH): m/z = 569.1 (calcd. for $\{[Rh^{III}(dmdmp^-)Cl^-(MeBPA)]\}^+$: m/z = 569.1). ^{1}H NMR ($(CD_3)_2OD$): δ 2.03 (s, 3H, 7-Me), 2.15 (s, 3H, -NMe), 2.68 (s, 6-Me), 4.86 and 4.93 (ABq, J_{AB} = 14.4 Hz, 4H, -CH_2-), 7.56 – 7.62 (m, 2H, H5 of pyridines), 7.62 – 7.69 (m, 2H, H3 of pyridines), 8.05 – 8.11 (m, 2H, H4 of pyridines), 9.37 (d, J = 5.3 Hz, 1H, H6 of pyridine), 9.46 (d, J = 5.7 Hz, 1H, H6 of pyridine).

6–3 X-ray Diffraction Analyses

All crystallographic measurements were performed at 120 K on a Bruker APEXII diffractometer with graphite-monochromated Mo Kα radiation (λ = 0.71073 Å). The structures were solved by a direct method (SIR–97) and expanded with differential Fourier technique. All non–hydrogen atoms were refined anisotropically and the structure refinements were carried out with full matrix least squares on F. All calculations were performed by using the Yadokari–XG program package.[14]

6–3–1 [{(terpy)(OH_2)Ru^{II}(μ-PQQTME)Ag^{I}(OTf)(μ-OTf)}$_2${(OTf)Ag^{I}(μ-OTf)$_2Ag^{I}$(OTf)}] (4)

A single crystal of **4** was obtained by slow concentration of the filtrate of the reaction mixture with crude $[Ru^{II}(OH_2)_3(terpy)]^{2+}$ (containing silver salt) and PQQTME in 1,2-dichloroethane (see 6-2-4). Crystallographic data: $C_{36}H_{25}Ag_2F_{12}N_5O_{21}RuS_4$, FW = 1536.66, green-brown, triclinic, $P\bar{1}$, a = 13.628(2) Å, b = 13.863(2) Å, c = 15.446(2) Å, α = 102.265(2)°, β = 100.557(2)°, γ = 96.661(2)°, V = 2766.5(7) Å^3, Z = 2, D_{calc} = 1.845 g/cm^3, F_{000} = 1508, $R1$ = 0.0541 ($I > 2.00\sigma(I)$), wR = 0.1043 (all data), GOF = 0.905.

6–3–2 [Ru^{II}(terpy)(η^2-PQQTME)(MeCN)](PF_6)$_2$ (**3**·(PF_6)$_2$)

A single crystal of **3**·(PF_6)$_2$ was obtained by slow concentration of an MeCN solution of **1** in the presence of $CHCl_3$ as a poor solvent. Crystallographic data: $C_{34}H_{26}F_{12}N_6O_8P_2Ru$, FW = 1037.61, green, monoclinic, $P2_1/n$, a = 27.114(3) Å, b = 12.8194(16) Å, c = 33.802(4) Å, β = 98.429(2)°, V = 11622.2(3) Å^3, Z = 8, D_{calc} = 1.186 g/cm^3, F_{000} = 4144, $R1$ = 0.0686 ($I > 2.00\sigma(I)$), wR = 0.0888 (all data), GOF = 1.065.

6–3–3 [Ru^{II}(dmdmp)Cl(MeBPA)] (**7**)

A single crystal of **7** was obtained by slow concentration of an CD_3CN solution of **7**. Crystallographic data: $C_{23}H_{27}ClN_8ORu$, FW = 568.04, brown, monoclinic, $P2_1$, a = 8.702(3) Å, b = 12.587(4) Å, c = 11.310(4) Å, β = 106.492(4)°, V = 1187.9(7) Å^3, Z = 2, D_{calc} = 1.588 g/cm^3, F_{000} = 580, $R1$ = 0.0398 ($I > 2.00\sigma(I)$), wR = 0.1124 (all data), GOF = 0.850.

6–3–4 [Ru^{II}Cl(MeBPA)(Hdmdmp)] (**7**-H^+·(PF_6))

A single crystal of (**7**-H^+)·(PF_6) was obtained by slow concentration of an $(CD_3)_2CO$ solution of (**7**-H^+)·(PF_6). Crystallographic data: $C_{23}H_{28}ClF_6N_8OPRu$, FW = 714.02, purple, monoclinic, $P2_1/c$, a = 9.1261(12) Å, b = 17.015(2) Å, c = 18.767(2) Å, β = 96.562(2)°, V = 2894.9(6) Å^3, Z = 4, D_{calc} = 1.638 g/cm^3, F_{000} = 1440, $R1$ = 0.0376 ($I > 2.00\sigma(I)$), wR = 0.1456 (all data), GOF = 1.201.

6–3–5 [Rh^{III}(dmdmp)Cl(TPMOM)]Cl (**8**·Cl)

A single crystal of **8**·Cl was obtained by slow concentration of a CH_2Cl_2 solution of **8**·Cl. Crystallographic data: $C_{27}H_{27}Cl_2N_8O_3Ru$, FW = 685.37, yellow, monoclinic, $C2/c$, a = 20.3867(18) Å, b = 13.1090(11) Å, c = 21.5581(19) Å, β = 100.0270(10)°, V = 5673.4(9) Å^3, Z = 8, D_{calc} = 1.605 g/cm^3, F_{000} = 2784, $R1$ = 0.0458 ($I > 2.00\sigma(I)$), wR = 0.1315 (all data), GOF = 1.060.

6–4 DFT Calculations

The structures of free PQQTME, **1**, **2**, 1e$^-$-reduced species of **2** ([Ru^{II}(PQQTME$^{\bullet-}$)(terpy)]$^+$), **5**, and 1e$^-$-reduced species of **5** ([{Ru^{II}(terpy)(OH_2)}(PQQTME$^{\bullet-}$){Ag^{I}(OTf)$_2$}]) were optimized by using the B3LYP functional.[15] The SDD basis set[16] was used for Ru and Ag atoms and the D95** basis set[17] for H, C, N, F, and S atoms. The Gaussian 09 program package[18] was used for all DFT calculations.

6–5 Kinetic Measurements

Kinetic measurements described in Chapter 4 were performed on a UNISOKU RSP-2000 stopped-flow spectrometer equipped with a multi-channel photodiode array using a double-mixing mode at 296 K in superdehydrated grade MeCN (Wako Pure Chemical Industries) as a solvent. Ru^{II}-dmdmp complexes (**7** or **10**: 15 μM) were treated with [Fe^{III}(bpy)$_3$](PF_6)$_3$ (15 μM) to generate the corresponding Ru^{III}-dmdmp complexes (**7**$_{OX}$ and **10**$_{OX}$). After an incubation time of 1.0 s, substrates were added to the solution. The

spectral changes were monitored by the rise of the absorption band centered at 530 nm due to the formation of Ru^{II}-Hdmdmp complexes (**7**-H^+ and **10**-H^+). The kinetic measurements were carried out at 296 K under pseudo first-order conditions, where the concentrations of the substrate were set at more than 100-fold excess to the Ru^{III}-dmdmp complexes. Pseudo first-order rate constants (k_{obs}) were determined by least-square curve fittings for the absorbance changes at 530 nm on the basis of eq 2:

$$A = A_\infty \exp(1 - k_{obs}t) \quad (2)$$

where A and A_∞ refer to the absorbance at 530 nm at the moment of t and at the infinite time after the initiation of the reaction. A linear fit to the plot of the k_{obs} values obtained against the concentration of the substrate gave the second-order rate constant, k, as the slope (eq 3).

$$k_{obs} = k\,[\text{substrate}]_0 \quad (3)$$

6–6 Determination of the pK_a values in MeCN

UV-vis titrations of **6**-H^+ were performed with use of 2,4,6-trimethylpyridine (Me_3Py) as a base for the determination of pK_a values of **6**-H^+. A solution of Me_3Py (37.9 mM) in MeCN was added dropwise to a MeCN solution (3.0 mL) of **6**-H^+ (18.9 μM) in a quartz cell and UV-vis spectrum was measured after each addition. The absorbance change at 560 nm was analyzed using eq 4:

$$A - A_0 = (\varepsilon_{\mathbf{6}\text{-H+}} - \varepsilon_{\mathbf{6}})[K_1([Me_3Py]_0 + [\mathbf{6}\text{-H}^+]_0) - \{K_1^2([Me_3Py]_0 + [\mathbf{6}\text{-H}^+]_0)^2 - 4K_1(K_1 - 1) \times [Me_3Py]_0[\mathbf{6}\text{-H}^+]_0\}^{1/2}]/2(K_1 - 1) \quad (4)$$

where A_0 refers to the absorbance of **6**-H^+ at the wavelength and K_1 represents the equilibrium constant of the reaction between **6**-H^+ and Me_3Py; $\varepsilon_{\mathbf{6}\text{-H+}} = 4060$, $\varepsilon_{\mathbf{6}} = 1660$ at 560 nm. Based on eq 4, K_1 was determined to be 0.37 ± 0.02. Thus, the pK_a value of **6**-H^+ was calculated using the K_1 value obtained and the pK_a value of Me_3Py (14.98)[19] based on eq 5.

$$pK_a = -\log K_1 + pK_a(HMe_3Py^+) \quad (5)$$

The pK_a of **6**-$2H^+$ was determined through a similar procedure using trifluoromethane-sulfonic acid (TfOH) as an acid. A solution of TfOH (56.5 mM) in MeCN was added dropwise to a MeCN solution (3.0 mL) of **6**-H^+ (18.9 μM) in a quartz cell, and UV-vis spectra were measured after each addition. The absorbance change at 660 nm was analyzed using eq 6:

$$A' - A_0' = (\varepsilon_{\mathbf{6}\text{-H+}} - \varepsilon_{\mathbf{6}\text{-2H+}})[K_2([TfOH]_0 + [\mathbf{6}\text{-H}^+]_0) - \{K_2^2([TfOH]_0 + [\mathbf{6}\text{-H}^+]_0)^2 - 4K_2(K_2 - 1) \times [TfOH]_0[\mathbf{6}\text{-H}^+]_0\}^{1/2}]/2(K_2 - 1) \quad (6)$$

where A_0' refers to the absorbance of **6**-H^+ at the wavelength and K_2 is the equilibrium constant of the reaction between **6**-H^+ and TfOH; $\varepsilon_{\mathbf{6}\text{-H+}} = 1580$, $\varepsilon_{\mathbf{6}\text{-2H+}} = 1200$ at 549 nm. Based on eq 6, K_2 was determined to be 0.15 ± 0.01. Thus, the pK_a value of **6**-$2H^+$ was calculated on the basis of the K_2 value obtained and the pK_a value of TfOH (2.6)[20] based on eq 7.

$$pK_a = \log K_2 + pK_a(TfOH) \quad (7)$$

UV-vis titrations of **7**-H$^+$, which was formed by addition of 1 equiv of TfOH, were performed with use of Me_3Py as a base for the determination of pK_a values of **7**-H$^+$. A solution of Me_3Py (37.9 mM) in MeCN was added dropwise to a MeCN solution (3.0 mL) of **7**-H$^+$ (20.1 μM) in a quartz cell and UV-vis spectrum was measured after each addition. The absorbance change at 430 nm was analyzed using eq 8:

$$A - A_0 = (\varepsilon_{\mathbf{7}\text{-H+}} - \varepsilon_{\mathbf{7}})[K_3([Me_3Py]_0 + [\mathbf{7}\text{-H}^+]_0) - \{K_3^2([Me_3Py]_0 + [\mathbf{7}\text{-H}^+]_0)^2 - 4K_3(K_3 - 1) \times [Me_3Py]_0[\mathbf{7}\text{-H}^+]_0\}^{1/2}]/2(K_3 - 1) \quad (8)$$

where A_0 refers to the absorbance of **7**-H$^+$ at the wavelength and K_3 represents the equilibrium constant of the reaction between **7**-H$^+$ and Me_3Py; $\varepsilon_{\mathbf{7}\text{-H+}} = 2340$, $\varepsilon_{\mathbf{7}} = 7960$ at 430 nm. Based on eq 8, K_3 was determined to be $(4.08 \pm 0.02) \times 10^{-2}$. Thus, the p$K_a$ value of **7**-H$^+$ was calculated using the K_3 value obtained and the pK_a value of Me_3Py (14.98)[19] based on eq 9.

$$pK_a = -\log K_3 + pK_a(HMe_3Py^+) \quad (9)$$

The pK_a of **7**-2H$^+$ was determined through a similar procedure using TfOH as an acid. A solution of TfOH (56.5 mM) in MeCN was added dropwise to a MeCN solution (3.0 mL) of **7**-H$^+$ (17.4 μM) in a quartz cell, and UV-vis spectra were measured after each addition. The absorbance change at 549 nm was analyzed using eq 10:

$$A' - A_0' = (\varepsilon_{\mathbf{7}\text{-H+}} - \varepsilon_{\mathbf{7}\text{-2H+}})[K_4([TfOH]_0 + [\mathbf{7}\text{-H}^+]_0) - \{K_4^2([TfOH]_0 + [\mathbf{7}\text{-H}^+]_0)^2 - 4K_4(K_4 - 1) \times [TfOH]_0[\mathbf{7}\text{-H}^+]_0\}^{1/2}]/2(K_2 - 1) \quad (10)$$

where A_0' refers to the absorbance of **7**-H$^+$ at the wavelength and K_4 is the equilibrium constant of the reaction between **7**-H$^+$ and TfOH; $\varepsilon_{\mathbf{7}\text{-H+}} = 9390$, $\varepsilon_{\mathbf{7}\text{-2H+}} = 2400$ at 549 nm. Based on eq 10, K_4 was determined to be 19 ± 2. Thus, the pK_a value of **7**-2H$^+$ was calculated on the basis of the K_4 value obtained and the pK_a value of TfOH (2.6)[20] based on eq 11.

$$pK_a = \log K_4 + pK_a(TfOH) \quad (11)$$

UV-vis titrations of **10**-H$^+$, which was formed by addition of 1 equiv of TfOH, were performed with use of Me_3Py as a base for the determination of pK_a values of **10**-H$^+$ *via* a similar procedure to that of **6**-H$^+$. A solution of Me_3Py (37.9 mM) in MeCN was added dropwise to a MeCN solution (3.0 mL) of **10**-H$^+$ (19.6 μM) in a quartz cell and UV-vis spectrum was measured after each addition. The absorbance change at 430 nm was analyzed using eq 12:

$$A'' - A_0'' = (\varepsilon_{\mathbf{10}\text{-H+}} - \varepsilon_{\mathbf{10}})[K_5([Me_3Py]_0 + [\mathbf{10}\text{-H}^+]_0) - \{K_5^2([Me_3Py]_0 + [\mathbf{10}\text{-H}^+]_0)^2 - 4K_5(K_5 - 1) \times [Me_3Py]_0[\mathbf{10}\text{-H}^+]_0\}^{1/2}]/2(K_5 - 1) \quad (12)$$

where A_0'' refers to the absorbance of **10**-H$^+$ at the wavelength and K_5 represents the equilibrium constant of the reaction between **10**-H$^+$ and Me_3Py; $\varepsilon_{\mathbf{10}\text{-H+}} = 9970$, $\varepsilon_{\mathbf{10}} = 14870$ at 430 nm. Based on eq 12, K_5 was determined to be 5.4 ± 0.3. Thus, the pK_a value of **10**-H$^+$ was calculated using the K_5 value obtained and the pK_a value of Me_3Py (14.98)[19] based on eq 13.

$$pK_a = -\log K_5 + pK_a(HMe_3Py^+) \quad (13)$$

The pK_a values of protonated rhodium-pterin complexes, **8**-H^+ and **9**-H^+ were also determined *via* a similar procedure to those of ruthenium-pterin complexes. A solution of TfOH (56.5 mM) in MeCN was added dropwise to a MeCN solution (3.0 mL) of **8** (20.0 μM) in a quartz cell, and UV-vis spectra were measured after each addition. The absorbance change at 420 nm was analyzed using eq 14:

$$A' - A_0' = (\varepsilon_{\mathbf{8}} - \varepsilon_{\mathbf{8}\text{-H+}})[K_6([\text{TfOH}]_0 + [\mathbf{8}]_0) - \{K_6^2([\text{TfOH}]_0 + [\mathbf{8}]_0)^2 - 4K_6(K_6 - 1) \times [\text{TfOH}]_0[\mathbf{8}]_0\}^{1/2}]/2(K_6 - 1) \quad (14)$$

where A_0' refers to the absorbance of **8** at the wavelength and K_6 is the equilibrium constant of the reaction between **8** and TfOH; $\varepsilon_{\mathbf{8}} = 5030$, $\varepsilon_{\mathbf{8}\text{-H+}} = 200$ at 420 nm. Based on eq 15, K_6 was determined to be 5.1 ± 0.6. Thus, the pK_a value of **8**-H^+ was calculated on the basis of the K_6 value obtained and the pK_a value of TfOH (2.6)[20] based on eq 15.

$$pK_a = \log K_6 + pK_a(\text{TfOH}) \quad (15)$$

A solution of TfOH (56.5 mM) in MeCN was added dropwise to a MeCN solution (3.0 mL) of **9** (22.0 μM) in a quartz cell, and UV-vis spectra were measured after each addition. The absorbance change at 411 nm was analyzed using eq 16:

$$A' - A_0' = (\varepsilon_{\mathbf{9}} - \varepsilon_{\mathbf{9}\text{-H+}})[K_7([\text{TfOH}]_0 + [\mathbf{9}]_0) - \{K_7^2([\text{TfOH}]_0 + [\mathbf{9}]_0)^2 - 4K_7(K_7 - 1) \times [\text{TfOH}]_0[\mathbf{9}]_0\}^{1/2}]/2(K_7 - 1) \quad (16)$$

where A_0' refers to the absorbance of **9** at the wavelength and K_7 is the equilibrium constant of the reaction between **9** and TfOH; $\varepsilon_{\mathbf{9}} = 5250$, $\varepsilon_{\mathbf{9}\text{-H+}} = 220$ at 420 nm. Based on eq 16, K_7 was determined to be 6.0 ± 0.6. Thus, the pK_a value of **9**-H^+ was calculated on the basis of the K_7 value obtained and the pK_a value of TfOH (2.6)[20] based on eq 17.

$$pK_a = \log K_7 + pK_a(\text{TfOH}) \quad (17)$$

6–7 Attempt to Formation of pterin-OO-metal Species with 6-2H^+ in Propionitrile

To 3.0 mL of a propionitrile solution of **6**-H^+ (49.9 μM, 150 nmol) in a quartz cell was added 10.0 μL (113 μmol) of TfOH under Ar at RT. Color of the solution was changed into green, indicating that **6**-2H^+ was formed. The green solution was cooled to –85 °C, and cobaltocene (~ 4 mM) in propionitrile was added dropwise to the **6**-2H^+ solution, and UV-vis spectra were measured after each addition. After addition of ~1800 nmol of cabaltocene, the MLCT band of the **6**-2H^+ around 660 nm was completely disappeared. To the solution a mixture of KO_2 (63 mg, 0.89 mmol) and 18-crown-6 (118 mg, 0.451 mmol) in 2 mL of benzene was added dropwise by 10 μL. In the course of the addition of KO_2 into the reduced **6**-2H^+, no

absorption bands were observed over 400 nm.

Reference and Notes

(1) MacKenzie, A. R.; Moody, C. J.; Roes, C. W. *Tetrahedron* **1986**, *42*, 3259.

(2) Glansdorp, F. G.; Spandl, R. J.; Swatton, J. E.; Loiseleur, O.; Welch, M.; Spring, D. R. *Org. Biomol. Chem.* **2008**, *6*, 4120.

(3) Carrigan, C. N.; Bartlett, R. D.; Esslinger, C. S.; Cybulski, K. A.; Tongcharoensirikul, P.; Bridges, R. J.; Thompson, C. M. *J. Med. Chem.* **2002**, 45, 2260.

(4) Alewood, P. F.; Hussian, S. A.; Jenkins, T. C.; Perkins, M. J.; Sharma, A. H.; Siew, N. P. Y.; Ward, P. *J. Chem. Soc., Perkin Trans. 1* **1978**, 1066.

(5) Winter, A.; Hummel, J.; Risch, N. *J. Org. Chem.* **2006**, *71*, 4862.

(6) Wong, Y.-L.; Mak, C.-Y.; Kwan, H. S.; Lee, H. K. *Inorg. Chim. Acta* **2010**, *363*, 1246.

(7) Luo, J.; Rath, N. P.; Mirica, L. M. *Inorg. Chem.* **2011**, *50*, 6152.

(8) Jonas, R. T.; Stack, T. D. P. *Inorg. Chem.* **1998**, *37*, 6615.

(9) Huynh, M. H. V.; Lasker, J. M.; Wetzler, M.; Mort, B.; Szezepura, L. F.; Witham, L. M.; Cintron, J. M.; Marschilok, A. C.; Ackerman, L. J.; Castellano, R. K.; Jameson, D. L.; Churchill, M. R.; Jircitano, A. J.; Takeuchi, K. J. *J. Am. Chem. Soc.* **2001**, *123*, 8780.

(10) Funahashi, Y. *private communications*. See also: Yamauchi, O.; Odani, A.; Masuda, H.; Funahashi, Y. In *Bioinorganic Chemistry of Copper*; Karlin, K. D.; Tyeklár, Z., Eds.; Chapman & Hall: New York, 1993; p363.

(11) Miyazaki, S.; Kojima, T.; Sakamoto, T.; Matsuyama, T.; Ohkubo, K.; Fukuzumi, S. *Inorg. Chem.* **2008**, *47*, 333.

(12) Shimizu, Y.; Fukui, S.; Oi, T.; Nagao, H. *Bull. Chem. Soc. Jpn.* **2008**, *81*, 1285.

(13) Taher, D.; Thibault, M. E.; Mondo, D. D.; Jennings, M.; Schlaf, M. *Chem.–Eur. J.* **2009**, *15*, 10132.

(14) (a) Wakita, T. Yadokari–XG, Software for Crystal Structure Analysis, **2001**. (b) Kabuto, C.; Akine S.; Nemoto, T.; Kwon, E, Release of Software (Yadokari–XG 2009) for Crystal Structure Analyses. *J. Cryst. Soc. Jpn.* **2009**, *51*, 218.

(15) (a) Becke, A. D. *Phys. Rev. A* **1988**, *38*, 3098. (b) Lee, C.; Yang, W.; Parr, R. G. *Phys. Rev. B* **1988**, *37*, 785. (c) Becke, A. D. *J. Chem. Phys.* **1993**, *98*, 5648.

(16) Andrae, D.; Haussermann, U.; Dolg, M.; Stoll, H.; Preuss, H. *Theor. Chim. Acta* **1990**, *77*, 123.

(17) (a) Raghavachari, K. Trucks, G. W. *J. Chem. Phys.* **1989**, *91*, 1062; (b) Dunning, T. H.; Hay, J. P. In *Modern Theoretical Chemistry*; Schaefer, H. F. III, Ed.; Plenum: New York, 1976; Vol. 3, pp 1-27.

(18) Gaussian 09 (Revision A.02), Gaussian, Inc., Wallingford CT, 2009.

(19) Kaljurand , I.; Kütt, A.; Sooväli, L.; Rodima, T.; Mäemets, V.; Leito. I.; Koppel, I. A. *J. Org. Chem.* **2005**, *70*, 1019.

(20) Izutsu, K. *Acid-Base Dissociation Constants in Dipolar Aprotic Solvents*; Blackwell Scientific: Boston, MA, 1990.

List of Publications

1) Heteronuclear $Ru^{II}Ag^{I}$ Complexes Having a Pyrroloquinolinequinone Derivative as a Bridging Ligand Hiroumi Mitome, Tomoya Ishizuka, Yoshihito Shiota, Kazunari Yoshizawa, Takahiko Kojima, *Inorganic Chemistry* **2013**, *52*(5), 2274-2276.

2) Controlling the redox properties of a pyrroloquinolinequinone (PQQ) derivative in a ruthenium(II) coordination sphere,Hiroumi Mitome, Tomoya Ishizuka, Yoshihito Shiota, Kazunari Yoshizawa, Takahiko Kojima, *Dalton Transaction* **2015**, *44*(7), 3151-3158.

Acknowledgments

The author would like to give special thanks to Professor Takahiko Kojima for his excellent tutelage, encouragements, and great generosity that inspired the author to devote oneself to research. The author is also deeply grateful to him for engaging me in fruitful discussions that cultivated author's understanding about natural science and one's thinking ability. The author would appreciate very much Dr. Tomaya Ishizuka's patient guidance throughout author's student life in the Kojima laboratory, which not only initiated the author into scientific research but also enlightened the author on how the author should behave one's life. The author's thanks also go to Dr. Hiroaki Kotani for his helpful advices in one's research.

The author would like to express one's sincere gratitude to Prof. Kazunari Yoshizawa and Prof. Yoshihito Shiota in Institute for Materials Chemistry and Engineering, Kyushu University, for their kind collaboration in DFT calculations to gain important insights that cannot be obtained with any experimental methods. The author would like to appreciate Prof. Masaki Kawano in Graduate School of Science and Engineering, Tokyo Institute of Technology, for their kind collaboration in X-ray Diffraction Analyses. The author also would like to appreciate Prof. Shinobu Itoh in Department of Material and Life Science, Osaka University, for the gift of the Na_2HPQQ salt. The author would like to thank Prof. Tai-Chu Lau in City University of Hong Kong for hosting the author during a short stay in his laboratory, and the author also expresses one's sincere thanks to the members of Lau's laboratory, especially Dr. Wai-Lun Man, for their careful instructions not only in various experimental techniques but also in the author's life in Hong Kong.

The author would like to thank all the labmates in the Kojima laboratory, Department of Chemistry, University of Tsukuba, for their tough questions and for the long nights we were working together. The author would also like to express one's gratitude to Ms. Miyuki Nakahara for her daily assistance in administrative processes.

Finally, the author sincerely appreciates one's parents for their spiritual supports and pecuniary assistance throughout one's life.

February 2016

Hiroumi Mitome

Kojima laboratory
Department of Chemistry
University of Tsukuba